From Childhood Stress to Adult Inflammatory Response: Conditional Vulnerability in Late Avar-Period Austria

by
Mirina Van Der Veen

A Thesis submitted to the Faculty of Graduate and
Postdoctoral Studies at
The University of Manitoba

In partial fulfilment of the requirements of the degree

MASTER OF ARTS

Department of Anthropology
University of Manitoba
Winnipeg

Abstract

This research investigates the relationship between early life stress and adult skeletal-dental inflammatory burden in two late Avar-period cemetery samples from eastern Austria: Bruckneudorf and Hirschstetten. It examines whether retained skeletal and dental indicators of early life stress correspond with adult skeletal-dental inflammatory burden, including periodontal disease, periosteal new bone formation, and osteoarthritis. The study sample included 68 adults and late adolescents. Early life stress was assessed through dental enamel defect count, maximum defect depth, defect timing, estimated stature, cortical thickness index, and bilateral appendicular asymmetry. Adult inflammatory burden was assessed through periodontal disease and periosteal new bone formation, which were combined into a SINDEX (Crespo 2020) score. Osteoarthritis was included as contextual adult skeletal remodelling. Population-level, sex-stratified, correlation, and exploratory regression analyses were used to examine relationships among developmental indicators, inflammatory lesions, osteoarthritis, age, sex, and cemetery population.

Results show that the strongest population-level difference was concentrated in periodontal disease. Bruckneudorf had higher SINDEX and periodontal disease scores than Hirschstetten, while periosteal new bone formation did not reproduce the same site-level pattern. Early life stress indicators showed weaker and more fragmented associations with adult inflammatory burden. Dental enamel defect timing demonstrated the clearest developmental direction, showing weak positive relationships with periosteal new bone formation severity, activity, and anatomical extent. Osteoarthritis was structured primarily by age. These findings support a complex, non-linear relationship between retained developmental stress and adult inflammatory burden. Early life stress is interpreted as conditional vulnerability: a developmental history that may shape inflammatory-repair response when later exposure, pathology, repair demand, and survival make that vulnerability visible in bone.

Table of Contents

Table of Figures

Acknowledgements

I would first like to thank my advisor, Dr. Julia Gamble, for her guidance, patience, and encouragement throughout this project. Julia created the space for me to develop my own research questions, follow unexpected directions, and find a research niche that I have grown to care about deeply. I am grateful for her mentorship, her trust in my ideas, and the many conversations that helped this thesis take shape. I would also like to thank my committee members, Dr. Stacie Burke and Dr. Fabian Crespo, for their time, expertise, and thoughtful feedback. Their perspectives strengthened this project and helped me think more carefully about the interpretation of skeletal inflammation, life-course stress, and bioarchaeological method.

I am grateful to the Department of Anthropology at the University of Manitoba and to the supporters of the Emőke Szathmáry Fellowship in Biological Anthropology, which helped make this research possible. I also thank the Department of Anthropology at the Naturhistorisches Museum Wien for access to the Bruckneudorf skeletal collection, use of imaging equipment, and assistance during data collection. I especially thank Karin Wiltschke-Schrotta, Doris Pany-Kucera, Margit Berner, and Barbara Ankerl for their help while we were working at the museum. They did an enormous amount to support us during that time. I am grateful to the City Archaeology Department at the Museum der Stadt Wien for permission to conduct research on the Hirschstetten collection. I also thank Jasmin Özyurt and Paul Klostermann for sharing their knowledge of Avar-period archaeology in Austria.

I also want to acknowledge the many women scholars I was surrounded by while completing this thesis, including peers, mentors, and colleagues in Winnipeg and Vienna. It has been deeply inspiring to work alongside so many talented, intelligent, and generous women. Their knowledge, support, and example shaped both this project and my sense of what kind of scholar I want to become.

Artificial Intelligence Disclosure

Copilot was used during revision in response to advisor comments for limited editorial support, including checking clarity and continuity, identifying repetition, and considering sentence-level wording alternatives. Copilot was also used during R script development to help identify syntax errors, troubleshoot error messages, and refine code execution.

All research questions, data collection, variable construction, statistical test selection, model specification, citation selection, interpretation of results, and final writing decisions were completed and reviewed by the author.

Ethics Statement

Formal Research Ethics Board approval was not required. All sampling and data collection were conducted with the permission and full oversight of the Department of Anthropology at the Naturhistorisches Museum Wien, the Museum der Stadt Wien, and Novetus Archaeologie, using methods and procedures designed to minimize destruction.

1. Introduction

The human skeleton is a complex organ system that materializes the biosocial conditions of life. Nutrition, infection, care, labour, and ecological constraint become embodied in skeletal and dental tissues, shaping growth, maintenance, and repair across the life course (Agarwal 2016; Gowland 2015; Schrader and Torres-Rouff 2020). Bone and enamel preserve traces of these conditions at different biological scales: enamel records disruption during crown formation (Goodman and Rose 1990; Hillson 2014), while bone grows, remodels, and repairs through overlapping energetic, endocrine, mechanical, and immune systems (Cunningham et al. 2016; Pappalardo et al. 2023; Ruff 2003). Skeletal tissues reflect lived experience within social and ecological worlds (Gowland and Caldwell 2023; Temple and Klaus 2022). A biocultural approach reads developmental and inflammatory skeletal indicators as embodied traces of social life, ecological exposure, and biological response.

Skeletal and dental indicators do not record the same moments in the life course or form through the same biological pathways. Developmental stress can shape later immune regulation, inflammatory response, and repair capacity (Anderson et al. 2025; Fagundes and Way 2014; Heim et al. 2019), but skeletal lesions do not only preserve developmental history. They also record exposure, tissue-specific lesion ecology, age, activity, repair, frailty, and survival (DeWitte and Wood 2008; Klaus 2014; J. Wood et al. 1992). A dental enamel defect preserves evidence of a disruption during crown formation (Goodman and Rose 1990; Hillson 2014). A thin cortex, altered adult stature, or bilateral appendicular asymmetry may preserve longer histories of skeletal investment and growth (Cunningham et al. 2016; De Coster et al. 2013; Parsons 1992; Ruff 2003). Periodontal disease records chronic alveolar destruction around the dentition (Cekici et al. 2014; Zhou and Graves 2022). Periosteal new bone formation records cortical surface response after infection, injury, irritation, vascular disturbance, or

repair demand (Weston 2008; Klaus 2014). Osteoarthritis records joint-level remodelling through age, movement, loading, repair, and survival (Becker 2020; Molnar et al. 2011).

This study applies this life-course problem to two late Avar-period cemetery populations from the Vienna Basin, Bruckneudorf (Pany-Kucera and Wiltschke-Schrotta 2022) and Hirschstetten (Penz and Lehofer 2023). The Avar Khaganate was a politically and culturally diverse polity that extended across much of the Carpathian Basin from the late sixth to the early ninth century. During the seventh and eighth centuries CE, the Vienna Basin formed part of its western zone, where communities participated in shared material and mortuary traditions that included furnished inhumations and animal deposits (Curta 2021; Daim 2003; Pohl 2018). Both populations belong to a shared late Avar regional setting, but their communities may have differed in diet, land use, mobility, livestock contact, and patterns of interaction (Herold 2013; Faragó et al. 2022). These differences could have produced distinct nutritional and infectious exposures across the two communities. Comparing early-life stress indicators with adult inflammatory markers at Bruckneudorf and Hirschstetten examines variation in their immunological landscapes within a shared regional context.

Cemetery membership does not provide direct access to childhood developmental ecology. Childhood conditions were structured through household provisioning, food access, disease exposure, care, mobility, and recovery. Adult conditions added further exposures through labour, oral disease, infection, movement, injury, and survival with chronic tissue change. Recent ancient DNA studies of Avar-period cemeteries, including geographically proximate late Avar sites south of Vienna, have identified patrilocality, female exogamy, remarriage, and household incorporation, complicating any assumption that adults buried in the same cemetery shared the same childhood locality or developmental ecology (Gnecchi-Ruscone et al. 2024; Wang et al. 2025).

The thesis analysis tests whether retained developmental stress indicators correspond with adult skeletal-dental inflammatory burden. Developmental stress was assessed through dental enamel defects, defect timing, appendicular growth, cortical thickness, and appendicular asymmetry. Adult inflammatory burden was assessed through periodontal disease and periosteal new bone formation, combined into a SINDEX (Crespo 2020) score and examined as separate components. Osteoarthritis was included as contextual adult joint remodelling because it can involve inflammatory participation (Fernandes et al. 2002; Thielen et al. 2021), but its macroscopic expression remains strongly structured by age, mechanics, activity, and repair (Molnar et al. 2011). These variables were compared by sample population, sex, and life-course association to evaluate whether developmental disruption, adult inflammation, and skeletal maintenance formed a shared pattern.

Stronger retained developmental stress signatures were expected to correspond with greater adult inflammatory burden. That expectation follows clinical and living-population evidence linking early adversity with later immune regulation, inflammatory response, and repair capacity (Fagundes and Way 2014; Heim et al. 2019; McDade et al. 2017), as well as bioarchaeological work connecting developmental indicators, adult lesions, frailty, and mortality risk (DeWitte and Wood 2008; Wigley et al. 2025). The archaeological record filters that relationship through tissue timing and selective visibility (DeWitte and Wood 2008; McFadden and Oxenham 2020; Wood et al. 1992). Individuals must survive stress long enough for enamel defects, growth changes, alveolar destruction, periosteal response, or joint remodelling to form and remain observable. Lesion absence can reflect limited exposure, effective buffering, repair, rapid death, tissue loss, or preservation.

The purpose of this thesis is to evaluate the proposed relationship between retained developmental stress and greater adult inflammatory burden in the Bruckneudorf and Hirschstetten late Avar cemetery samples by comparing developmental stress indicators and

adult skeletal-dental inflammatory lesions. Chapter 2 establishes the archaeological, biological, and theoretical frameworks through late Avar lifeways, early life stress, developmental embodiment, osteoimmune vulnerability, and adult inflammatory lesion patterning. Chapter 3 presents the research questions, aims, and hypotheses. Chapter 4 outlines the study samples, variable construction, and statistical approach. Chapters 5 and 6 present and interpret the results, and Chapter 7 summarizes the thesis contribution, limitations, and directions for future work.

2. Literature Review

Adult inflammatory lesions represent adult tissue responses shaped by developmental history, pathological exposure, repair, frailty, and survival. Life-course bioarchaeology treats skeletal and dental tissues as cumulative records of growth, maintenance, stress, and repair, but those records preserve different moments and durations in the life course (Agarwal 2016). A visible inflammatory lesion marks tissue response that persisted long enough to form, remodel, and survive observation; its absence may reflect limited exposure, rapid death, effective repair, tissue loss, or preservation constraints (DeWitte and Wood 2008; Klaus 2014; Wood et al. 1992). Developmental stress can shape later physiological reserve, immune response, and repair capacity (Gowland 2015; Fagundes and Way 2014; Temple 2019), but adult lesion patterning also reflects later exposure, age, activity, local tissue ecology, frailty, and survival. Studies that place developmental indicators, adult inflammatory burden, and mortality risk within the same life-course framework make this relationship archaeologically testable while preserving its limits (DeWitte and Bekvalac 2010, 2011; Wigley et al. 2025).

Skeletal histories develop through social arrangements as well as tissue processes. Biocultural bioarchaeology treats developmental ecology as a route through which social worlds become embodied in growth and repair, including the distribution of food, labour, care, and inequality (Farmer 2004; Leatherman and Goodman 2020; Schrader and Torres-Rouff 2020). A child's capacity to grow, rest, recover, and resist infection depends on household provisioning, care ecology, and the organization of daily exposure. Embodiment gives those arrangements biological consequence because exposure, susceptibility, resistance, recovery, and survival are produced through lived social worlds (Krieger 2012). Stress becomes evident in skeletal and dental tissues when disruption intersects with tissue growth timing, physiological reserve, recurrence, and the conditions that permit recovery or continued damage (Temple and Edes 2022; Temple and Klaus 2022). Life-course analysis asks how

developmental ecology becomes a skeletal history of growth, repair, resilience, or vulnerability.

Linking developmental stress to adult immune or inflammatory phenotype requires a model of timing, survival, physiological reserve, and later exposure. DOHaD, the thrifty phenotype, and predictive adaptive responses connect early conditions to later physiological capacity through growth, metabolic allocation, developmental plasticity, and trade-off (Barker 2012; Bateson et al. 2014; Hales and Barker 2013). In bioarchaeology, these models shift developmental stress markers away from isolated signs of childhood disruption and toward questions of timing, survival, physiological reserve, and adult phenotype (Gowland 2015; Temple 2019). Developmental skeletal markers have been linked with adult immune function in a living population (Anderson et al. 2025), while DeWitte and Bekvalac (2011) and Wigley et al. (2025) have placed developmental stress indicators, adult inflammatory lesions, frailty, survival, and mortality risk within the same life-course frame. Developmental stress may remain biologically consequential, but its archaeological expression has to be read through the adult lesion systems in which later vulnerability becomes evident.

2.1 Late Avar Lifeways in the Vienna Basin

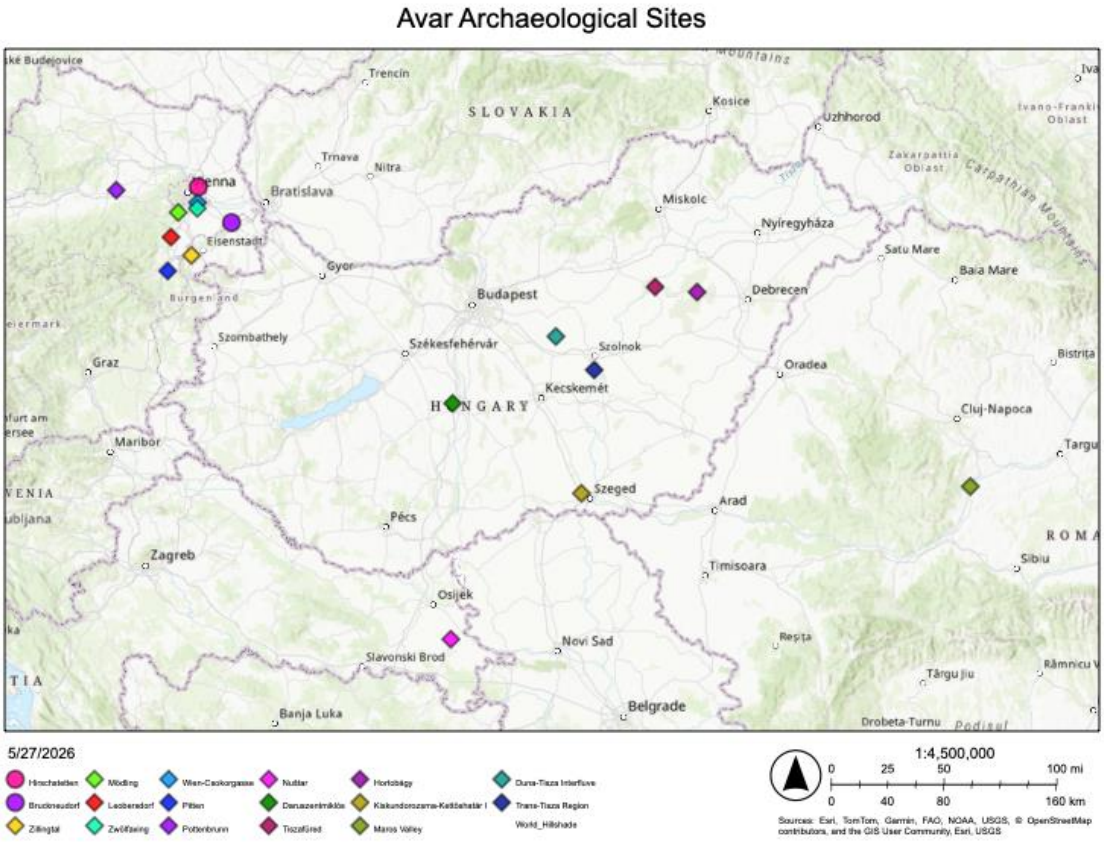

Figure 1 Geographic distribution of Avar-period and early medieval comparative sites discussed in this literature review. The mapped sites indicate the geographic range of the osteological, isotopic, settlement, and palaeopathological evidence considered, extending from eastern Austria and the Vienna Basin through Hungary, the Duna–Tisza and Trans-Tisza regions, the Maros Valley, and eastern Croatia. Site and regional locations were compiled from Herold (2008, 2013), Gausterer et al. (2011), Vidal-Ronchas et al. (2019), Kondé et al. (2019), Pany-Kucera and Wiltschke-Schrotta (2022), Bühler and Kirchengast (2022), Faragó et al. (2022), Spekker et al. (2022, 2023), Penz and Lehofer (2023), Pópity (2023), Gnecchi-Ruscone et al. (2024), Tihanyi et al. (2024), Wang et al. (2025), and Klostermann et al. (2025). Made in ArcGIS Online by author using World Hillshade and World Topographic Maps (Esri 2012b, 2012a).

The study populations derive from two late Avar-period cemetery samples in the Vienna Basin, a western zone of the Avar Khaganate during the seventh and eighth centuries CE (Daim 2003; Pohl 2018). Their burials belong to a late Avar cemetery tradition that included furnished inhumations and animal deposits, although grave contents varied by site, sex, age, and status (Curta 2021; Daim 2003; Stadler 2008). Cemetery evidence provides only partial access to the developmental ecologies that structured childhood conditions. Because associated domestic evidence is limited for the Vienna Basin cemeteries considered here, late Avar lifeways are reconstructed through a wider comparative geography of Austrian and Carpathian Basin

evidence. Figure 1 shows the comparative sites discussed in this section, extending from the Vienna Basin and eastern Austria through the Carpathian Basin and eastern Croatia.

Settlement comparisons suggest that late Avar cemetery communities were embedded in landscape ecologies where water access, arable land, pasture, craft activity, and movement routes structured daily life. At Zillingtal (Austria), an Avar-period settlement lay near a stream and across from its associated cemetery, with evidence for pits, postholes, ceramic phases, Avar-period activity within a Roman villa area, and iron-smelting furnaces (Herold 2013). In the Maros Valley (Hungary), Avar-period settlements were arranged in relation to former floodplains, higher flood-free ground, fertile soils, freshwater bodies, and river corridors (Pópity 2023). At Daruszentmiklós (Hungary), cooking vessels, storage vessels, tablewares, workshop evidence, and specialised production show how domestic assemblages can preserve food preparation, storage, craft activity, and possible social differentiation (Kondé et al. 2019). These features of everyday life help identify conditions that could buffer or intensify stress, as access to water and land, household storage and production, craft activity, and movement shaped provisioning, labour demands, mobility, and exposure to environmental or animal-associated risks.

By the later Avar period, settlement and cultivation had expanded across parts of the Carpathian Basin after seventh-century political and military disruptions, including conflict with Byzantium and challenges to Avar authority (Pohl 2018; Preiser-Kapeller 2018). Preiser-Kapeller (2018) describes this expansion alongside a variable climate record that included cold and dry phases, droughts, floods, changing lake levels, regional differences in precipitation, and later instability. Floodplain systems along major rivers and tributaries created fertile agricultural zones, while seasonal inundation, snowmelt, and ice-jam floods affected settlement placement, movement, fields, and grazing land (Preiser-Kapeller 2018). Millet, barley, rye, wheat, and other cereals occur in Avar-period archaeobotanical and isotopic evidence,

alongside cattle, pigs, sheep, goats, poultry, and horses (Vidal-Ronchas et al. 2019). Cereals point to cultivation, storage, processing, and cooking, while domestic animals point to grazing, foddering, dairying, slaughter, and husbandry (Preiser-Kapeller 2018; Vidal-Ronchas et al. 2019).

Nearby communities did not necessarily share a uniform provisioning system. At Nuštar (Croatia), $\delta^{13}C$ and $\delta^{15}N$ values, interpreted alongside local faunal values and archaeobotanical evidence, supported a mixed late Avar food economy involving C^3 grain crops (wheat, barley, and rye), millet (C^4), and animal resources, without strong dietary differentiation by sex, age, or burial status (Vidal-Ronchas et al. 2019). This included individuals with richer burial treatment, including horse-associated graves, whose isotope values remained within the cemetery range (Vidal-Ronchas et al. 2019). Faragó et al. (2022) found sharper dietary differences between neighbouring early medieval communities in the Carpathian Basin. Tiszafüred (Hungary) followed a pattern of C^3 grain and millet consumption with animal protein, while Hortobágy (Hungary) produced higher nitrogen values linked to greater animal protein intake and possible freshwater resources (Faragó et al. 2022).

At Leobersdorf (Austria), males averaged 10.9‰ $\delta^{15}N$[1] and females 10.5‰ $\delta^{15}N$, and males had higher $\delta^{15}N$ values in 14 of 17 sex and age comparisons across the investigated sites (Herold 2008). Leobersdorf, Zwölfaxing (Austria), and Wien-Csokorgasse (Austria) also had higher $\delta^{15}N$ and $\delta^{13}C$[2] values than the Slavic comparison sites of Pitten (Austria) and Pottenbrunn (Austria), suggesting greater animal protein consumption and a stronger millet signal in the Avar-period samples (Herold 2008). Dental pathology at Bruckneudorf (Austria) complicates how far oral disease can be used to reconstruct diet. Pany-Kucera and Wiltschke-

[1] Higher $\delta^{15}N$ values generally indicate greater trophic-level protein intake, especially animal protein. Animal foddering, manuring, and local ecology can also affect these values (Caut et al. 2009; Stephens et al. 2022).
[2] Higher δ13C values indicate a stronger contribution from C^4 plants (Caut et al. 2009; Stephens et al. 2022), most plausibly millet in this regional setting (M. Herold 2008).

Schrotta (2022) recorded a permanent-tooth caries frequency of 6.2%, with posterior teeth affected more often than anterior teeth, alongside 750 teeth lost antemortem and calculus on 3,185 of 3,688 assessable teeth. The low caries frequency does not necessarily indicate low carbohydrate exposure, because heavy occlusal wear can remove crown surfaces where lesions may have formed, while exposed roots can shift caries expression toward cervical and root surfaces (Meinl et al. 2010). Antemortem tooth loss further reduces the observable dentition, including teeth that may have carried carious or periodontal lesions during life.

The large pedigrees reconstructed by Gnecchi-Ruscone et al. (2024) show male descent lines persisting across generations, while females more often entered cemetery communities through exogamous marriage. In the sampled cemeteries, patrilocal residence and patrilineal descent produced sex-differentiated residence histories: locally rooted male lines, incoming females, children of exogamous unions, and individuals incorporated through later partnerships could occupy different positions within the same burial community (Gnecchi-Ruscone et al. 2024). Multiple reproductive partnerships and levirate unions further indicate that household affiliation could shift through remarriage, widowhood, and alliance formation (Gnecchi-Ruscone et al. 2024). South of Vienna, Wang et al. (2025) found neighbouring late Avar cemeteries with shared material culture but different ancestry profiles, biological relatedness, reproductive boundaries, and marriage networks. Shared grave forms indicate participation in the same late Avar mortuary tradition, while individual cemeteries could maintain distinct marriage boundaries, residence histories, and biological relatedness patterns (Gnecchi-Ruscone et al. 2024; Wang et al. 2025).

At Mödling (Austria) and Leobersdorf, adolescent pathology clusters in growth stages associated with the transition into heavier work and adult responsibility. Klostermann et al. (2025) examined individuals aged 8 to 25 years and found that joint disease, Schmorl's nodes, osteochondritis dissecans, and trauma appeared from peak height velocity and later adolescent

growth stages, while non-specific stress indicators and inflammatory or respiratory lesions varied across development. The timing of these lesions places increased bodily demand within adolescence, when growing individuals could begin entering adult labour regimes involving animals, fields, food preparation, domestic production, movement, and load-bearing tasks (Klostermann et al. 2025). In the Vienna Basin cemeteries examined here, this regional pattern suggests that bodily demand could intensify during adolescence, before skeletal maturation was complete. At Wien-Csokorgasse, Bühler and Kirchengast (2022) identified proposed skeletal indicators associated with habitual horse riding in a nearby Avar cemetery population. Males showed higher frequencies of Poirier's facet[3] and higher acetabular index of ovalization[4], while some females also showed proposed riding indicators, especially in earlier cemetery phases (Bühler and Kirchengast 2022).

Bruckneudorf provides a direct adult osteological baseline for one cemetery population examined here. Pany-Kucera and Wiltschke-Schrotta (2022) report low postcranial fracture frequencies, rare skull fractures, limited signs of interpersonal violence, infectious disease indicators in some individuals, and spinal degenerative changes in many adults over 40, with males affected more often than females. Pany-Kucera and Wiltschke-Schrotta (2022) recorded infectious disease indicators, including lesions interpreted as tuberculosis, osteomyelitis, and possible brucellosis. Brooks (2025) examined the same Bruckneudorf collection alongside Hirschstetten and estimated tuberculosis in 35.58% of assessed individuals and brucellosis in nearly 7.40%. Tuberculosis and brucellosis imply different exposure pathways and different conditions of skeletal visibility. Tuberculosis circulated through respiratory exposure involving shared indoor air, household contact, mobility, and repeated interaction between people

[3] An accessory articular extension on the anterior femoral neck, often interpreted as a response to repeated contact or loading at the hip joint (Bühler and Kirchengast 2022).
[4] A metric measure of acetabular shape; values above 1 have been associated with habitual riding (Bühler and Kirchengast 2022).

(Brooks 2025; Kramer and Assadian 2014). Skeletal tuberculosis represents the subset of infections that persisted long enough to involve bone, whether originating in the lungs or elsewhere. In addition to airborne transmission, livestock contact could have exposed Avar communities to zoonotic *M. bovis* through inhalation, unpasteurized dairy products, animal tissues, or wounds during animal work (Olea-Popelka et al. 2017). Brucellosis involved a more specific animal-associated exposure pathway, including contact with infected livestock, unpasteurized milk, meat, animal tissues, and wounds sustained during routine animal work (Brooks 2025; Fournié et al. 2017).

Gamble et al. (2024) report a possible case of leprosy in an individual from the Hirschstetten collection. Gausterer et al. (2011) identified *Mycobacterium leprae* DNA in an early medieval individual from Pottenbrunn, Lower Austria, confirming leprosy in the broader regional record. At Kiskundorozsma–Kettőshatár I, an eighth-century late Avar cemetery in the Duna-Tisza Interfluve, Spekker et al. (2022) described a middle-aged male with lepromatous leprosy affecting the rhinomaxillary region of the face and the lower limbs. The skeletal changes included severe deformation and functional impairment, including difficulty with eating, drinking, standing, and walking; Spekker et al. (2022) argue that survival with this degree of impairment would have required regular care from others. The individual was buried within the cemetery boundaries, with body position, orientation, and grave goods conforming to local mortuary practice (Spekker et al. 2022). Spekker et al. (2023) and Tihanyi et al. (2024) identify leprosy as part of a recurring Avar-period disease record, where skeletal involvement could affect movement and daily activity while burial treatment generally remained consistent with community cemetery practice.

Childhood histories at Bruckneudorf and Hirschstetten require inference beyond burial wealth, sex, or cemetery membership. Avar-period and regional isotope studies show that foodways varied in the available evidence by community, sex, animal protein intake, millet

consumption, and possible aquatic resource use, while burial status did not always produce detectable dietary differences (Faragó et al. 2022; Herold 2008; Vidal-Ronchas et al. 2019). For children, these differences operated through household provisioning: stored grain, processed cereals, animal products, weaning foods, food sharing, and the adults responsible for feeding and care. Patrilocal residence and female exogamy further complicate childhood inference, since adults buried in the same cemetery may have grown up in different households or communities before joining the same mortuary population (Gnecchi-Ruscone et al. 2024; Wang et al. 2025). Sex-structured adult patterning may therefore reflect residence history, marriage mobility, provisioning, food practice, and adult incorporation into cemetery communities.

Infectious disease could also shape developmental ecology through proximity, care, and household disruption. The study collections include evidence for multiple infectious processes, including tuberculosis, brucellosis, osteomyelitis, and a possible case of leprosy in the Hirschstetten collection (Brooks 2025; Gamble et al. 2024; Pany-Kucera and Wiltschke-Schrotta 2022). Their relevance for childhood conditions lies in the household responses they could require. Illness could reorganize labour, food support, care, and mobility assistance. Avar-period leprosy cases make that care burden visible: severe impairment could limit eating, standing, walking, and social participation, while survival required sustained support and could still end in burial within community cemetery practice (Spekker et al. 2022; Tihanyi et al. 2024). Childhood exposure included pathogen contact as well as household capacity to maintain care, provisioning, and labour when illness changed daily life.

2.2 Early Life Stress and Skeletal Growth

Barker's work helped establish the Developmental Origins of Health and Disease (DOHaD) by linking fetal and infant growth to adult cardiovascular, metabolic, and respiratory

disease, shifting attention from adult exposure alone to the developmental conditions under which organs, endocrine systems, and metabolic capacity are formed (Barker 1986; Barker and Osmond 1987; Barker et al. 1989; Barker 1990; Barker et al. 1990, 2010; Barker 2012). The thrifty phenotype hypothesis refined this argument by proposing that poor fetal and infant nutrition could produce lasting metabolic trade-offs, including altered pancreatic and insulin-regulatory development, that increase later disease risk when adult conditions place unexpected demands on systems built under constraint (Hales and Barker 2013). Later DOHaD work expanded this model beyond birthweight alone by emphasizing maternal nutritional history, placental function, nutrient transfer, glucocorticoid signalling, and maternal-fetal inflammation as mechanisms through which early developmental environments are produced (Jackson et al. 2010; Vaughan et al. 2010; Goldstein et al. 2020). Gluckman, Hanson, and Bateson reframed this relationship through developmental plasticity and predictive adaptive response theory, emphasizing that early-life cues can shape phenotypes calibrated to anticipated ecological conditions (Gluckman and Hanson 2004; Bateson et al. 2014; Hanson and Gluckman 2014). Early life stress (ELS) names a process of constraint, plasticity, and trade-off, in which responses that support survival under immediate conditions may alter later physiological reserve.

Early life is a period of heightened developmental plasticity, when growth depends on physiological stability and protection from infectious burden. ELS refers to the nutritional, infectious, and/or endocrine disruption from late gestation through childhood that redirects physiological resources away from growth and toward survival, immune defence, and homeostasis (Cunningham et al. 2016; Entringer and Heim 2024; Goodman and Rose 1990; Pappalardo et al. 2023). These disturbances are embedded in developmental ecology: household provisioning, care, pathogen exposure, labour demands, mobility, and buffering capacity condition the circumstances in which growth proceeds (Farmer 2004; Krieger 2012;

Leatherman and Goodman 2020; Temple and Edes 2022; Temple and Klaus 2022). Figure 2 summarizes this physiological reallocation, linking energetic scarcity, endocrine disruption, and inflammatory burden to altered growth and tissue development (Jackson et al. 2010; Goldstein et al. 2020; Pappalardo et al. 2023; Vaughan et al. 2010). These shifts can reduce resources available for cell proliferation, matrix deposition, and skeletal expansion, causing growth to slow, pause, or reorganize depending on the timing, duration, and intensity of disruption (Cunningham et al. 2016; Lewis 2018).

Enamel and bone register these changes at different temporal resolutions because they form, mineralize, and remodel through different tissue processes. Enamel forms incrementally and does not remodel after maturation, so interruptions to ameloblast[5] activity can remain fixed as hypoplastic defects, including linear furrows or broader pitted and plane-form defects depending on the severity and pattern of disruption (Hillson and Bond 1997; Hillson 2014; Witzel et al. 2008). Bone remains metabolically active across the life course and integrates repeated or sustained constraint through longitudinal growth, cortical accrual, diaphyseal geometry, porosity, and bilateral asymmetry (Cunningham et al. 2016; Pappalardo et al. 2023; Ruff 2003; Temple 2019; Temple and Klaus 2022; Parsons 1992). In enamel, systemic infection, malnutrition, and inflammatory burden can disrupt ameloblast metabolism and matrix secretion (Goodman and Rose 1990; Hillson 2014; Witzel et al. 2008; Armelagos et al. 2009); in bone, similar stressors can alter growth-plate activity, osteoblast[6] function, periosteal apposition, and cortical osteogenesis (Pappalardo et al. 2023).

Living-population and clinical evidence shows that developmental regulation can remain biologically consequential beyond the period of exposure. Heijmans et al. (2008)

[5] Specialized enamel-forming cells active during crown formation and enamel maturation (Goodman and Rose 1990; Hillson 2014; Hillson and Bond 1997; Witzel et al. 2008).
[6] Bone-forming cells derived from mesenchymal osteoprogenitors. They produce osteoid, regulate mineralization, and contribute to coupling between bone resorption and formation (Katsimbri 2017; Kim et al. 2020).

provide a clear example of long-term biological embedding, showing altered IGF2[7] methylation six decades after prenatal famine exposure. Fagundes and Way (2014) link ELS to adult inflammatory activity and inflammation-mediated chronic disease, while Chen et al. (2016) and Dietert and Grammer (2016) identify immune development as a major target of adverse intrauterine and early-life environments. McDade et al. (2017) further grounds this process in social and ecological context, showing that early nutritional, microbial, and psychosocial conditions predict methylation patterns in inflammatory genes in young adulthood. Early adversity may alter regulatory thresholds in ways that become most visible under later challenge, while baseline inflammation remains variable (Heim et al. 2019; Dutcher et al. 2020). Anderson et al. (2025) connect skeletal markers formed during development with adult immune phenotype in a living Tsimane forager-farmer population. Porous cranial lesions, commonly treated as nonspecific childhood stress markers in archaeological assemblages (Brickley 2024; McFadden and Oxenham 2020; Morgan 2014; Watts 2013), remained visible into later adulthood and corresponded with adult immune function in the Tsimane sample (Anderson et al. 2025). These findings connect a developmental skeletal marker with adult immune phenotype, although porous cranial lesions were not among the variables recorded in this study.

Archaeological developmental stress markers preserve tissue disruption among individuals who survived long enough for those disruptions to become visible and persist. Bioarchaeologists have linked enamel hypoplasia to the Barker tradition by connecting childhood physiological disruption with adult mortality risk (Armelagos et al. 2009; Goodman and Armelagos 1989), while growth disturbance, cortical gracility, and developmental stress indicators show how childhood constraint can persist among individuals who survived into

[7] Growth factor gene involved in fetal and early postnatal growth; altered methylation after prenatal famine reflects long-term changes in growth factor signalling (Godfrey et al. 2007; Heijmans et al. 2008).

adolescence or adulthood (Gamble and Bentley 2022; Temple and Klaus 2022). Pubertal timing adds a maturational scale to this evidence, since developmental environments can alter adolescent growth tempo, reproductive scheduling, and sex-specific allocation (DeWitte and Lewis 2021; Klostermann et al. 2025).

Wigley et al. (2025) tested whether first permanent molar fluctuating asymmetry, used as a proxy for fetal and early postnatal stress, predicted later inflammatory lesions and age-at-death in archaeological skeletal remains. Higher M1 fluctuating asymmetry was linked to active and bilateral periosteal new bone formation and shorter adult survival. The immature cohort showed a positive association between fluctuating asymmetry and age-at-death. They interpret this pattern as evidence that early developmental stress may support short-term survival while increasing later inflammatory vulnerability.

For this study, enamel defects and cortical growth indicators provide complementary but non-equivalent evidence of developmental stress. Enamel preserves discrete disruptions during crown formation (Goodman and Rose 1990; Hillson and Bond 1997; Hillson 2014), while long-bone dimensions, cortical development, and bilateral asymmetry preserve slower histories of skeletal investment, developmental regulation, mechanical loading, and later remodelling (Cunningham et al. 2016; Ruff 2003; Temple and Klaus 2022). Figure 2 summarizes how physiological reallocation may appear as disrupted amelogenesis in enamel or altered cortical osteogenesis during growth.

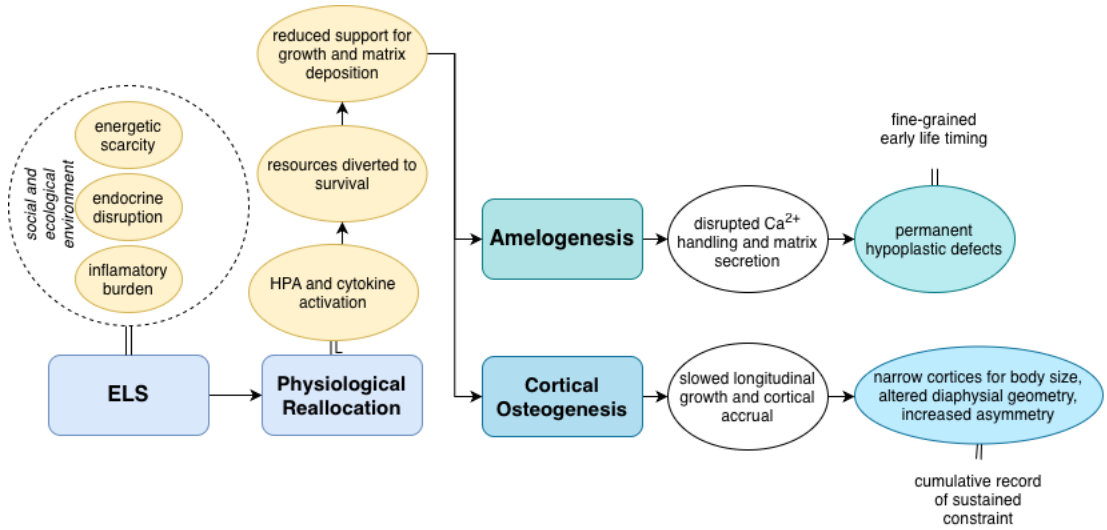

Figure 2 Early life stress, physiological reallocation, and mineralized tissue outcomes: Schematic showing how social and ecological environments shape early-life energetic scarcity, endocrine disruption, and inflammatory burden, and how physiological reallocation may be registered differently in enamel and cortical bone. Colour groupings distinguish contextual fields, regulatory and allocative pathways, and enamel and cortical growth outcomes corresponding to sections 2.2.1 and 2.2.2. Diagram made in draw.io (2021).

2.2.1 Dental Enamel Defects

Dental enamel defects (DED) are hypoplastic disturbances in enamel formation, including linear or furrow-form defects, pitted defects, and plane-form defects (Goodman and Rose 1990; Hillson 2014). The broader dental literature often uses the terms enamel hypoplasia or linear enamel hypoplasia (LEH), while DED is used here as the operational term for recorded enamel stress indicators. Linear or furrow-form defects are transverse grooves that follow the direction of crown growth and mark disruption along the forming enamel front (Bocaege and Hillson 2016; Goodman and Rose 1990; Hillson and Bond 1997; Hillson 2014). Pitted defects reflect more localized interruptions in ameloblast activity, where smaller groups of cells were affected during secretion (Hillson 2014; Moro et al. 2025). Plane-form defects represent broader surfaces of interrupted secretion, where a larger region of the forming crown was affected (Hillson 2014; Moro et al. 2025; Witzel et al. 2008).

Amelogenesis is incremental, metabolically demanding, and irreversible, making enamel sensitive to systemic disruption during defined prenatal and postnatal windows (Atar and Körperich 2010; Hillson 2014; Hillson and Bond 1997; Rokade et al. 2023). During

amelogenesis, ameloblasts secrete and organize enamel matrix in a regular developmental sequence; interruption to secretion cannot be remodelled or repaired after crown maturation (Goodman and Rose 1990; Hillson and Bond 1997; Hillson 2014; Witzel et al. 2008; Antoine et al. 2009, 2018). Ameloblast activity depends on mineral regulation, oxygenation, substrate availability, and cellular energy support, making enamel formation vulnerable to systemic disease, malnutrition, maternal stress, and other physiological disturbances during growth (Atar and Körperich 2010; Austin et al. 2016; Hillson 2014; Mountain et al. 2021; Rokade et al. 2023).

Different stressors can produce similar enamel defects because enamel has a limited morphological response to disrupted secretion. Infection, fever, malnutrition, systemic disease, maternal stress, endocrine disruption, inflammatory burden, and reduced oxygen or substrate availability can each alter the environment in which enamel is produced (Atar and Körperich 2010; Goodman and Rose 1990; Hillson 2014; Moro et al. 2025; Mountain et al. 2021). A single enamel defect can indicate that physiological stress reached the threshold needed to interrupt crown formation, but it cannot separate infection, nutritional stress, endocrine disturbance, or inflammatory burden as the sole cause. Reduced or interrupted enamel secretion presents on the finished crown as a limited set of recurring hypoplastic forms.

Histological analyses refine external morphology by showing that enamel defects reflect graded impairments in secretory ameloblast function. Witzel et al. (2008) describe a sequence in which reduced secretion alters incremental spacing, greater impairment disrupts the Tomes' process[8] and produces aprismatic enamel[9], and severe disturbance can temporarily or permanently halt secretion, exposing incremental planes. Hillson and Bond (1997) and

[8] The secretory extension of an ameloblast that contributes to enamel prism formation during amelogenesis (Witzel et al. 2008)
[9] Enamel that lacks the normal prism or rod organization produced during typical ameloblast secretion (Witzel et al. 2008).

Hillson (2014) show why these disturbances do not appear uniformly across the crown. Perikymata[10] spacing changes from the occlusal to cervical crown, and defects formed in different crown regions may appear wider, deeper, shallower, or less visible even when they belong to the same physiological episode. External breadth and depth are shaped by enamel growth geometry as well as by the stress event itself, making timing, recurrence, and distribution across teeth and individuals more informative than the apparent size of a single defect.

Incremental enamel structures allow defects to be placed within developmental time. Daily cross-striations record short-period enamel growth, while long-period Retzius lines[11] and their surface expressions, perikymata, mark repeated intervals in crown formation (Antoine et al. 2009; Birch and Dean 2014; Hillson 2014). Because enamel forms through regular incremental rhythms, disruptions to ameloblast secretion are expressed in relation to the growth structures already being laid down, allowing defects to be aligned with tooth formation schedules (Antoine et al. 2009, 2018; Reid and Dean 2000, 2006; Birch and Dean 2014). Deciduous teeth record late gestation and early infancy, while permanent anterior teeth capture disruptions during early childhood (Birch and Dean 2014; Reid and Dean 2000, 2006). Elemental and structural signatures in primate teeth have been associated with growth disruption, illness, and stress-related pathways (Austin et al. 2016). In human primary teeth, neonatal line width has been associated with maternal psychosocial stress and social support, connecting enamel growth structures to prenatal and perinatal conditions at the maternal-infant boundary (Mountain et al. 2021). Macaques exposed to seasonal food scarcity developed recurring defects aligned with developmental timing, showing how repeated ecological stress

[10] Fine transverse ridges or grooves visible on the outer enamel surface, marking where internal long-period growth lines reach the crown surface (Hillson 2014; Hillson and Bond 1997; Reid and Dean 2000, 2006).
[11] Internal long-period incremental growth lines within enamel that form rhythmically during amelogenesis and record repeated intervals of enamel secretion inside the crown (Hillson 2014; Hillson and Bond 1997; Reid and Dean 2000, 2006).

can become organized as a visible sequence of crown disruption (Skinner 2021; Skinner et al. 2025).

DED require caution because their expression is partly shaped by tooth formation itself. Tooth type, crown position, perikymata spacing, and enamel growth geometry influence whether a disruption appears broad, narrow, shallow, pronounced, or visible during macroscopic observation (O'Hara and Guatelli-Steinberg 2020; O'Hara et al. 2023). Recording scale adds another source of variation: macroscopic observation can miss subtle defects, especially in cervical regions, while microscopic and technology-assisted approaches identify smaller disruptions that may be excluded from field-based scoring (Hassett 2012; Kobayashi et al. 2020). Quantitative profilometry further complicates direct readings of defect severity, since defect depth is influenced by normal growth increment depth and broader differences in enamel growth patterns (McGrath et al. 2018, 2021). Prevalence, depth, and apparent severity must be interpreted as products of physiology, enamel development, preservation, and observation.

2.2.2 Growth Disruption and Cortical Development

Long bone shafts lengthen through endochondral ossification at the growth plate and change in thickness through modelling and remodelling on periosteal and endosteal surfaces (Cunningham et al. 2016). These processes make cortical development sensitive to nutritional status, endocrine conditions, mechanical loading, and osteogenic capacity. Periosteal expansion along the diaphysis depends on osteoblast differentiation, collagen deposition, and mineralization, all of which require sustained nutritional and hormonal support (Cunningham et al. 2016; Ruff 2003; Temple and Klaus 2022). Endosteal activity shapes the inner cortical boundary at the same time that periosteal apposition expands the outer surface, so cortical thickness emerges from the balance between formation, resorption, and modelling during growth.

Physiological stress can constrain longitudinal growth and cortical accrual. Malnutrition, systemic infection, and inflammatory burden can slow chondrocyte proliferation at the growth plate, reduce osteoblast activity along modelling surfaces, and limit mineralized matrix deposition during growth (Cunningham et al. 2016; Lewis 2018; Pappalardo et al. 2023; Temple and Klaus 2022). Inflammatory burden adds another pathway, since cytokine activity and immune activation can alter bone remodelling and shift the balance between formation and resorption (Wippert et al. 2017; Wuertz-Kozak et al. 2020). Endocrine stress also affects this system: elevated glucocorticoids[12] and altered growth hormone or thyroid signalling can constrain growth-plate dynamics, vascular support, and osteoblast-mediated formation during sensitive windows (Cunningham et al. 2016; Pappalardo et al. 2023; Wippert et al. 2017).

Archaeological and clinical evidence link chronic infection and undernutrition to altered maturational timing (DeWitte and Lewis 2021; Lewis et al. 2016; Klostermann et al. 2025). Puberty is a major period of skeletal accrual, so delayed maturation can affect cortical development (Ruff 2003; Temple and Klaus 2022). Adolescents experiencing chronic physiological stress may show delayed puberty and delayed epiphyseal fusion, reflecting disruption to the regulatory signals that coordinate growth tempo and skeletal maturation. Sex steroids are especially important in this period because they contribute to the adolescent growth spurt, epiphyseal fusion, periosteal and endosteal modelling, and the attainment of adult cortical structure (Ruff 2003; Temple and Klaus 2022). Delayed fusion may extend the chronological period of growth, but it does not necessarily produce equivalent cortical accrual if nutritional, infectious, or endocrine stress continues to limit bone formation (DeWitte and Lewis 2021; Klostermann et al. 2025). Linear growth and cortical accrual do not always respond to stress in parallel. Stature may recover through catch-up growth or extended

[12] Steroid hormones involved in stress physiology and immune regulation; sustained exposure can impair osteoblast and osteocyte survival and reduce bone formation (Lee et al. 2022; Wippert et al. 2017).

maturation, while cortical thickness can retain evidence of constrained periosteal investment during earlier developmental windows.

Catch-up growth complicates the interpretation of adult skeletal size because longitudinal growth, periosteal expansion, and maturational timing do not necessarily recover together. Clark et al. (1986) show that general body size can mask poor early growth, since measures that continue growing into later childhood and adolescence may recover after early constraint, while earlier-forming skeletal dimensions retain evidence of disrupted development. Ruff (2003) makes a related point for cortical strength: stature alone is a poor proxy for bone structural development, since long-bone strength is more closely tied to body size, muscle loading, and mechanical adaptation than to linear growth alone. Periosteal apposition is sensitive to the timing of nutritional, hormonal, and mechanical conditions during growth, so improvement in stature or segment length may coexist with reduced cortical area or altered diaphyseal robusticity (Gowland et al. 2023; Ruff 2003; Temple and Klaus 2022). Adult skeletal form may preserve divergence between recovered length and constrained cortical investment, especially when early childhood stress is followed by altered pubertal timing or reduced endocrine support for peak cortical accrual.

Paired skeletal elements generally develop under shared systemic regulation, with chondrocyte cycling, osteoblast recruitment, endocrine rhythms, circulating growth factors, and mechanical loading coordinating growth between antimeres[13] (Cunningham et al. 2016; De Coster et al. 2013; Parsons 1992; Ruff 2003; Temple and Klaus 2022). Malnutrition, systemic infection, and glucocorticoid elevation can disturb the signals that maintain parallel growth trajectories, allowing small deviations between sides to accumulate during development (Cunningham et al. 2016; Lee et al. 2022; Lewis 2018; Temple and Klaus 2022).

[13] Paired anatomical structures on opposite sides of the body, such as the left and right femora, tibiae, humeri, or radii.

Fluctuating asymmetry may indicate reduced developmental buffering when paired elements diverge beyond expected variation, although activity, trauma, preservation, side dominance, and biomechanical loading can also produce bilateral differences (De Coster et al. 2013; Parsons 1992; Ruff 2003).

2.3 Developmental Embodiment and Inflammatory Vulnerability

ELS markers preserve tissue consequences of childhood conditions during growth. Food access, care, pathogen exposure, labour demands, mobility, and buffering capacity shaped the energetic and immunological context in which children grew, mounted immune responses, repaired tissue, and survived disruption (Carroll et al. 2017; Gamble and Bentley 2022; Gowland 2015; Leatherman and Goodman 2020; Temple and Edes 2022). Bioarchaeological DOHaD uses skeletal and dental markers to trace these conditions across the life course, treating DED, altered growth, cortical investment, and later vulnerability as tissue evidence of developmental embodiment (Gamble and Bentley 2022; Gowland 2015; Gowland and Caldwell 2023).

Childhood exposure emerged through the social and economic organization of daily life. Scarcity, infection, workload, rest, protection, and care were structured through household economies, social position, labour obligations, settlement ecology, and buffering resources. Farmer (2004) locates illness, suffering, and premature death within these historically situated arrangements, where inequality structures who encounters harm and who has the resources to recover. During development, those arrangements determine whether hunger is episodic or recurrent, infection is buffered or prolonged, care interrupts illness, and growth proceeds under repeated energetic demand. Biocultural approaches treat these material conditions as routes through which inequality is incorporated into the body, since provisioning, protection, and recovery define the physiological context of childhood growth and survival (Leatherman and Goodman 2020). Under these conditions, duration and recurrence are as consequential as

exposure itself: a short illness in a buffered household may leave little skeletal trace, while recurrent scarcity, infection, or labour burden without recovery can alter growth, immune regulation, and repair across sensitive developmental windows, consistent with allostatic load and reactive scope models (McEwen 2000; Romero et al. 2009).

Krieger proposes an ecosocial model of embodiment in which exposure, susceptibility, resistance, and survival are produced through historical and biological processes across the life course (Krieger 2012). The same childhood insult can carry different consequences depending on timing, recurrence, prior stress history, and recovery conditions. A short disruption during a buffered period may be absorbed with little lasting tissue change, while repeated disruption during a sensitive window can alter developmental regulation, including endocrine response, immune activation, growth tempo, and repair capacity.

Mineralized tissues preserve partial histories of embodiment because each marker forms through a different tissue process and developmental window. DED, altered growth, cortical investment, and later inflammatory burden mark different moments in a life-course sequence, each passing through a different tissue filter (Gamble and Bentley 2022; Gowland 2015; Temple and Edes 2022). Timing, repair, survivorship, and visibility therefore differ by marker.

Selective visibility limits every skeletal and dental marker used here. DED, altered growth, cortical thickness index (CTI), PD, PNBF, and other lesions form only when an individual survives long enough for tissue response to be initiated, mineralized, remodelled, or retained after death (McFadden and Oxenham 2020; Wood et al. 1992). A visible marker is a preserved tissue trace that records stress, response, repair, duration, and survival only when these processes leave retained tissue change. The osteological paradox places this problem at the centre of palaeopathological interpretation, since skeletal assemblages are composed of the dead and are filtered by hidden heterogeneity in frailty and selective mortality (Wood et al.

1992). DeWitte and Wood's (2008) analysis of Black Death mortality demonstrates that even epidemic mortality was selective with respect to pre-existing frailty.

Frailty is used here to describe reduced physiological reserve across multiple systems, which can make some individuals more vulnerable to morbidity and death under similar exposure conditions. In skeletal assemblages, frailty is approached through lesion patterning, preservation, and survivorship across skeletal-dental systems (Marklein et al. 2016; Gaddis 2018). Associations among dental pathology, PD, PNBF, and mortality risk show that anatomically distinct lesions can still participate in broader vulnerability patterns: PD and dental pathology have been linked to higher mortality risk, while PD and PNBF have been shown to co-occur independently of age, suggesting possible connections among immune competence, shared exposure, inflammatory response, and frailty (DeWitte and Bekvalac 2010, 2011; Wigley et al. 2025). Individuals with developmental stress markers survived long enough for defects, growth alteration, or remodelling change to become visible, yet survival through early constraint may still carry later physiological consequences if developmental regulation was altered by repeated nutritional, infectious, or endocrine stress (Gowland 2015; McFadden and Oxenham 2020; Wigley et al. 2025; Wood et al. 1992).

2.3.1 Developmental Programming in DOHaD

Developmental programming describes how early nutritional, infectious, inflammatory, endocrine, and maternal-fetal conditions can alter later physiological regulation (Figure 3). Within DOHaD, early development is a period when systems governing growth, repair, stress response, and disease susceptibility remain especially plastic (Barker 2012; Godfrey et al. 2007). Early adversity has been linked to durable changes in stress-response and immune regulation (Heim et al. 2019). These effects are probabilistic: early conditions alter regulatory thresholds rather than producing a single fixed disease outcome. Inflammatory vulnerability

can emerge through altered activation and resolution, even when baseline inflammation is not consistently elevated (Entringer and Heim 2024; Fagundes and Way 2014).

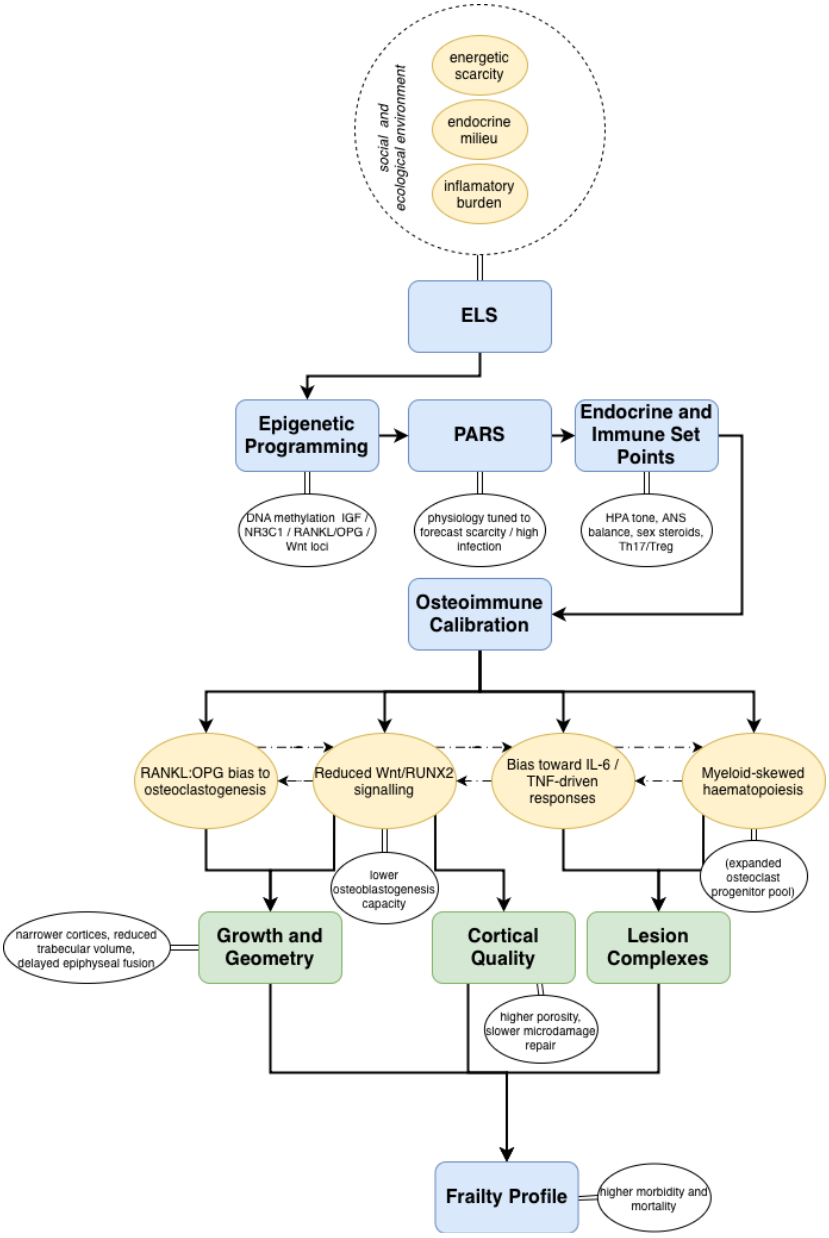

Figure 3 Developmental programming, osteoimmune calibration, and skeletal vulnerability. Conceptual model showing how socially and ecologically patterned early-life stress may become embedded through epigenetic regulation, predictive adaptive responses, and endocrine and immune set points. These pathways may bias osteoimmune regulation through RANKL:OPG balance, Wnt/RUNX2-mediated formation, IL-6/TNF-driven response, and osteoclastogenic potential, shaping growth geometry, cortical quality, lesion complexes, and frailty profiles across the life course. Diagram made in draw.io (2021).

Maternal-placental-fetal regulation is an early interface between embodied maternal conditions and developmental programming. Maternal nutritional history and metabolic capacity influence the substrates available for fetal growth, while placental transport and vascular adaptation regulate the movement of nutrients, oxygen, and endocrine signals into fetal tissues (Barker et al. 2010; Jackson et al. 2010; Vaughan et al. 2010). Glucocorticoid

regulation adds another layer to this interface: placental enzymatic activity helps modulate fetal exposure to maternal stress hormones during sensitive periods of tissue differentiation and organ development (Vaughan et al. 2010). Inflammatory or vascular disturbance within the placenta can alter nutrient transfer, oxygenation, and fetal immune signalling, linking maternal-fetal inflammatory environments to later metabolic and immune phenotypes (Goldstein et al. 2020).

During sensitive windows of growth, epigenetic regulation can give developmental exposure durable effects on gene expression potential. Epigenetic processes regulate how genes respond to intracellular and extracellular signals without changing DNA sequence (Godfrey et al. 2007; Waterland and Michels 2007). These include DNA methylation, histone modification, chromatin remodelling, and non-coding RNA activity. Early nutritional, endocrine, inflammatory, and psychosocial conditions can alter developmental regulation while tissues and stress-response pathways are still being organized (Godfrey et al. 2007; Heim et al. 2019). Prenatal famine research provides a human example of this persistence: individuals exposed to the Dutch Hunger Winter around conception showed altered methylation at IGF2, a growth-related imprinted locus, six decades later (Heijmans et al. 2008). Stress-axis research has examined NR3C1, which encodes the glucocorticoid receptor, as a regulatory site through which early adversity can affect HPA-axis feedback and later stress responsiveness (Daskalakis and Yehuda 2014; Heim et al. 2019). Developmental exposure can persist because growth and repair systems remain responsive to regulatory marks established under earlier nutritional, inflammatory, or psychosocial conditions.

McDade et al. (2017) linked early nutritional, microbial, and psychosocial conditions with methylation patterns in inflammation-related genes in young adulthood, placing immune responsiveness within socially patterned developmental ecology. Adverse intrauterine and early-life environments have also been associated with altered immune development and later

susceptibility to inflammatory and immune disorders, including changes in fetal immune programming, glucocorticoid exposure, and inflammatory regulation (Chen et al. 2016; Dietert and Grammer 2016).

The predictive adaptive response (PAR) hypothesis proposes that early development may involve anticipatory calibration to expected later environments (Bateson et al. 2014). During gestation, the fetus receives cues about the expected environment through maternal condition, stress physiology, infectious exposure, and early postnatal ecology (Bateson et al. 2014; Gluckman and Hanson 2004; Hanson and Gluckman 2014). Those cues can alter the regulatory phenotype, including growth tempo, metabolic allocation, stress responsiveness, and immune vigilance, before the later environment is directly encountered. PARs are adaptive in principle because they may increase the fit between phenotype and anticipated conditions, but the forecast is never guaranteed. Later conditions may diverge from early cues, or developmental ecology may be severe enough to produce disruption and immediate survival responses alongside predictive calibration (Bateson et al. 2014; Hanson and Gluckman 2014).

The thrifty phenotype emphasizes the cost of physiological systems built under nutritional constraint. Fetal or infant undernutrition can constrain organ and tissue development in ways that support short-term survival while reducing later reserve, especially when later metabolic, immune, reproductive, or mechanical demands increase (Hales and Barker 2013). Bone growth and repair require sustained physiological support; developmental environments that favour stress-axis mobilization, immune vigilance, or energetic conservation may reduce investment in periosteal apposition, maturation, cortical accrual, and later repair capacity (Gowland and Caldwell 2023; Pappalardo et al. 2023).

Early adversity can shape inflammation as a conditional response, with later vulnerability emerging most clearly when the body encounters a new challenge. Severe or recurrent ELS has been linked to adult inflammatory activity and to chronic diseases in which

inflammation contributes to morbidity, including cardiovascular, metabolic, immune-mediated, and musculoskeletal disease (Fagundes and Way 2014). Baseline cytokine levels may remain modest, while later challenge can reveal altered activation thresholds, higher inflammatory peaks, slower resolution, or reduced regulatory restraint (Entringer and Heim 2024; Heim et al. 2019; Nusslock and Miller 2016). Early nutritional, microbial, and psychosocial conditions have also been associated with methylation patterns in inflammation-related genes, linking developmental ecology to later immune responsiveness (McDade et al. 2017). Later challenges can reveal earlier regulatory settings through inflammatory activation, resolution, and repair demand, including the endocrine and immune signals that regulate skeletal resorption, formation, and repair.

2.3.2 Osteoimmune Calibration

Bone is an osteoimmune[14] tissue maintained through coupled osteoclast-mediated resorption and osteoblast-mediated formation. Osteoclasts[15] remove mineralized matrix, osteoblasts replace it with osteoid and mineralized bone, and osteocytes coordinate local remodelling by sensing mechanical and physiological signals within the matrix (Kim et al. 2020; Okamoto et al. 2017; Weitzmann and Ofotokun 2016). Osteoimmune, endocrine, and mechanical signals regulate the tempo and coupling of this cycle, so bone maintenance depends on more than local skeletal demand alone (De Leon-Oliva et al. 2023; Lorenzo et al. 2016; Torres et al. 2023). Glucocorticoid tone, autonomic balance, inflammatory thresholds, and immune response patterns all contribute to remodelling balance. Chronic stress and inflammatory signalling can alter bone turnover through endocrine-immune pathways that

[14] The reciprocal regulation of skeletal and immune systems, especially the ways immune cells and inflammatory mediators influence osteoclast and osteoblast activity, bone turnover, and repair (Lorenzo et al. 2016).
[15] Multinucleated bone-resorbing cells derived from the monocyte/macrophage lineage. They attach to mineralized bone, acidify the resorption surface, and degrade bone matrix during remodelling and repair (Galson and Roodman 2011; Kim et al. 2020).

affect osteoblast survival, osteocyte survival, osteoclast recruitment, and remodelling balance (De Leon-Oliva et al. 2023; Wippert et al. 2017; Wuertz-Kozak et al. 2020). Developmental calibration may shape how strongly bone responds to later inflammatory or mechanical challenge, altering remodelling balance across the life course.

Osteoclast recruitment is regulated by the balance between RANKL and OPG. RANKL is produced by osteoblast-lineage cells, stromal cells, osteocytes, and activated immune cells, and it binds RANK on osteoclast precursors to promote osteoclast differentiation, fusion, survival, and resorptive activity (Galson and Roodman 2011; Kim et al. 2020; Okamoto et al. 2017). OPG limits this process by binding RANKL before it activates RANK, acting as a restraint on osteoclast recruitment (Galson and Roodman 2011; Okamoto et al. 2017; Xu et al. 2023). The RANKL:OPG ratio helps determine how readily osteoclast precursors are recruited into active bone resorption. Inflammatory signalling can shift this balance by increasing RANKL expression, reducing OPG restraint, or increasing precursor sensitivity to osteoclastogenic signals (Epsley et al. 2021; Torres et al. 2023; Xu et al. 2023). Developmentally shaped inflammatory thresholds and response duration may make later challenges more likely to favour osteoclast recruitment and sustained matrix removal.

Skeletal vulnerability can arise when osteoblast-lineage cells lose formation and repair capacity. Osteoblast differentiation depends on osteogenic transcriptional and signalling pathways, including RUNX2[16], SP7/osterix[17], BMP[18], and Wnt/β-catenin[19] activity, which support progenitor commitment, matrix deposition, mineralization, and organized replacement

[16] Runt-related transcription factor 2, a transcription factor required for osteoblast lineage commitment and early osteoblast differentiation(Katsimbri 2017).
[17] An osteoblast-lineage transcription factor acting downstream of RUNX2 during osteoblast differentiation and bone formation (Katsimbri 2017).
[18] Bone morphogenetic proteins, signalling molecules that promote osteogenic differentiation, skeletal development, and bone repair (Katsimbri 2017).
[19] A signalling pathway that promotes osteoblast differentiation and bone formation; inhibition of this pathway can reduce bone-forming activity (Katsimbri 2017).

after resorption (Katsimbri 2017; Kim et al. 2020; Ponzetti and Rucci 2021). Wnt antagonists such as DKK1[20] and sclerostin[21] reduce this formation signal by limiting osteoblast activity and suppressing bone-forming capacity (Katsimbri 2017; Xu et al. 2023). Sustained inflammatory signalling can interfere with osteoblast differentiation and survival, while glucocorticoid exposure can reduce osteoblast proliferation, increase osteoblast and osteocyte apoptosis, and weaken the cellular support needed for organized repair (Epsley et al. 2021; Lee et al. 2022; Martín-Márquez et al. 2023; Torres et al. 2023). Under sustained inflammatory or endocrine strain, skeletal vulnerability can emerge through impaired replacement as well as increased removal, because resorbed matrix must be followed by stable osteoblast-mediated formation for remodelling to preserve tissue structure.

IL-6 and TNF-α connect conditional inflammation to remodelling imbalance because they act across both osteoclast and osteoblast lineages. IL-6 can increase osteoclastogenic signalling through RANKL-related pathways and sustain inflammatory bone turnover, while TNF-α can amplify osteoclast precursor activation and strengthen resorptive signalling in inflamed bone environments (De Leon-Oliva et al. 2023; Epsley et al. 2021; Xu et al. 2023). The same cytokine milieu can interfere with osteoblast differentiation, reduce osteoblast and osteocyte survival, and weaken organized repair, especially when inflammatory activation is prolonged or repeatedly reactivated (Epsley et al. 2021; Torres et al. 2023; Xu et al. 2023). Remodelling becomes uncoupled when bone removal continues or increases while replacement becomes delayed, reduced, or structurally disorganized. Conditional inflammatory responses shaped by earlier adversity may intensify this imbalance when later challenges produce higher inflammatory peaks, slower resolution, or prolonged repair demand (Entringer and Heim 2024; Wippert et al. 2017; Wuertz-Kozak et al. 2020). Cortical maintenance then depends on whether

[20] Dickkopf-related protein 1, a Wnt antagonist that can suppress osteoblast differentiation and bone formation .
[21] An osteocyte-derived inhibitor of Wnt/β-catenin signalling that suppresses osteoblast activity and bone formation (Katsimbri 2017).

resorption and formation remain coordinated, or whether repeated inflammatory activation pushes repair into a less stable remodelling state.

Figure 3 places osteoimmune calibration between developmental programming and later skeletal vulnerability. The calibrated system is not itself visible archaeologically; it is inferred through the patterned ways bone grows, remodels, repairs, and responds to later challenge. Early energetic scarcity, endocrine disruption, and inflammatory burden may shape the regulatory conditions under which later bone turnover occurs, but skeletal expression still passes through lesion ecology, mechanical demand, repair capacity, and survivorship. This distinction makes the interpretation probabilistic: altered osteoimmune regulation can contribute to growth geometry, cortical quality, delayed repair, or lesion clustering, while each skeletal change remains constrained by its lesion ecology.

2.3.3 Translation into Skeletal Vulnerability

Developmentally shaped remodelling becomes archaeologically relevant when later demands alter bone maintenance. Later demands place pressure on resorption, formation, and repair, but skeletal expression depends on inflammatory thresholds and lesion ecology. Infection, injury, nutritional strain, mechanical loading, metabolic stress, ageing, and chronic inflammatory burden can each enter that process (Klaus 2014; Torres et al. 2023). Chronic stress and inflammatory signalling have been linked to altered bone turnover, reduced bone quality, and disrupted osteoblast-osteoclast coupling, suggesting that endocrine and immune regulation shape how bone responds to repeated challenge (Wippert et al. 2017; Wuertz-Kozak et al. 2020). Exposure duration, lesion timing, preservation, and survival determine what can be observed archaeologically (Klaus 2014). Life-course studies linking developmental disruption, adult inflammatory burden, and mortality risk support a cautious reading of skeletal vulnerability as the interaction between earlier developmental regulation and later challenge (Gowland 2015; Wigley et al. 2025). The same developmental history may leave no adult

skeletal trace, support repair, or become visible through altered remodelling after later challenge.

Skeletal vulnerability is expressed through the quality and distribution of bone formed, maintained, and repaired across the life course. During growth, cortical expansion, trabecular development, and pubertal skeletal accrual depend on sustained physiological and mechanical support (Cunningham et al. 2016; Pappalardo et al. 2023; Ruff 2003; Temple and Klaus 2022). Across adulthood, cortical quality depends on remodelling balance and microdamage repair, processes that can be altered under chronic stress physiology and inflammatory signalling (Epsley et al. 2021; Torres et al. 2023; Wippert et al. 2017; Wuertz-Kozak et al. 2020). Clinical work linking early adversity or developmental constraint to later bone mineral density and fracture-related outcomes supports a cautious life-course interpretation in which earlier regulatory conditions may influence later skeletal reserve without directly diagnosing the origin of any single cortical feature (Ghaseminejad-Raeini et al. 2025). Cortical thinning, cortical porosity, and delayed repair indicate compromised bone maintenance when formation, resorption, and repair do not remain coordinated across later life. PD, PNBF, and OA preserve different tissue responses, so their distributions must be read through the local conditions under which each lesion forms, remodels, and remains visible.

2.4 Adult Inflammatory Lesion Patterning

Adult inflammatory lesion patterning is interpreted through the distribution and association of lesions across tissue systems. PD, PNBF, and OA arise in different anatomical contexts and preserve different combinations of local stimulus, host response, repair, age, activity, preservation, and survivorship. Inflammatory burden is therefore inferred from how lesions are distributed across individuals, tissues, and anatomical regions, since immune competence and inflammatory response vary among individuals and are shaped by environmental, social, and biological histories (Crespo 2020; Klaus 2014). Selective mortality

remains part of that pattern: visible lesions identify individuals who survived long enough for tissue change to form or remodel, while frailty shapes which individuals are represented at a given age (DeWitte and Wood 2008; Wood et al. 1992).

2.4.1 Bioarchaeological Inflammation, SINDEX, and Frailty

Inflammation is part of normal tissue defence and repair. Acute inflammatory responses recruit immune cells, remove pathogens or damaged tissue, and initiate cellular repair processes needed to restore local tissue function (Abbas et al. 2012; Chavda et al. 2024; Kiss 2022; McDade 2005). The same response becomes costly when activation persists, recurs, exceeds local regulation, or fails to resolve. Under those conditions, immune defence can contribute to tissue breakdown, altered bone remodelling, incomplete repair, and skeletal lesion formation (Crespo 2020; Epsley et al. 2021; Torres et al. 2023).

Visible inflammatory lesions indicate survival through tissue response. A lesion forms only when an individual experienced a stimulus strong or sustained enough to provoke tissue change and survived long enough for bone to form, remodel, or persist after the episode began (Wood et al. 1992). Lesion absence can reflect no exposure, rapid death, effective buffering, healing or remodelling that reduced macroscopic visibility, or preservation limits. Because mortality is selective with respect to pre-existing frailty, adult inflammatory lesion patterning must be read as exposure, response, repair, and survival compressed into observable tissue change (DeWitte and Wood 2008; Marklein et al. 2016). At St Mary Graces, PD and PNBF co-occurred independently of age, linking oral and periosteal lesion systems within a broader pattern of inflammatory burden (DeWitte and Bekvalac 2010). PD and dental caries were also associated with elevated mortality risk, placing oral pathology within patterns of frailty (DeWitte and Bekvalac 2010). Developmental indicators did not explain these relationships in a uniform way: enamel hypoplasia was associated with PD but not periosteal lesions, while femur length was not associated with either lesion system (DeWitte and Bekvalac 2011). These

mixed findings support considering several developmental and inflammatory indicators together, since each records a different tissue history.

Crespo's (2020) SINDEX model treats skeletal-dental inflammatory burden as a patterned distribution across tissue systems. Lesion severity and cross-system association can identify skeletal inflammatory phenotypes while preserving the anatomical specificity and etiological nonspecificity of each lesion category. Each lesion remains constrained by its own ecology, timing, repair history, and skeletal visibility.

2.4.2 Periodontal Disease

PD develops when oral biofilm and host inflammatory response sustain remodelling of the alveolar bone environment. Bacterial products stimulate gingival epithelial cells, neutrophils, macrophages, fibroblasts, and osteoblast-lineage cells, which release inflammatory mediators that recruit additional immune cells and alter local tissue turnover (Cekici et al. 2014; Zhou and Graves 2022). In the periodontal ligament and gingival tissues, inflammatory mediators and matrix-degrading enzymes break down collagen and weaken the soft-tissue structures that anchor the tooth (Cekici et al. 2014). At the alveolar crest, the same host response can shift RANKL-OPG balance toward osteoclast recruitment, increasing resorption of the bone supporting the tooth (Xu et al. 2023; Zhou and Graves 2022). PD reflects an interaction between microbial challenge and host regulation. Bacterial exposure initiates the local inflammatory field, while alveolar loss depends on immune response, osteoclast activity, repair capacity, and lesion duration.

2.4.3 Periosteal New Bone Formation

PNBF develops from the periosteum's capacity to respond rapidly to disturbance at the cortical surface. The periosteum is vascular, innervated, and osteogenic; its cambium layer contains progenitor and osteoblast-lineage cells that can be activated by inflammatory,

infectious, traumatic, vascular, or mechanical stimuli (Li and Fennessy 2021; Maia Ferreira Alencar et al. 2020). When the periosteal environment is irritated, vascular change and osteogenic activation can produce new bone on the cortical surface, often beginning as woven bone and later undergoing lamellar remodelling if the individual survives long enough for repair to continue (Allen et al. 2023; Klaus 2014; Weston 2008). The resulting surface change can include both resorptive and formative activity because inflammation and repair may occur together or in sequence within the same lesion ecology (Allen et al. 2023; Klaus 2014). A woven, porous, or irregular surface can reflect active or recent stimulation, while a smoother remodelled surface preserves a later phase of the same periosteal response after repair has begun.

2.4.4 Osteoarthritis as Contextual Life-Course Skeletal Change

Osteoarthritis (OA) develops within the whole joint, where mechanical strain, local tissue repair, and low-grade inflammatory remodelling act across the cartilage-bone interface through chondrocytes, synoviocytes, subchondral osteoblasts, and local immune-cell activity (Fernandes et al. 2002; Mukherjee and Das 2024; Thielen et al. 2021). Inflammatory mediators such as IL-1β, TNF-α, IL-6, NF-κB/MAPK signalling, MMPs, and aggrecanases can weaken cartilage matrix, alter synovial activity, and change the tissue environment in which repair occurs (Fernandes et al. 2002; Mukherjee and Das 2024; Thielen et al. 2021). OA is a joint-level process in which immune activity, matrix degradation, mechanical strain, and repair shape the local conditions that later become visible as skeletal change.

Subchondral bone remains active during OA, as trabecular architecture, sclerosis, and bone turnover change beneath mechanically stressed articular surfaces (Bultink and Lems 2013; Mündermann et al. 2024). Osteoblast and osteoclast activity participate in this response, with altered formation and resorption shaping the subchondral plate and trabecular compartment during joint degeneration (De Leon-Oliva et al. 2023; Mündermann et al. 2024).

Repair occurs in the same local environment as loading, cartilage damage, and synovial inflammation. Skeletal change reflects the history of a joint surface under repeated stress. Systemic inflammatory tone[22] may modulate OA severity or symptom burden in clinical contexts, especially where inflammatory markers correspond with joint degeneration or pain (He et al. 2024; Wippert et al. 2017).

In archaeological assemblages, OA appears through osteophytes, eburnation, porosity, and articular remodelling on joint surfaces (Becker 2020; Crubézy et al. 2002; Molnar et al. 2011). These features record local joint remodelling and repair, with expression shaped by age, mobility, loading regimes, task-related movement, local mechanics, injury, and survival long enough for change to accumulate (Becker 2020; Molnar et al. 2011). Osteophytes and articular remodelling can reflect repeated stimulation at the joint margin and joint surface, while eburnation marks advanced cartilage loss and bone-on-bone contact (Becker 2020; Crubézy et al. 2002). Porosity can preserve local remodelling, vascular change, and repair within the articular environment (Bultink and Lems 2013; Mündermann et al. 2024).

OA provides adult life-course context, but it should not be treated as an inflammatory equivalent to PD or PNBF. Its skeletal expression remains rooted in age, mobility, loading, local mechanics, and survivorship (Becker 2020; Crubézy et al. 2002; Molnar et al. 2011). When OA is read beside PD and PNBF, it provides a way to test whether adult inflammatory change is broadly distributed across joint, oral, and periosteal systems, or whether OA remains a separate pattern of adult joint remodelling (DeWitte and Bekvalac 2011; Crespo 2020; Klaus 2014; Molnar et al. 2011; J. Wood et al. 1992). Joint-specific patterning keeps biomechanical history visible through the distribution of change across hips, knees, shoulders, spine, hands, or other loaded regions.

[22] The broader circulating inflammatory state of the body, reflected in markers such as cytokines (McDade 2005).

2.5 Conclusion

Adult inflammatory lesions preserve late-forming tissue responses within longer life-course histories. By the time individuals entered the cemetery assemblage, developmental ecology, adult exposure, repair, and survival had already shaped the tissues available for observation. Children's food access depended on household provisioning and the adults responsible for feeding, care, and recovery. Provisioning could differ by community, resource use, and sex, while mortuary display offered an uneven guide to what people ate while growing (Faragó et al. 2022; M. Herold 2008; Vidal-Ronchas et al. 2019). People buried in the same cemetery did not necessarily share a childhood locality, since female exogamy and other forms of mobility could incorporate individuals raised elsewhere into local households (Gnecchi-Ruscone et al. 2024; Wang et al. 2025). Illness could shape childhood conditions through exposure, care demands, and household labour redistribution. Disease exposure involved shared air, animal contact, wounds, and chronic infection, while illness and impaired mobility could redirect provisioning, labour, movement, and household support (Brooks 2025; Spekker et al. 2022; Tihanyi et al. 2024).

Developmental ecology became biologically consequential when it intersected with periods of growth. A short illness or scarcity could be managed with food, rest, care, and other recovery measures, but repeated or prolonged disruption could divert physiological resources to immune defence, repair, and maintaining homeostasis (Goodman and Rose 1990; Gowland 2015; Temple and Klaus 2022). Growing bodies allocated limited resources among tissue formation, metabolic stability, immune response, and survival, so the duration and timing of disruption shaped growth tempo, skeletal investment, and repair (Cunningham et al. 2016; Pappalardo et al. 2023). Physiological allocation can have lasting consequences because fetal life, infancy, childhood, and adolescence differ in growth tempo, maturational sensitivity, and physiological reserve (Barker 2012; Bateson et al. 2014; Hales and Barker 2013; Gluckman

and Hanson 2004). Exposure, recovery, and survival were also socially patterned, since developmental ecology shaped whether disruption was brief, repeated, or prolonged (Krieger 2012; Leatherman and Goodman 2020). Mineralized tissues preserve only parts of these developmental histories because tissues form, mineralize, remodel, and persist through different temporal limits. Enamel records disruption during crown formation, while cortical growth and long-bone structure integrate slower histories of skeletal investment, maturation, mechanical demand, and remodelling (Cunningham et al. 2016; Hillson 2014; Ruff 2003; Temple and Klaus 2022). The record that remains is selective: it contains disruptions that crossed a biological threshold and were retained in tissue, while buffered exposures, repaired damage, and rapidly fatal episodes may leave little lasting trace.

Reconstructing the relationship between developmental stress markers and adult inflammatory lesions remains difficult in populations shaped by specific lifeways, selective mortality, and selective tissue visibility. Recent work has connected developmental skeletal markers with adult immune function, inflammatory burden, and mortality risk (Anderson et al. 2025; Wigley et al. 2025). PD, PNBF, and OA form in different tissues, so their distributions preserve distinct oral, periosteal, and joint histories (Crespo 2020; Klaus 2014). Lesion presence marks stimulus, response, duration, repair, and survival; lesion absence may reflect limited exposure, rapid death, buffering, healing, or preservation limits (DeWitte and Wood 2008; Wood et al. 1992). In the study populations, adult inflammatory patterning reflects a microregional life-course history: developmental conditions structured early vulnerability, adult labour and disease exposure contributed to later tissue response, and selective mortality determined what remained observable in the skeleton.

3. Research Questions, Aims, and Hypotheses

Developmental stress, appendicular growth, and skeletal-dental inflammatory burden are treated here as linked life-course distributions. The analysis evaluates whether these distributions differ by cemetery population, by sex, or by population-sex patterning. Because each marker preserves a different tissue history, the variables are compared as related but non-equivalent records of developmental and adult skeletal experience.

Dental enamel defects record disruption during crown formation. Stature reflects cumulative linear growth where long bone preservation permits estimation. CTI reflects cortical structure shaped through modelling and remodelling across growth, ageing, activity, and health history. Appendicular asymmetry provides a cautious proxy for developmental instability where paired elements are preserved. SINDEX captures skeletal-dental inflammatory burden through oral and periosteal lesion systems, while OA is treated separately as contextual adult skeletal change. Population- and sex-structured patterning are evaluated within the inflammatory, developmental, and life-course association analyses.

3.1 Inflammatory Lesion Patterning

The first stage evaluates adult skeletal-dental inflammatory burden using SINDEX. Periodontal disease (PD) and periosteal new bone formation (PNBF) are also examined as component-level scores. Osteoarthritis (OA) is assessed separately because its expression involves age, mechanical loading, joint use, degeneration, and low-grade inflammatory processes.

Research Question: How does adult skeletal-dental inflammatory burden differ between Bruckneudorf and Hirschstetten, and are those differences patterned by sex?

Aim: To compare SINDEX, PD, and PNBF scores between Bruckneudorf and Hirschstetten, including sex-stratified comparisons where sample size permits.

Hypothesis: If site-level conditions structured adult inflammatory burden, Bruckneudorf and Hirschstetten will differ in SINDEX and/or its component scores. If the pattern is primarily site-level, female and male analytical groups will show the same directional contrast across sites. If inflammatory burden was sex-structured, female and male analytical groups will show different within-site or cross-site patterns.

3.2 Developmental Stress and Appendicular Growth

The second stage compares developmental stress and appendicular growth indicators across the two populations. These indicators record different tissue processes and developmental windows, so they are not expected to produce identical patterns.

Research Question: Do developmental stress and appendicular growth indicators differ between Bruckneudorf and Hirschstetten, and are these differences structured by sex?

Aim: To compare DED event count, maximum DED depth, DED timing, stature z-scores, sex-standardized CTI z-scores, and appendicular asymmetry scores between populations and, where sample size permits, between sex groups.

Hypothesis: If retained developmental histories differed between the two cemetery populations or between females and males within them, one population or sex group will show higher DED burden, greater defect severity, altered DED timing, reduced stature z-scores, lower CTI z-scores, or greater appendicular asymmetry. Because these variables capture different tissue histories, population or sex differences may vary across indicators.

3.3 Developmental Stress and Adult Inflammatory Expression

The third stage evaluates whether developmental stress and appendicular growth indicators manifest patterned association with adult skeletal-dental inflammatory burden.

Research Question: Are developmental stress and appendicular growth indicators associated with adult skeletal and dental inflammatory burden?

Aim: To assess whether DED burden, DED severity, DED timing, stature reduction, lower CTI, or greater appendicular asymmetry correspond with higher SINDEX scores. PD, PNBF, and OA are examined to evaluate whether any association is concentrated in particular adult lesion systems.

Hypothesis: Individuals with stronger developmental stress signatures are expected to show higher adult inflammatory burden. Higher DED event count, greater maximum defect depth, earlier DED timing, lower stature z-scores, lower CTI z-scores, and higher appendicular asymmetry scores are expected to correspond with higher SINDEX values. These associations are expected to be partial because adult inflammatory burden also reflects age, sex, activity, oral ecology, preservation, and survivorship.

4. Materials and Methods

4.1 Archaeological Collections and Case Selection

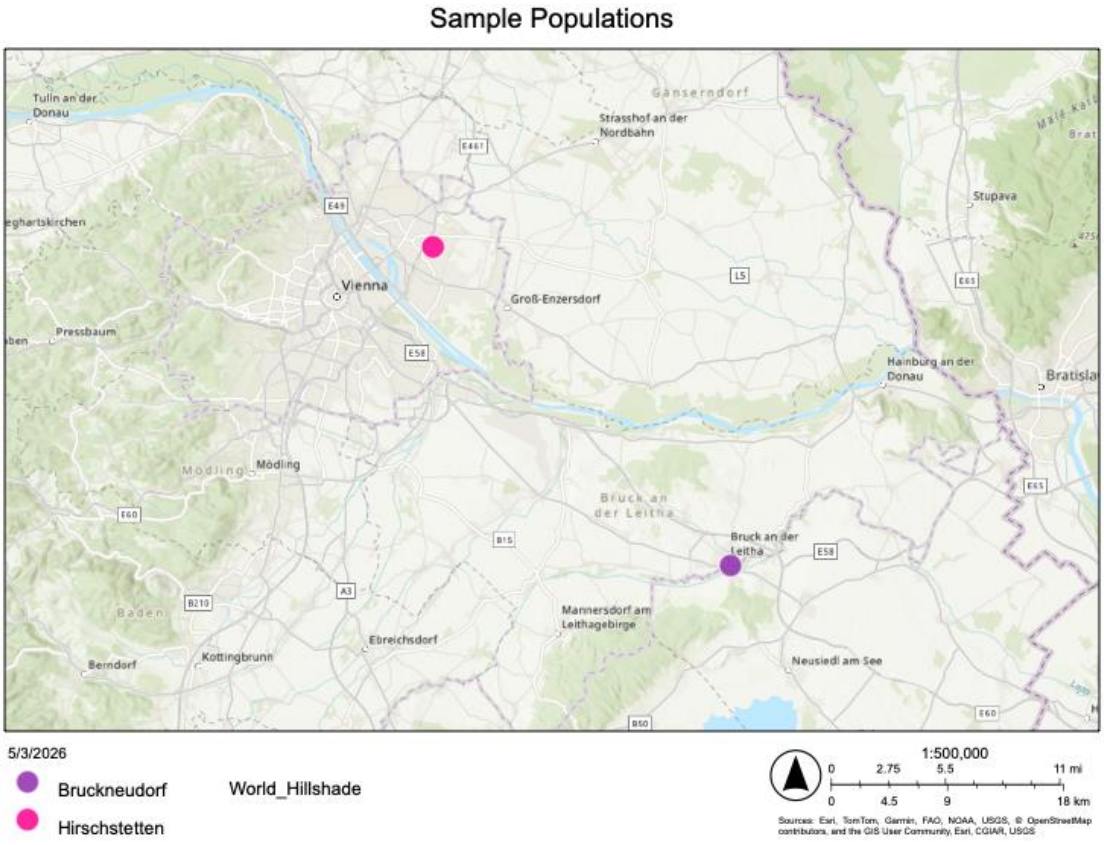

Figure 4 Microregional setting of the study cemeteries in eastern Austria. Hirschstetten and Bruckneudorf are located within approximately 34 km of one another in the Vienna Basin region (Penz and Lehofer 2023; Pany-Kucera and Wiltschke-Schrotta 2022).Made in ArcGIS Online by author using World Hillshade and World Topographic Maps (Esri 2012b, 2012a).

The study sample consists of 68 adults and late adolescents from two late Avar-period cemeteries in eastern Austria (Figure 4): Bruckneudorf (n=35) and Hirschstetten (n=33). Both cemeteries date to the seventh and eighth centuries CE, when the region formed part of the western zone of the Avar Khaganate (Csáky et al. 2020; Daim 2003; Pohl 2018). Their burials belong to a late Avar cemetery tradition that included furnished inhumations and animal deposits, although grave contents varied by site, sex, age, and status (Curta 2021; Daim 2003; Stadler 2008). The two assemblages are broadly comparable in chronology and regional setting, but differ in excavation history, preservation, and prior documentation.

Bruckneudorf was excavated between 2003 and 2005 and comprises more than 400 inhumations. Pany-Kucera and Wiltschke-Schrotta (2022) examined 383 Avar-period individuals and recorded preservation, demography, stature, trauma, infectious disease indicators, dental disease, antemortem tooth loss, enamel defects, and degenerative change. The cemetery is generally well preserved and currently provides a more fully published osteological baseline than Hirschstetten for late Avar-period skeletal variation in the Vienna Basin. Hirschstetten was excavated more recently, between 2022 and 2023, and contains more than 200 individuals (Penz and Lehofer 2023). Its skeletal and contextual record remains less fully characterized, and preservation is more variable due to soil conditions, groundwater fluctuation, and modern disturbance.

Local landscape ecology also differs between the collections. Bruckneudorf lies near two streams (Figure 4), while Hirschstetten lies within a few kilometres of the Danube, although modern urbanization has obscured parts of the earlier Hirschstetten landscape. No associated domestic evidence exists for either cemetery, so settlement location, household activity, subsistence practice, and mobility cannot be directly reconstructed.

Individuals were included when preservation permitted assessment of at least one of the study's major skeletal or dental indicators. These included dental enamel defects, periosteal new bone formation (PNBF), periodontal disease (PD), osteoarthritis (OA), cortical thickness index (CTI), stature, and bilateral appendicular asymmetry (BAA). Because preservation varied across individuals, sample sizes differ by variable. Missing observations were treated as missing rather than as absence of pathology or stress.

4.2 Age and Sex Estimation

Age-at-death estimations were conducted by Dr. Julia Gamble. For adults, age estimation was based on Transition Analysis 3 (Milner et al. 2026). For individuals with unfused epiphyses, age estimation relied primarily on dental development, with epiphyseal

fusion used as supporting developmental evidence (AlQahtani et al. 2010; Schaefer et al. 2009). These age estimates were used to define sample inclusion and to provide age-related covariates for analysis. Age is included as a primary covariate due to its strong association with cumulative lesion development. Biological sex was assessed using standard pelvic and cranial morphological criteria (Buikstra et al. 1994) and is treated here as an osteological estimate rather than a direct measure of lived gender. Age and sex were included because both structure skeletal and inflammatory outcomes. Age is associated with cumulative lesion expression, cortical remodelling, PD, and OA. Sex was considered because of known differences in skeletal morphology, bone remodelling, immune regulation, and potential socially structured exposure.

4.3 Early Life Stress Markers

4.3.1 Dental Enamel Defects

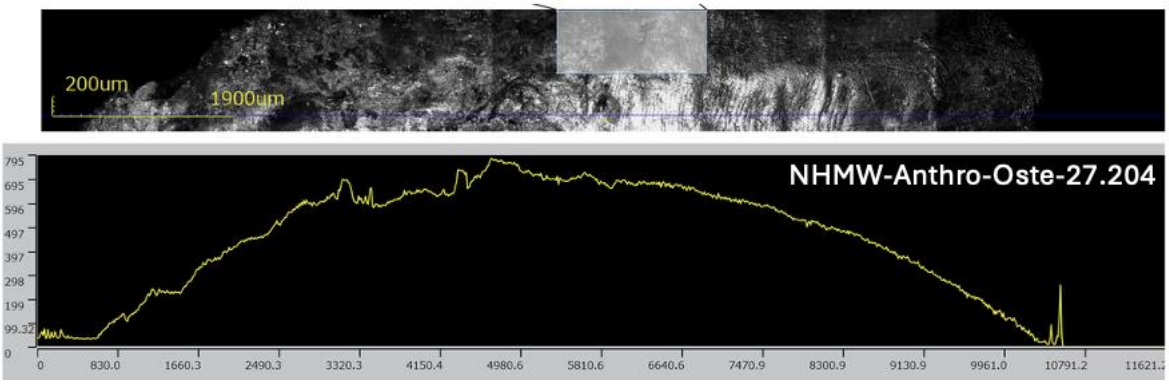

Figure 5 Example of LEXT crown surface profile acquisition for DED analysis (NHMW-Anthro-Oste27.204). A scan region was selected on the preserved enamel crown surface, and a linear surface profile was extracted across the crown to capture height variation in micrometres. The resulting profile was used to compare the observed enamel surface with an estimated crown contour during defect identification.

Dental enamel defects (DEDs) were analysed from high-resolution crown surface profiles generated at 10x magnification with an Olympus LEXT OLS4000 laser scanning confocal microscope at the Bioanthropology Digital Image Analysis Laboratory, University of Manitoba. One permanent tooth was analysed per individual where preservation permitted, usually a maxillary or mandibular canine with sufficient crown surface preservation for LEXT profiling (Figure 5). The goal was to identify and quantify enamel surface depressions

consistent with disruptions in enamel formation. This study used a profile-based method in which the observed enamel surface was compared to an estimated expected crown contour.

This approach follows the logic of quantitative LEH profile methods developed by Cares Henriquez and Oxenham (2020), the LEXT-based workflow used by Gamble and Milne (2018) and the spline-based adaptation evaluated by Jensby (2022). Because only one tooth was analysed per individual, detected tooth-level events were treated as the individual-level DED record. For each tooth, the LEXT profile was converted into paired x- and y-coordinates (Figure 5). The x-coordinate represented position along the crown profile, and the y-coordinate represented enamel surface height in micrometres. Profiles were reconstructed in Excel (Figure 6). Where necessary, profile ends were trimmed to remove non-enamel portions of the scan, including empty space, edge noise, or cementum below the cementum-enamel junction (CEJ). The observed enamel profile was compared to a spline-derived expected crown contour. The spline-derived contour represents the overall crown shape in the absence of localized developmental depressions. Defect depth was calculated as the vertical difference between the observed profile and the expected contour. For normally oriented scans, depth was calculated as:

$$d_i = \max(0, norm_{y_i} - y_i)$$

Where d_i is the depth below the expected contour at point i, $norm_{y_i}$ is the spline-derived expected height at point i, and y_i is the observed enamel height at point i. This calculation returns positive values only where the observed surface falls below the expected contour.

For scans taken from impressions, the topography was inverted. In those cases, the calculation was reversed:

$$d_i = \max(0, y_i - norm_{y_i})$$

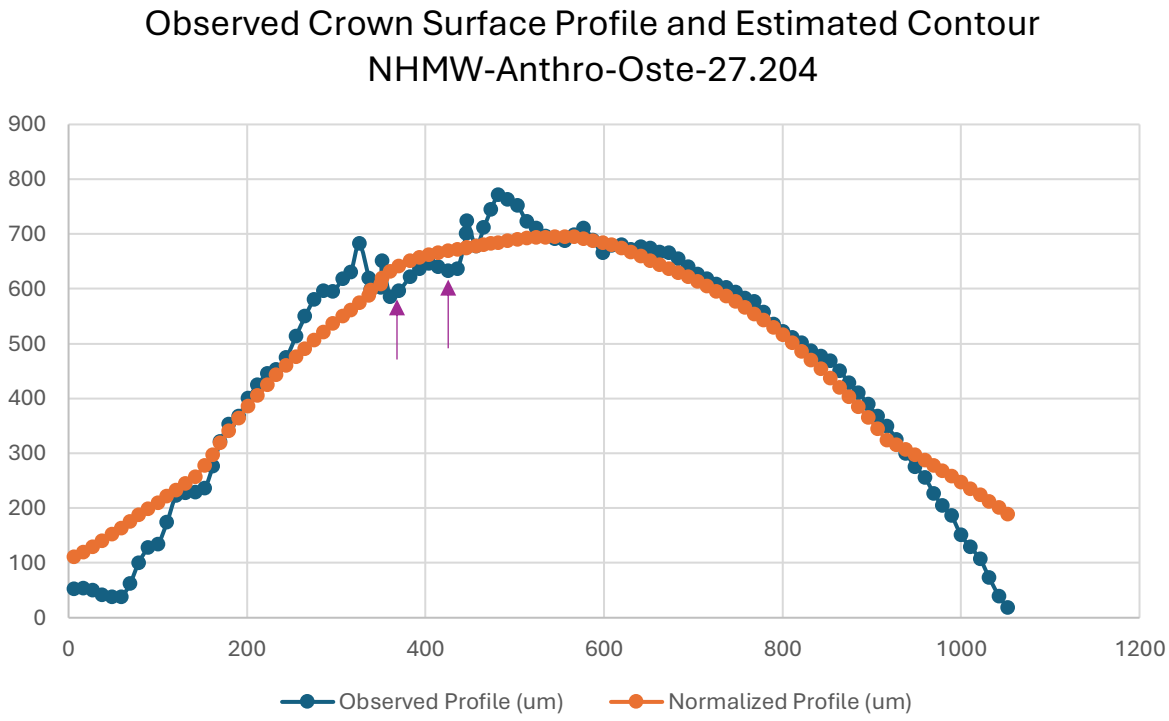

Figure 6 Example of DED profile processing for NHMW-Anthro-Oste-27.204. The observed crown surface profile was compared with a spline-estimated crown contour. Depressions below the estimated contour were used to identify enamel surface deviations consistent with dental enamel defects. Purple arrows indicate two detected defects. Graph generated in Excel.

Potential defects were identified using a local thresholding procedure. A moving standard deviation was calculated along the profile to evaluate deviations relative to local crown morphology rather than against a single global threshold:

$$SD_i = \sqrt{\frac{\sum_{j=i-k}^{i+k}(d_j - \overline{d}_i)^2}{n-1}}$$

where SD_i is the moving standard deviation at point i, d_j is the depth value for each point within the local window, $\overline{d}_i$ is the mean depth within that local window, k is the half-window size, and n is the number of points included in the window. Following the Jensby (2022) adaptation of Cares Henriquez and Oxenham's profile method (2020), k was set to

approximately one-eighth of the total number of profile points, producing a full window of approximately one-quarter of the profile.

A point was classified as part of a potential DED only if it met both of the following criteria:

$$d_i > SD_i \text{ and } d_i \geq 10\mu m$$

The first criterion identifies depressions exceeding local surface variation. The second criterion applies a minimum depth threshold to reduce false positives from scan noise, normal perikymata-scale surface variation, and minor irregularities. The same classification criteria were applied across the preserved crown profile, but local surface variation was recalculated within the moving window so that defect identification was evaluated relative to surrounding crown morphology rather than a single global surface threshold. Each point was coded as flagged or unflagged:

$$flag_i = \begin{cases} 1 \; if \; d_i > SD_i, and \; d_i \geq 10\mu m \\ 0 \; otherwise \end{cases}$$

Adjacent flagged points were treated as part of the same defect. A new DED event was counted only when the binary flag changed from 0 to 1:

$$event \; start_i = \begin{cases} 1 \; if \; flag_i = and \; flag_{i-1} = 0 \\ 0 \; otherwise \end{cases}$$

The total event count was calculated as:

$$event \; count = \Sigma_{event \; start_i}$$

This approach counts each continuous residual valley as one defect event rather than counting every flagged point as a separate event.

For each event, the following variables were recorded: event ID, start x-coordinate, end x-coordinate, maximum depth, x-coordinate at maximum depth, proportional timing, and timing bin. For the master dataset, these event-level values were summarized as:

- *event count* as a measure of DED burden,

- *maximum depth* as a measure of defect severity,
- *timing of deepest event* as the position of the most severe observed defect
- *timing of earliest event* as the earliest preserved defect observed on the crown.

Defect timing was estimated from the event's position along the preserved crown profile:

$$p = \frac{x_{defect} - x_{min}}{x_{max} - x_{min}}$$

where x_{defect} is the x-coordinate of the event, x_{min} is the CEJ end of the preserved profile, and x_{max} is the occlusal or incisal end of the preserved profile. Because x_{min} corresponded to the CEJ, lower values represent later-forming cervical enamel, and higher values represent earlier-forming occlusal or incisal enamel. This proportional approach follows the developmental logic of Reid and Dean's enamel formation studies (2000, 2006), but values were interpreted as relative timing estimates rather than absolute ages of defect formation.

Timing values were grouped into three broad developmental bins and coded numerically:

- $p \geq 0.66 = early, 1$
- $0.33 \leq p < 0.66 = mid, 2$
- $p < 0.33 = late, 3$

Because occlusal or incisal wear can remove early-forming enamel, preservation was evaluated from the LEXT images and profile outputs. Preserved profile length was calculated as:

$$preserved\ profile\ length = x_{max} - x_{min}$$

Cusp or occlusal/incisal preservation was scored from the LEXT images as present or absent. These variables were used to evaluate whether apparent timing differences could be explained by differential loss of early-forming enamel. Timing values were interpreted as the position of observed defects on preserved enamel, not as a complete reconstruction of all developmental disruptions.

4.3.2 Appendicular Growth and Skeletal Maintenance

Appendicular growth and skeletal maintenance were assessed using stature estimates, CTI, and BAA. These variables were used to evaluate different dimensions of skeletal growth and life-course skeletal response. Stature reflects cumulative linear growth outcome, CTI reflects cortical bone structure and remodelling, and appendicular asymmetry reflects bilateral developmental instability where paired elements were preserved.

Stature and Bilateral Asymmetry

Study population stature was estimated from long bone lengths measured by Dr. Julia Gamble as part of the original osteological data collection. Stature estimates were retained where long bone preservation permitted. Because element preservation varied across individuals, stature sample sizes vary by element and population. Stature was estimated using regression equations derived from Ruff's (2018) data for Bruckneudorf and Mödling reference populations. Regression coefficients were calculated as:

$$a = \frac{\left(Cov(X,Y)\right)}{Var\ (X)}$$

$$b = \mu_Y - a \times \mu_X$$

$$stature\ (cm) = a \times element\ length\ (mm) + b$$

where X is element length (mm), Y is stature (cm) in the reference sample, and μ_X and μ_Y are their respective means. $Cov(X,Y)$ is their covariance, $Var\ (X)$ is the variance in element length, a is the regression slope, and b is the intercept.

Table 1 Stature Coefficients

Element	a	b
Femur	0.2567	50.08
Tibia	0.2977	54.17
Humerus	0.3081	64.28

To assess relative adult stature, estimated statures were standardized against a late Avar comparative reference sample from Ruff's European dataset (Ruff 2018). The reference sample was restricted to the Bruckneudorf and Mödling individuals in rows 957 to 1017 of the dataset. Sex-specific mean stature and standard deviations were calculated from this reference subset. These values were then used to calculate a sex-specific stature z-score for each individual:

$$z_{stature} = \frac{stature_{individual} - \mu_{sex}}{\sigma_{sex}}$$

where μ_{sex} is the sex-specific reference mean and σ_{sex} is the sex-specific reference standard deviation. The male reference mean was 165.08 cm with a standard deviation of 6.00 cm, and the female reference mean was 158.48 cm with a standard deviation of 3.87 cm. Negative z-scores indicate reduced adult stature relative to the sex-specific late Avar comparative distribution. Individuals were categorized by relative stature rather than diagnosed as clinically stunted, since adult stature reflects the cumulative effects of genetic background, sex, nutrition, disease exposure, developmental stress, and life-course plasticity.

Bilateral appendicular asymmetry (BAA) was calculated from paired long bones where preservation permitted. Paired elements were included only when both left and right measurements were available for the same element. For each paired element, percent asymmetry was calculated as:

$$Asymmetry_{element} = \left(\frac{|L - R|}{(L + R)/2}\right) \times 100$$

where *L* is the left element length and *R* is the right element length. Asymmetry was calculated separately for preserved paired humeri, radii, ulnae, femora, and tibiae. An individual-level appendicular asymmetry score was then calculated as the mean percent asymmetry across all available paired elements:

$$Appendicular\ asymmetry\ score = \frac{\Sigma Asymmetry_{element}}{n_{paired\ elements}}$$

Higher values indicate greater bilateral asymmetry. This variable is conceptually related to developmental instability, as it is commonly used as a proxy for developmental stress (Parsons 1992; Graham and Özener 2016), but it is interpreted cautiously because BAA-stress relationships can be weak, trait-specific, and heterogeneous (De Coster et al. 2013). BAA can also reflect mechanical loading, activity, trauma, preservation, and measurement limitations (Graham and Özener 2016).

Cortical Bone Thickness

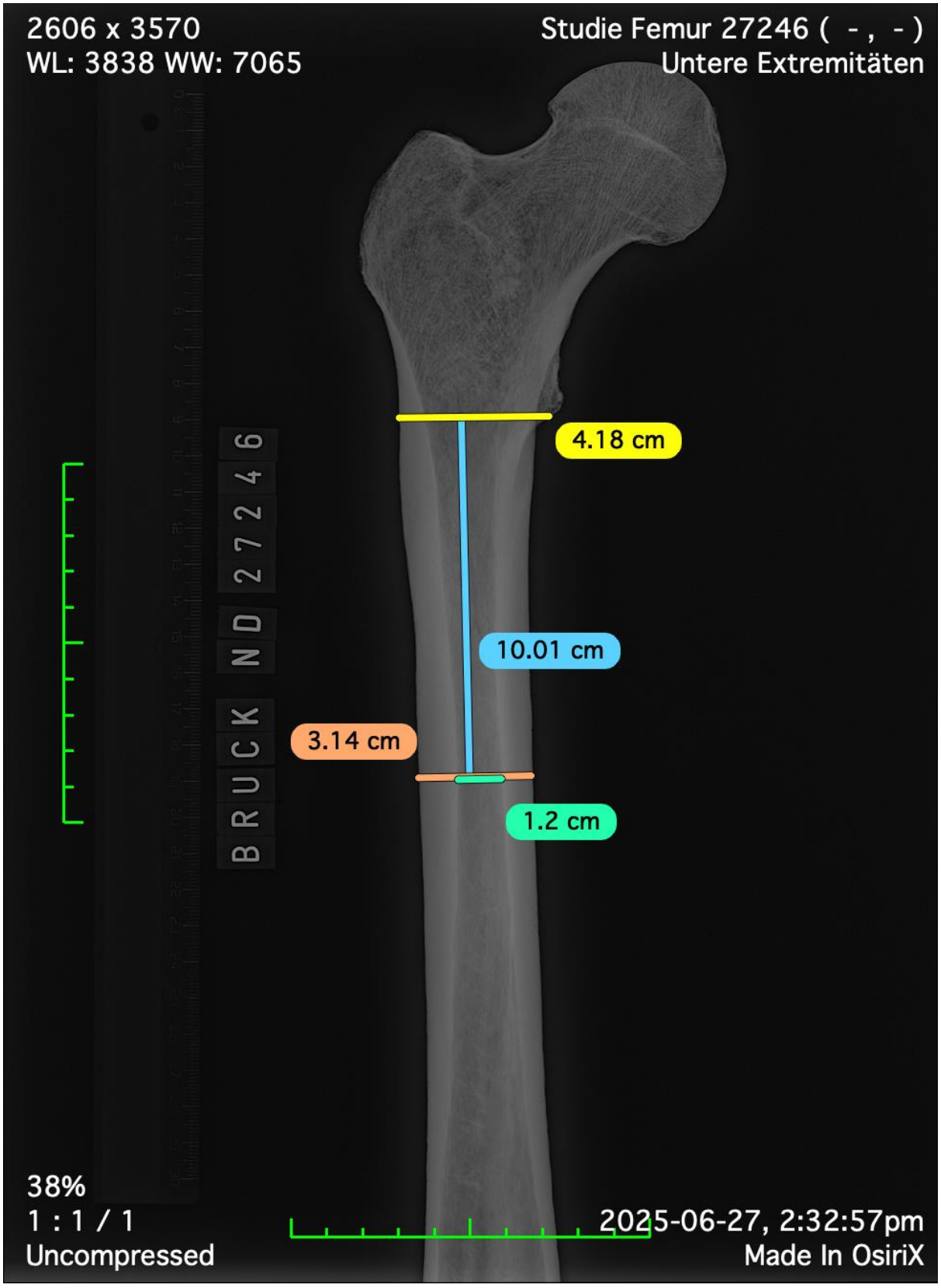

Figure 7 Example of femoral radiographic measurement for CTI in OsiriX (NHMW-Anthro-Oste-27.246). The yellow line marks the proximal reference level at the inferior margin of the lesser trochanter, the blue line marks the 10 cm distal location used for shaft measurement, the orange line marks total mediolateral shaft diameter, and the green line marks medullary cavity diameter.

Cortical bone structure was assessed using radiographic measures of cortical thickness index (CTI). Femoral radiographs were taken by the author at the Naturhistorisches Museum Wien. CTI was analysed for 44 individuals with usable femoral radiographs. Of these, 42 individuals had sex estimates that permitted calculation of sex-specific CTI z-scores. Standardized anteroposterior radiographs of the femur were used to measure cortical dimensions. Measurements followed Nguyen et al. (2018). Outer diameter (D_o) and inner diameter (D_i) are measured at the same standardized level on an anteroposterior femoral radiograph using OsiriX software (Figure 7). Nguyen et al. (2018) define CTI from the relationship between outer cortical diameter and inner medullary diameter and use this as a radiographic indicator of cortical bone structure. For each individual, D_o and D_i were measured from the radiographic image. CTI was calculated as:

$$CTI = \frac{(D_o - D_i)}{D_o}$$

where D_o is the outer diameter of the femoral shaft and D_i is the inner medullary diameter measured at the same location. Higher CTI values indicate proportionally greater cortical thickness, while lower values indicate a thinner cortical envelope relative to shaft size. Individuals with CTI z-scores ≤ -2 were classified as having markedly reduced cortical relative thickness within the sex-specific radiographed study subset. This was interpreted as markedly reduced study-relative cortical thickness and possible growth constraint.

Since cortical dimensions vary between sexes, CTI values were standardized by sex before analysis. Probable and definite females and males were grouped into separate analytical categories. Individuals with indeterminate sex were excluded from calculating sex-specific CTI z-scores. The mean and standard deviation of CTI were calculated for each sex group from the radiographed study subset. Individual CTI values were then converted to sex-specific z-scores using the formula:

$$zCTI = \frac{(CTI_{individual} - \bar{\mu}_{sex})}{\sigma_{sex}}$$

where μ_{sex} is the mean CTI for that individual's sex group, and σ_{sex} is the standard deviation of CTI for that sex group. The sex-standardized CTI z-score was used as the primary CTI variable in statistical analyses. Negative z-scores indicate lower CTI relative to same-sex individuals, while positive values indicate higher CTI relative to same-sex individuals. CTI was interpreted as an appendicular skeletal maintenance variable reflecting cumulative bone modelling and remodelling across the life course. It was not treated as a direct measure of ELS.

4.4 Inflammatory Activity

Inflammatory and degenerative skeletal-dental activity was assessed using periosteal new bone formation (PNBF), periodontal disease (PD), and osteoarthritis (OA). PNBF and PD were used to construct the SINDEX, a composite index of inflammatory skeletal-dental burden following Crespo (2020). OA was recorded separately to contextualize degenerative and mechanically mediated skeletal change following Ventades (2018), but it was not included as a primary SINDEX component. In this study, SINDEX is treated as a comparative index of observed skeletal-dental inflammatory burden.

4.4.1 Periosteal New Bone Formation

All observable skeletal elements were examined for periosteal change. Recording followed Crespo's PLS/SINDEX scoring structure (Form 1), which was converted into the study spreadsheet and applied across the observable skeleton. For each affected cortical surface, element, side, observability, lesion coverage, lesion severity, and lesion activity were recorded. Lesion coverage was scored as 1 for <25%, 2 for 25–50%, and 3 for >50% of the observable surface. Lesion severity was scored as 0 for unobservable bone, 1 for no periosteal lesion, 2 for mild striae with no thickening, 3 for moderate striae with mild thickening, and 4

for moderate to extreme thickening (Figure 8). Lesion activity was recorded as active, healing, or healed using SINDEX criteria (Crespo 2020). PNBF was summarized using two individual-level components:

$$PNBF_{severity}$$

and

$$PNBF_{activity}$$

The severity component captured cumulative extent and intensity of periosteal involvement. The activity component captured lesions expressing active or mixed inflammatory activity. These scores were treated as indicators of observed inflammatory skeletal response, not as evidence of specific diagnoses. No formal preservation correction was applied, so PNBF scores are interpreted as minimum observed inflammatory burden.

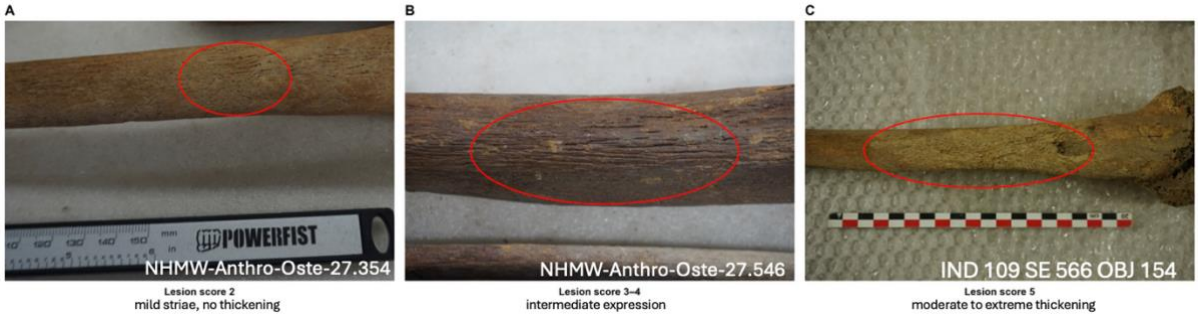

Figure 8 Examples of periosteal lesion severity scores used for PNBF recording. Red circles indicate affected cortical surfaces. Lesion score 2 indicates mild striae with no thickening, lesion score 2–3 indicates intermediate expression, and lesion score 4 indicates moderate to extreme thickening. More than one PNBF expression could be present on the same skeletal element; distinct affected areas were recorded separately when lesion form, severity, activity, or location differed.

4.4.2 Periodontal Disease

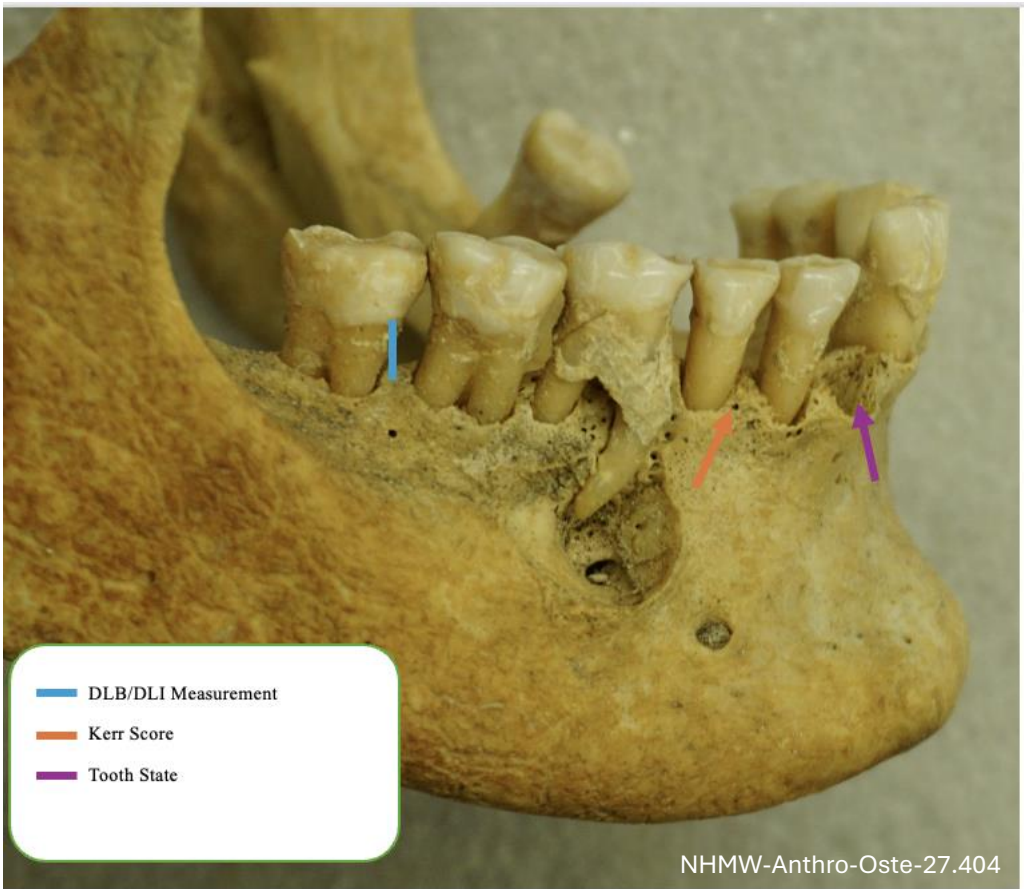

Figure 9 Example of PD scoring variables in preserved mandibular dentition. The blue marker indicates the CEJ–alveolar crest measurement location used to record DLB/DLI and the corresponding SLB/SLI score; these fields were recorded on the labial and lingual surfaces where observable. The orange marker indicates alveolar remodelling used for Kerr-based scoring, shown here by the porous, honeycomb-like appearance of the interseptal bone, consistent with a high Kerr score. The purple marker indicates tooth state, shown here as postmortem tooth loss with an unremodelled alveolus. Heavy calculus is visible on the first molar, with a dental abscess present inferior to the tooth.

PD was assessed from alveolar bone loss and alveolar remodelling using Crespo's PDS/SINDEX periodontal recording form (Form 2 Crespo PDS/SINDEX periodontal disease recording form. The form records labial and lingual CEJ–alveolar crest distances as DLB and DLI, and the corresponding CEJ–alveolar crest scores as SLB and SLI. Kerr-based alveolar remodelling was recorded separately (Crespo 2020; Kerr 1988).

), which was converted into an Excel spreadsheet for data entry. Where possible, CEJ–alveolar crest distance was recorded on the labial and lingual surfaces as DLB and DLI (Figure 9). These distances were then scored as SLB and SLI using the CEJ–AC scale: 0 for missing or unobservable tooth or bone, 1 for <2 mm or normal, 2 for 2–3 mm or mild PD, 3 for 3–5 mm or moderate PD, and 4 for >5 mm or severe PD. Kerr-based alveolar remodelling was recorded

separately from the interseptum, using a 0–5 scale from missing or not measurable bone to deep intra-bony defects (Crespo 2020; Kerr 1988). PD was summarized using two individual-level components:

$$PD_{SLB/SLI}$$

and

$$PD_{Kerr}$$

The SLB/SLI score captured alveolar bone loss, while the Kerr score provided an ordinal measure of interseptal remodelling. Unobservable teeth or alveolar regions were treated as missing. Where CEJ–AC values were unavailable, but Kerr scores could be assigned, Kerr values were used to retain periodontal information. Antemortem tooth loss (Figure 10) was recorded according to Crespo's SINDEX method as tooth state based on tooth presence intracryptal remodelling. Calculus was recorded as present or absent on each observable tooth and summarized for each individual as the proportion of observable teeth with calculus present; unobservable teeth were excluded from the denominator.

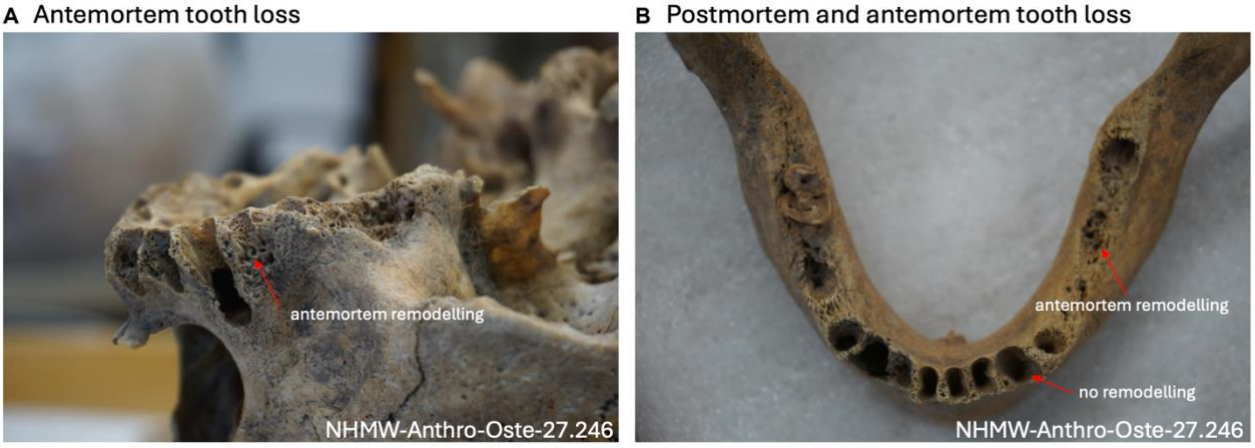

Figure 10 Antemortem and postmortem tooth loss in individual NHMW-Anthro-Oste-27.246. (A) Alveolar remodelling and closure indicate tooth loss during life; antemortem tooth loss (AMTL) counts were derived from alveolar-presence (AP) codes 4 and 5. (B) The same mandible shows both remodelled alveoli associated with AMTL and an open, unremodelled alveolus indicating tooth loss at or shortly after death. The latter was not counted as AMTL, and unavailable periodontal measurements remained coded as missing. Red arrows identify the relevant alveolar changes.

4.4.3 SINDEX Construction

A composite SINDEX score was calculated by combining periodontal and periosteal inflammatory indicators:

$$SINDEX_{raw} = PD_{SLB/SLI} + PD_{Kerr} + AMTL + PNBF_{severity} + PNBF_{activity}$$

Higher raw SINDEX values indicate greater observed inflammatory skeletal-dental burden. Because the components differ in scale and distribution, standardized component scores were also calculated:

$$z_i = \frac{x_i - \mu}{\sigma}$$

where x_i is the individual component value, μ is the sample mean, and σ is the sample standard deviation. Standardized PD and PNBF components were combined into domain-level sub-scores, and an equal-weight SINDEX score was calculated by giving the periodontal and periosteal domains equal contribution to the final composite index. This prevented components with larger raw ranges from dominating the composite score.

The equal-weight SINDEX score was used as the primary descriptive measure of observed inflammatory skeletal-dental burden. Age- and sex-adjusted SINDEX residuals were calculated for sensitivity analyses and exploratory models evaluating whether inflammatory burden exceeded expectations based on demographic structure. Positive adjusted residuals indicate inflammatory burden greater than expected for age and sex, while negative residuals indicate lower-than-expected burden.

4.4.4 Osteoarthritis

Figure 11 Examples of proximal ulnar changes considered during peripheral OA scoring. Panel A shows ulnae with little to no visible osteoarthritic change. Panel B shows non-articular bony remodelling on the olecranon and coronoid process, included here to show changes that were distinguished from scoreable articular OA. Panel C shows marginal lipping at the proximal ulna consistent with osteoarthritic change.

OA was assessed using osteophyte formation, articular surface porosity, eburnation, and subchondral surface alteration. OA scoring followed Form 3 Arthropathy identification and diagnosis recording form from Ventades et al. (2018). The form was used to structure macroscopic recording of osteoarthritis and other arthropathic changes, including osteophyte formation, porosity, eburnation, articular surface alteration, and joint distribution. Variables recorded from this form were used to construct peripheral, vertebral, and total OA scores for this study.

Form 3 in Ventades et al. (2018), which was used to record arthropathic changes relevant to osteoarthritis. Lesion severity was recorded on a 0–4 scale. OA variables were grouped into peripheral and vertebral domains. Peripheral OA included appendicular joint indicators such as hips, knees, elbows, shoulders, hands, and feet (Figure 12 and 12). Vertebral OA included cervical, thoracic, and lumbar involvement, apophyseal changes, vertebral osteophyte severity, and intervertebral preservation (Figure 13). Variables with categorical

multi-code entries rather than ordinal severity values were excluded from numeric scoring.

Peripheral OA was calculated as:

$$OA_{peripheral} = \frac{\Sigma\, OA_{peripheral\ indicators}}{n_{observed\ peripheral\ indicators}}$$

A vertebral OA score was calculated similarly:

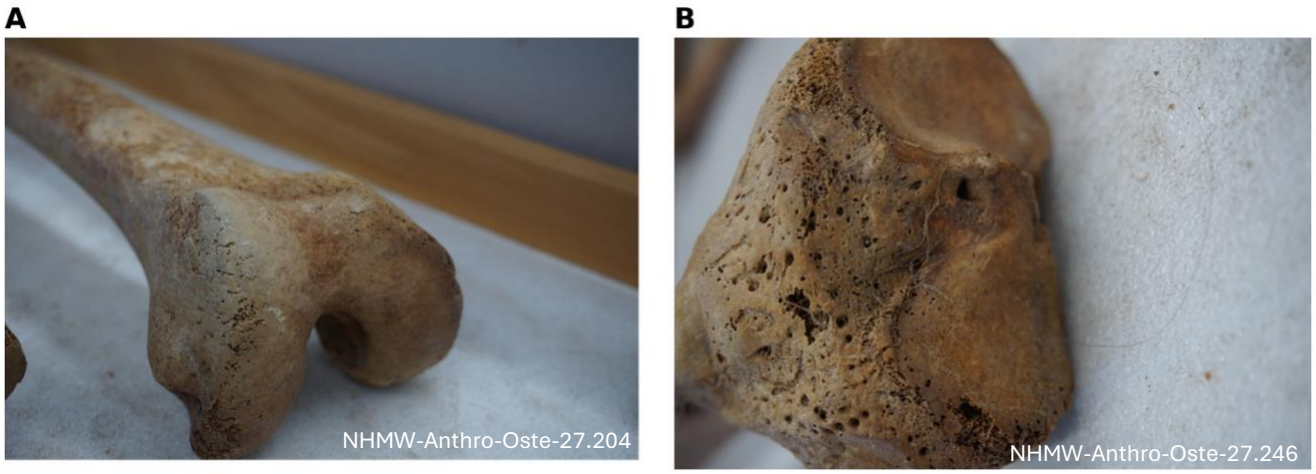

Figure 12 Example of appendicular OA scoring features. Panel A shows a femoral articular surface with little to no visible osteoarthritic change. Panel B shows a tibial articular surface with flattening and eburnation, recorded as advanced osteoarthritic surface change

$$OA_{vertebral} = \frac{\Sigma\, OA_{vertebral\ indicators}}{n_{observed\ vertebral\ indicators}}$$

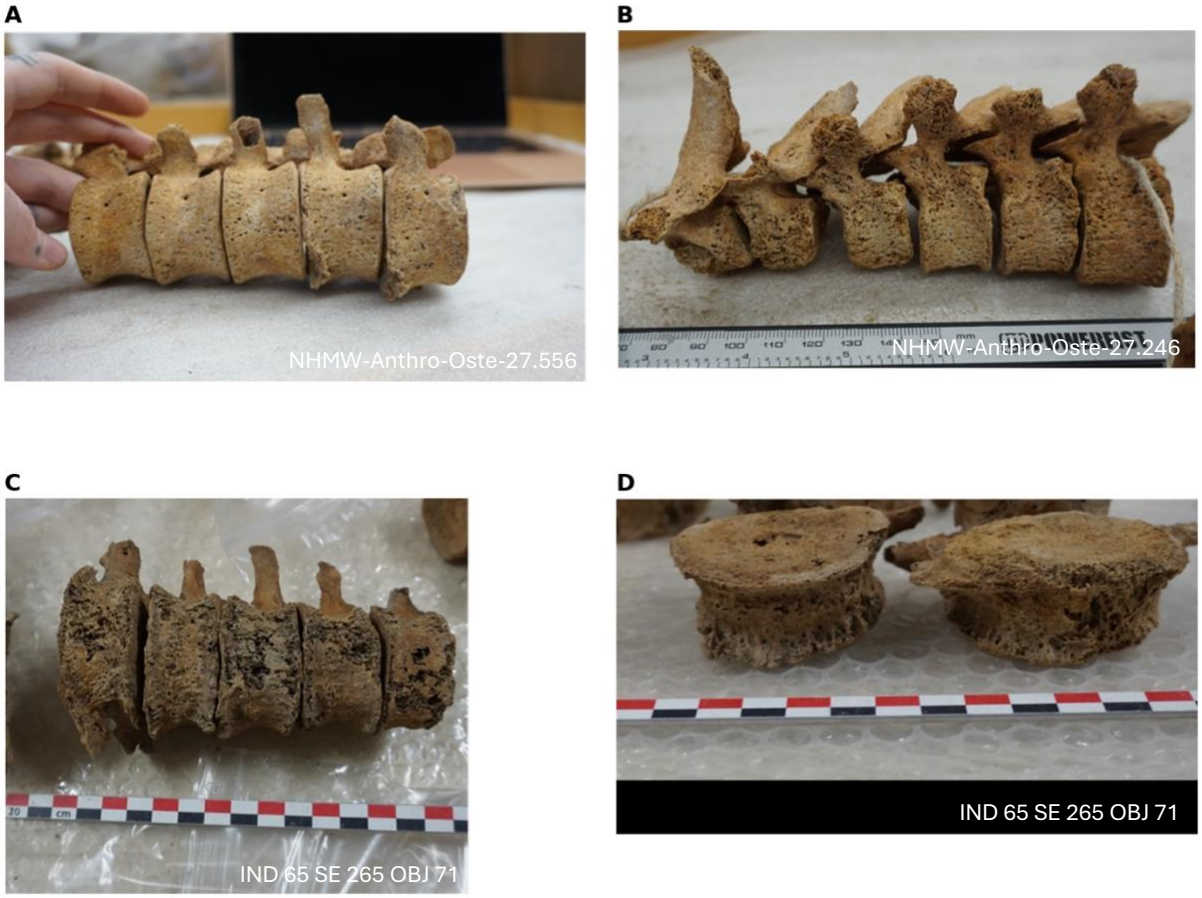

Figure 13 Examples of lumbar vertebral osteoarthritis scoring features. Panel A shows lumbar vertebrae with little to no osteoarthritic chang on L1-L3, with vertical osteophyte formation on the anterior aspect of the L4 and L5 bodies. Panel B shows marginal lipping on L1 and L2. Panel C shows more extensive horizontal osteophyte formation on L4 and L5. Panel D shows lumbar vertebrae with extensive horizontal osteophyte formation and body collapse.

A total OA score was then calculated as the mean of the peripheral and vertebral OA scores:

$$OA_{total} = \frac{OA_{peripheral} + OA_{vertebral}}{2}$$

Binary OA variables were also created. Any score greater than zero was coded as presence of OA. OA was interpreted as a contextual life-course skeletal variable rather than as a primary inflammatory burden equivalent to PNBF or PD.

4.5 Statistical Approach

All analyses were conducted at the individual level. Individuals were included in each analysis when the relevant variable was observable, recorded, and available. Missing observations were treated as missing rather than as absence of pathology, stress, or skeletal

response. Sample sizes vary across analyses because each variable depends on a differential preservation and observability structure. This treatment of missingness follows bioarchaeological concerns with differential preservation, observability, and variable-specific data loss in skeletal assemblages (Wissler et al. 2022). Data recording, derived variable construction, and preliminary calculations were conducted in Excel. These included DED profile processing, appendicular growth measures, stature estimates, sex-specific z-scores, CTI calculations, appendicular asymmetry scores, and categorical flags for marked growth constraint and reduced CTI. Final statistical analyses and visualizations were conducted in R (R Core Team 2020). Copilot was used during R script development to help identify syntax errors, troubleshoot error messages, and refine code execution. Analytical decisions, variable construction, statistical test selection, model specification, figure selection, interpretation, and written results were reviewed and finalized by the author. The R workflow merged the Master, DED, Appendicular Growth, SINDEX_summary, and OA worksheets using population and inventory ID as linking variables. Population names, inventory identifiers, sex categories, and numeric variables were cleaned before analysis.

Continuous variables were compared between Bruckneudorf and Hirschstetten using Welch's t-tests, Wilcoxon rank-sum tests, and Cohen's d. Welch's t-tests were used because group sizes and variances were not assumed to be equal. Wilcoxon tests were included for variables with skewed, bounded, ordinal, or count-like distributions. Cohen's d estimated the magnitude of group differences, with values near 0.2, 0.5, and 0.8 interpreted as small, moderate, and large, respectively. Due to the influence of preservation, missingness, and uneven sample sizes, p-values were interpreted within a broader inferential context that included effect sizes, confidence intervals, distributional shape, and biological plausibility (Baker and Pearson 2006; Cheverko and Hubbe 2017).

Sex-structured comparisons were conducted in two ways. First, females and males were compared within each population. Second, Bruckneudorf and Hirschstetten were compared within each sex. This allowed population-level patterning to be evaluated separately from sex-specific variation. These comparisons were conducted for ELS indicators, appendicular growth variables, and inflammatory skeletal-dental outcomes. Early-life and growth-related variables included DED event count, maximum DED depth, DED timing, sex-specific stature z-score, sex-specific CTI z-score, and appendicular asymmetry score. Inflammatory and degenerative variables included PD, PNBF, OA, and SINDEX.

Binary variables were analyzed using Fisher's exact tests because several comparisons had small or uneven cell counts. These binary variables included marked growth constraint, reduced CTI, peripheral OA presence, vertebral OA presence, and any OA presence. Marked growth constraint was defined as a sex-specific stature z-score $\leq$ -2 relative to the Ruff Bruckneudorf and Mödling comparative distribution. Reduced CTI was defined as a sex-specific CTI z-score $\leq$ -2 within the radiographed study subset. These binary classifications were used as conservative thresholds and were not treated as clinical diagnoses.

Dental enamel defect variables were analyzed according to their measurement structure. Event count was treated as a count-based measure of DED burden. Maximum depth was treated as a continuous measure of defect severity. Timing variables were treated as bounded proportional values between 0 and 1. Timing bins were treated as categorical variables representing early, mid, and late crown positions. Because preserved enamel affects defect visibility, DED timing was interpreted as the position of observed defects on preserved enamel rather than as a complete reconstruction of all developmental stress events.

Spearman rank correlations were used to evaluate associations among ELS indicators, appendicular growth variables, and inflammatory outcomes. ELS indicators included DED event count, DED maximum depth, DED timing, stature constraint, CTI constraint, and

appendicular asymmetry. Stature and CTI constraint variables were calculated by multiplying sex-specific z-scores by -1, so higher values represented greater stature reduction or cortical thinning. Inflammatory outcomes included PD, PNBF, total OA, peripheral OA, vertebral OA, and SINDEX. Correlations were calculated for the full sample and then stratified by sex and population where sample size permitted. Age-adjusted partial Spearman correlations were also calculated for selected variable pairs. Variables were rank-transformed, each variable was regressed on age-at-death, and the residuals were correlated. This approach evaluated whether associations between developmental stress indicators and adult outcomes persisted after accounting for age-related accumulation, especially for OA and SINDEX. P-values from correlation analyses were adjusted using the Benjamini-Hochberg (1995) procedure to control the false discovery rate.

Exploratory linear regression models assessed associations between developmental stress indicators and adult inflammatory outcomes while accounting for age, sex, and population where sample size permitted. Models were kept simple to reduce overfitting. These included models evaluating DED variables as predictors of SINDEX, appendicular growth variables as predictors of SINDEX, SINDEX as a predictor of OA, PD and PNBF as predictors of OA, and PD as a predictor of PNBF. Regression uncertainty was estimated with HC3 robust standard errors because residual variance was not assumed to be constant across observations in these small samples. HC3 adjusts standard errors, confidence intervals, and p-values, but does not change the estimated coefficients. These models were interpreted as exploratory associations rather than causal tests. This modelling strategy treats age, sex, and population as major observed covariates while recognizing that unmeasured differences in frailty, exposure history, preservation, and lesion formation can remain hidden in bioarchaeological datasets (Anderson and DeWitte 2026).

Exploratory individual-profile review was used to characterize upper-tail structure in SINDEX, PD, PNBF, DED timing, AMTL, OA, and appendicular asymmetry. Upper-tail profiles were defined using sample-wide upper quartiles and were interpreted descriptively, not as separate inferential tests.

Visualizations were generated in R (R Core Team 2020). Boxplots with jittered individual points were used to compare variable distributions by population and sex. Scatterplots with fitted trend lines were used to examine pairwise associations among selected variables. Spearman correlation heatmaps were used to visualize the broader life-course structure of the dataset, including age, stature, CTI, appendicular asymmetry, DED variables, PD, PNBF, OA, and SINDEX. A correlation network mapped moderate or stronger associations among variables. Network edges were retained when the absolute Spearman correlation coefficient was ≥ 0.30 and the pairwise sample size was ≥ 6. This network was interpreted as a descriptive map of covariance among developmental disruption, appendicular growth, cortical maintenance, and skeletal-dental inflammatory burden.

A conventional threshold of $p < 0.05$ was used as a reference point, but interpretation emphasized the broader inferential context. The statistical approach was designed to identify patterned relationships among life-course markers rather than produce definitive causal estimates.

5. Results

5.1 Sample Composition and Data Coverage

The merged dataset included 68 adults and late adolescents from Bruckneudorf and Hirschstetten. Sex estimates were available for 64 individuals, while four individuals had indeterminate or missing sex estimates. These individuals were retained in population-level analyses and excluded from sex-stratified comparisons. Data coverage varied across analytical domains because each measure had differential preservation and observability structure (Table 2). Age-at-death estimates were available for 67 individuals. Additional dental variables included AMTL count and calculus presence. AMTL was derived from AP codes 4 and 5. Calculus was summarized as an individual-level presence/absence variable. These variables were used to evaluate whether the population-level periodontal disease (PD) pattern aligned with AMTL, calculus presence, age, sex, and site-level differences.

Differences in data coverage influenced the statistical approach. Population-level tests used the available sample size for each variable, while sex-stratified analyses were limited to individuals with female or male sex estimates. Correlation and regression models involving multiple early-life indicators used complete cases, reducing sample size relative to single-variable comparisons. These models require cross-domain preservation and are interpreted with corresponding caution.

Table 2 Sample Composition and Data Coverage: Counts reflect the number of individuals with usable data for each measure. Sex-stratified analyses exclude individuals with indeterminate or missing sex estimates.

Domain	Measure	n
Sample	Total individuals	**68**
	Estimated sex	64
	Age at death	67
Early-Life Indicators	DED event count	59
	DED timing	54
	Estimated stature	53
	Stature z-score	53

	Growth-constraint flag	53
	CTI	44
	CTI z-score	42
	CTI-thinned flag	42
	Appendicular asymmetry	46
Adult Indicators	PD	68
	PNBF	68
	Total OA	68
	AMTL count	68
	Calculus presence/proportion	68
Derived Inflammatory Measures	PD component	68
	PNBF component	68
	Equal-weight SINDEX	**68**

5.2 Descriptive Patterns by Population

Descriptive statistics showed broad overlap between Bruckneudorf and Hirschstetten for most appendicular growth, DED, and OA variables (Table 3). Estimated stature differed by less than 1 cm between populations, and stature z-scores were close in both groups. CTI and CTI z-scores showed similarly close values.

Table 3 Population-specific descriptive statistics for developmental, inflammatory, demographic, and oral-health variables. Values are presented as n and mean ± SD; sample sizes vary with preservation and observability.

		Bruckneudorf		Hirschstetten	
Domain	**Variable**	**n**	**mean ± SD**	**n**	**mean ± SD**
Appendicular growth	BAA	27	0.77 ± 0.4	19	1.54 ± 1.77
	CTI	22	0.63 ± 0.07	22	0.62 ± 0.06
	CTI z-score	21	0.06 ± 1	21	-0.06 ± 1
	Estimated stature	30	161 ± 7.88	23	160.29 ± 6.97
	Stature z-score	30	-0.28 ± 1.22	23	-0.45 ± 1.12
DED	DED event count	30	1.87 ± 1.01	29	2.1 ± 1.35
	Maximum DED depth	28	34.52 ± 19.04	26	36.95 ± 18.75
	Timing of deepest DED	28	0.42 ± 0.17	26	0.36 ± 0.14
	Timing of earliest DED	28	0.56 ± 0.2	26	0.47 ± 0.2
OA	Peripheral OA score	35	0.32 ± 0.41	33	0.34 ± 0.5
	Total OA score	35	0.43 ± 0.5	33	0.41 ± 0.54
	Vertebral OA score	34	0.55 ± 0.65	33	0.48 ± 0.64
SINDEX	Equal-weight SINDEX score	35	0.18 ± 0.64	33	-0.19 ± 0.44

	PD	35	0.26 ± 0.64	33	-0.28 ± 0.67
	PNBF	35	0.09 ± 1.21	33	-0.1 ± 0.67
Oral ecology	AMTL count	35	4.71 ± 6.64	33	3.70 ± 6.53
	Calculus presence proportion	34	1.00 ± 0.00	31	0.98 ± 0.06
Demography	Age-at-death	35	38.29 ± 14.57	32	38.66 ± 16.79

Age-at-death distributions were similar between the two cemetery populations (Table 3;

Table A.16; Figure A.8). Bruckneudorf had a mean age-at-death of 38.29 years, while Hirschstetten had a mean age-at-death of 38.66 years. Sex-stratified age summaries also overlapped: Bruckneudorf females and males had mean ages of 38.20 and 40.50 years, while Hirschstetten females and males had mean ages of 39.63 and 38.55 years. Age distributions overlapped substantially (Figure A.8), although Bruckneudorf males were more concentrated in middle adulthood and Hirschstetten females showed greater dispersion. The population-level PD difference was not as simple as older ages in one cemetery.

Appendicular asymmetry was more dispersed in Hirschstetten. Hirschstetten had a higher mean asymmetry score and a larger standard deviation than Bruckneudorf, but the medians were nearly identical, 0.74 and 0.76 (Table A.1, **Error! Reference source not found.**). The higher Hirschstetten mean comes from the upper end of the distribution, which extends to 6.81. Bruckneudorf values remain below 1.70. **Error! Reference source not found.** shows most individuals clustered at low asymmetry values, with a small number of Hirschstetten individuals at the upper end of the distribution. Among these four, three had negative stature z-scores, while PD scores ranged from −0.79 to 1.07; only one had a positive PNBF score, and DED counts ranged from one to three among the three individuals with available DED data. The four upper-range individuals showed varied developmental and

inflammatory profiles. Sex-stratified summaries show wide Hirschstetten ranges in both females and males (Table A.2).

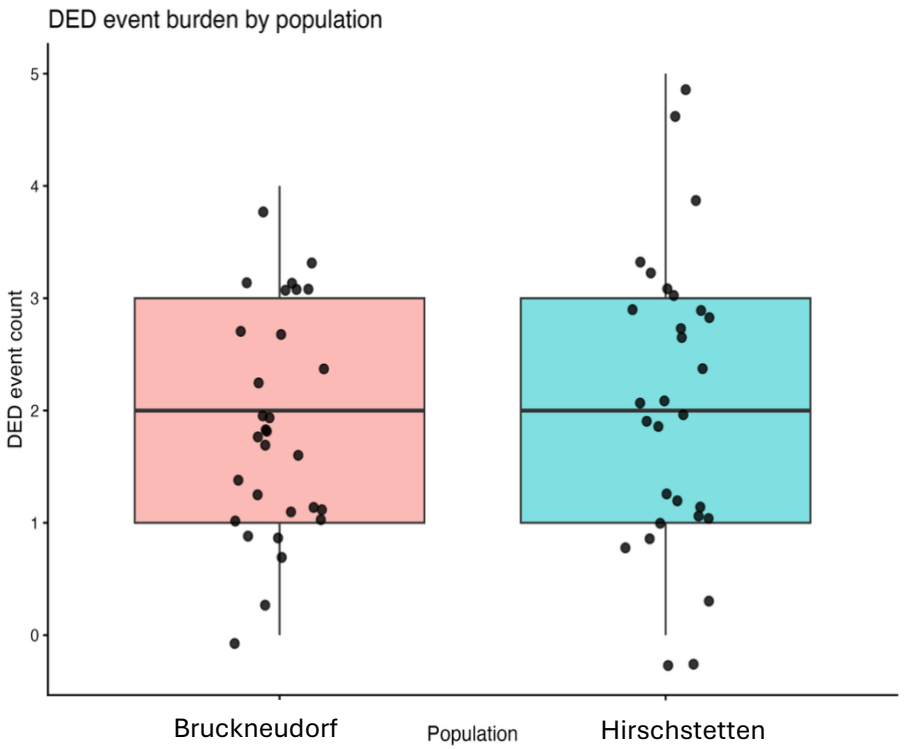

Figure 15 DED event burden by population. Median counts and interquartile ranges were similar, with substantial overlap between the cemetery populations

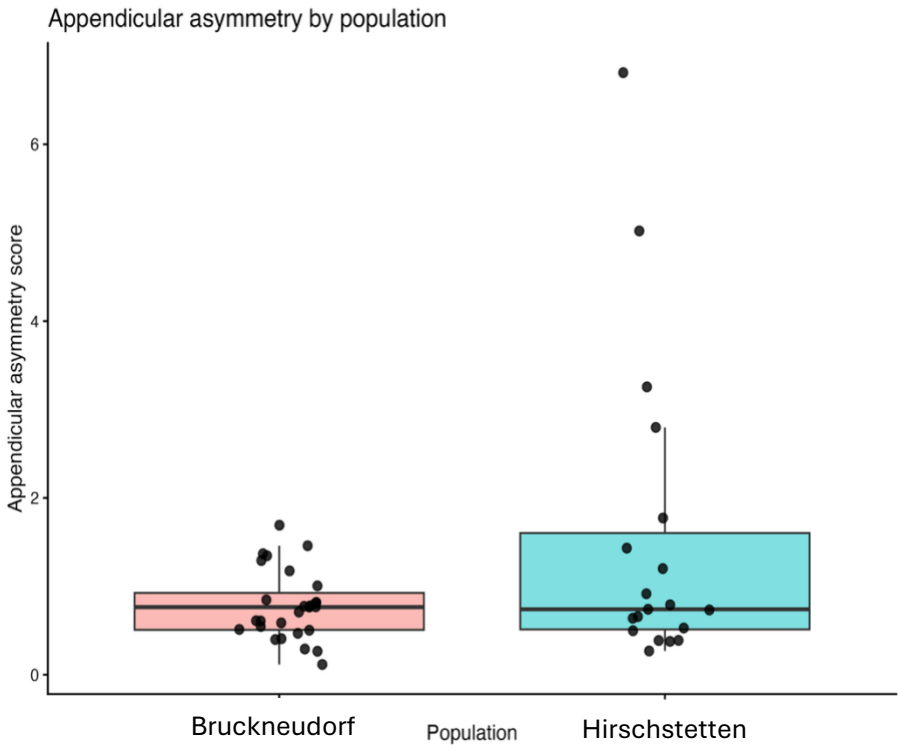

Figure 14 Appendicular asymmetry scores by population. Median scores were similar in Bruckneudorf (0.74) and Hirschstetten (0.76), but Hirschstetten had greater dispersion and a higher mean (1.54 versus 0.77), driven by several upper-range values.

DED event burden (Figure 14) and maximum DED depth (Figure 16) were similar between populations. Both populations had a median of two defects, and maximum defect depth showed overlapping ranges (Table A.1).

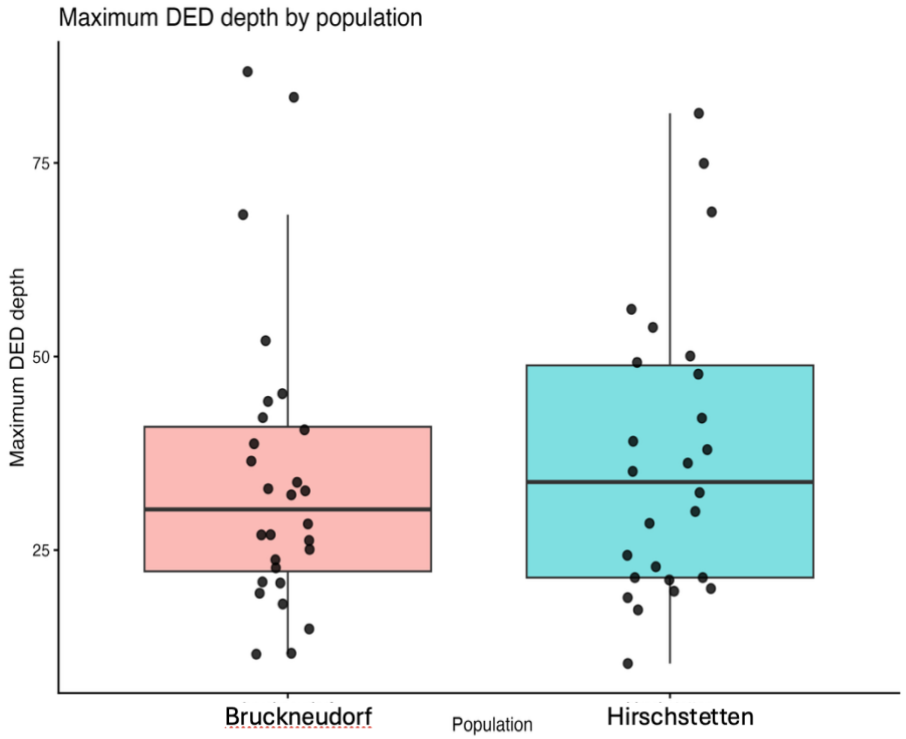

Figure 16 Maximum DED depth by population. Distributions overlapped substantially, with similar mean depths in Bruckneudorf (34.52 µm) and Hirschstetten (36.95 µm).

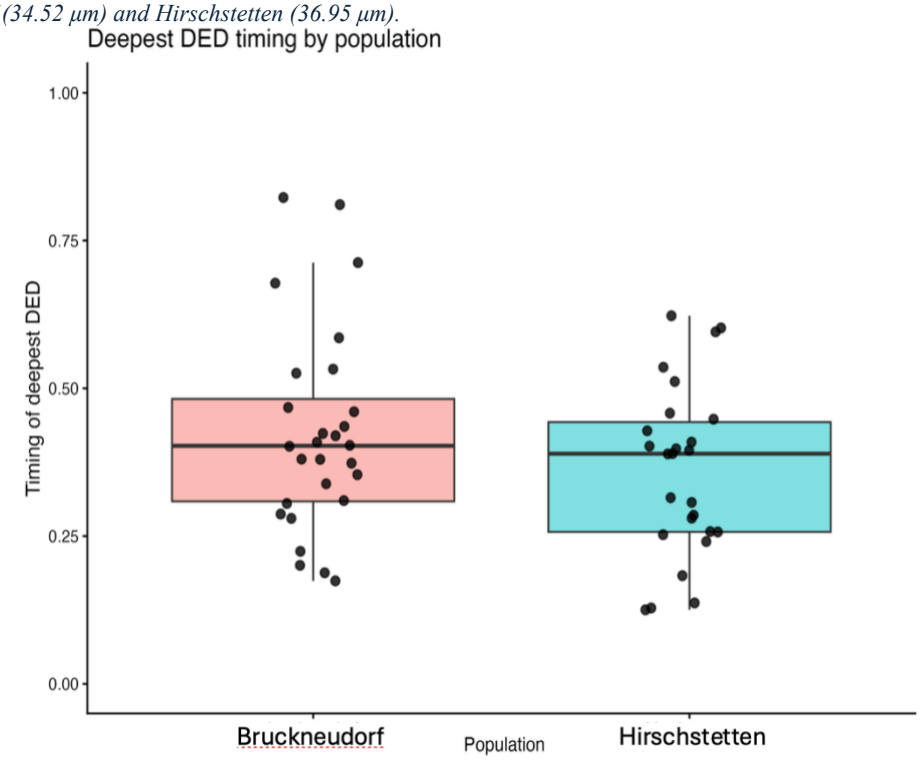

Figure 17 Timing of the deepest DED by population. Distributions overlapped, although Bruckneudorf had a slightly higher mean timing value (0.42 versus 0.36), indicating defects in earlier-forming enamel.

DED timing differed more than DED count or depth (Figure 17). Bruckneudorf had higher mean values for both deepest and earliest defect timing, and the median for earliest timing was also higher. The distributions nevertheless overlapped, with Hirschstetten including several individuals in the upper timing range but also extending further into the lower range. Overall, the central values indicate a modest shift toward earlier-forming enamel positions in Bruckneudorf. Attrition was not recorded as a formal variable, although occlusal or incisal crown wear was visible during DED profiling. For that reason, DED timing is not interpreted as a complete record of all developmental disruptions, since earlier-forming enamel may have

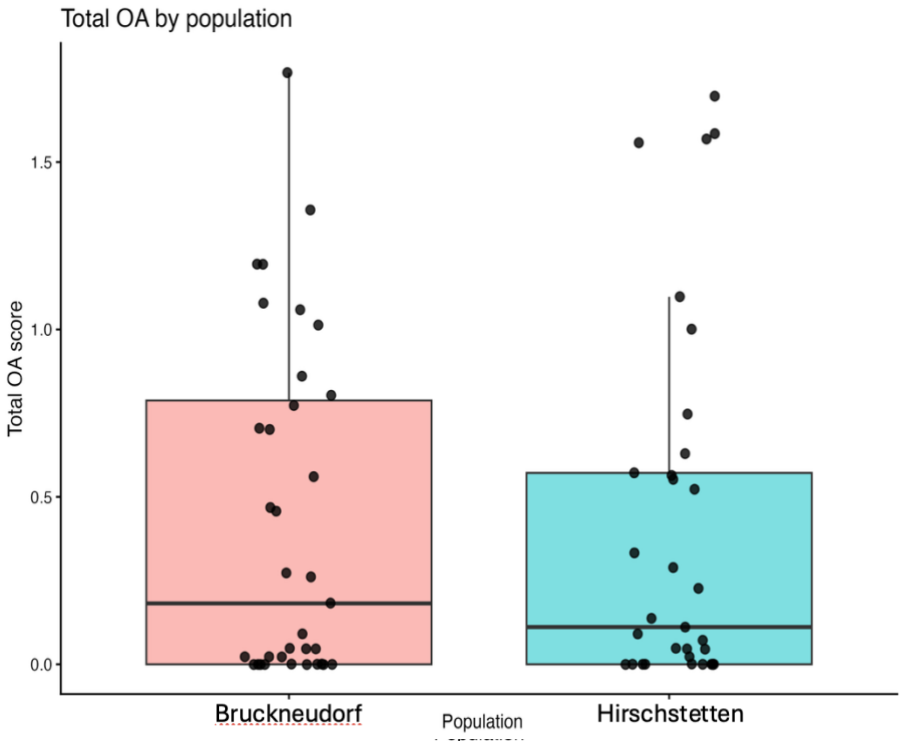

Figure 18 Total osteoarthritis (OA) scores by population. Distributions overlapped substantially, with similar mean scores in Bruckneudorf (0.43) and Hirschstetten (0.41).

been lost in some individuals. OA scores were also similar across populations (Figure 18). Total, peripheral, and vertebral OA means were close in Bruckneudorf and Hirschstetten (Table 3). The distributions were right-skewed, with many individuals scoring near zero and fewer carrying higher OA scores (Table A.1). Vertebral OA contributed more to total OA burden than peripheral OA in both populations. Sex-stratified summaries show higher total and vertebral

OA among Bruckneudorf males and higher peripheral OA among Hirschstetten females, though the ranges overlap (Table A.2).

SINDEX was higher in Bruckneudorf than Hirschstetten by both mean (0.18 versus −0.19) and median values (0.08 versus −0.23) (Table 3; Figure 19). Two PNBF-driven Bruckneudorf outliers contributed substantially to the higher mean, although the median was also higher in Bruckneudorf. The component scores place the broader difference mainly in PD. PD scores were higher in Bruckneudorf by both mean and median values, while PNBF had the same median and mode in both populations (Table A.1).

Figure 19 Equal-weight SINDEX scores by population. Scores were significantly higher in Bruckneudorf than Hirschstetten (mean 0.18 versus −0.19; p = .008).

PD increased with age in both cemetery populations, but Bruckneudorf values remained higher across much of the adult age range (Figure 20; Table 3; Table A.17). Bruckneudorf had higher antemortem tooth loss (AMTL) counts than Hirschstetten, with means of 4.71 and 3.70 and medians of 2 and 1, respectively. Calculus presence was high in both populations and showed little separation. The clearest population contrast was PD and tooth-loss burden, while calculus was widespread across both cemeteries.

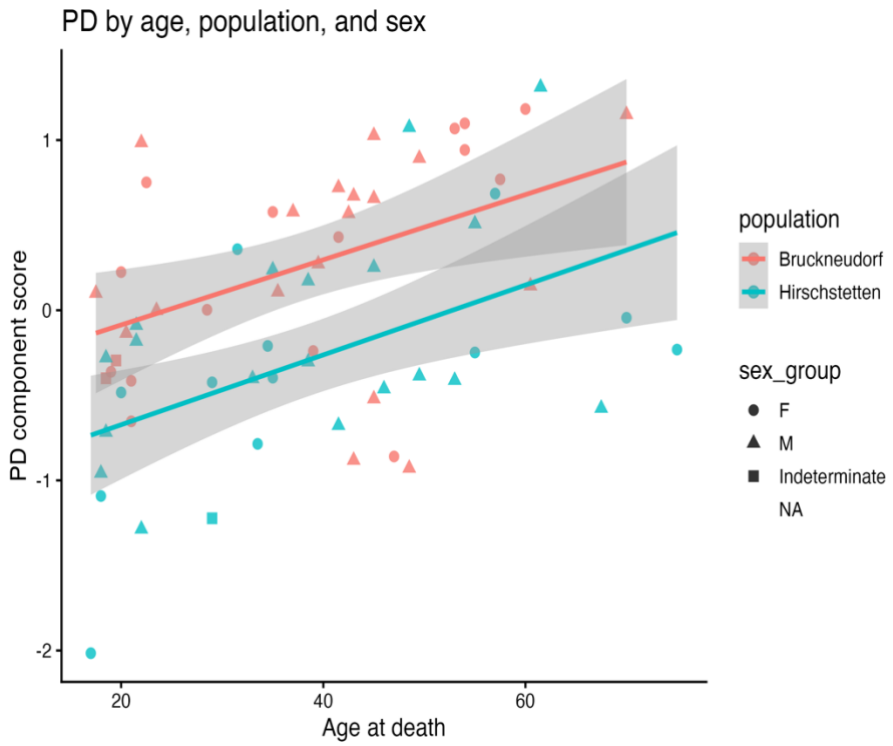

Figure 20 Periodontal disease (PD) scores by age, population, and sex. Scores increased with age in both populations but remained higher in Bruckneudorf, with no clear separation by sex. Shaded bands represent 95% confidence intervals.

5.3 Population Comparisons

Table 4 shows population-level tests for continuous variables. Most appendicular growth, DED, and OA comparisons showed non-significant group differences and small effect sizes. DED count and maximum depth showed little population separation, while DED timing had stronger directional effects. Bruckneudorf was shifted towards earlier-forming enamel positions for both deepest DED timing (Welch's $t(51.47) = 1.50$, $p = .140$, $d = 0.41$) and earliest DED timing (Welch's $t(51.70) = 1.58$, $p = .120$, $d = 0.43$). These timing comparisons did not reach statistical significance and may be affected by dental wear. Appendicular asymmetry was the main exception among the growth variables. Hirschstetten had a higher mean asymmetry score than Bruckneudorf, producing a moderate effect size (Welch's $t(19.27) = -1.85$, $p = .080$, $d = -0.60$; Wilcoxon $W = 219$, $p = .409$). This disagreement is due to the distribution: the mean increased for the upper-range Hirschstetten individuals, while the group medians stayed almost the same.

OA differed little between populations: total, peripheral, and vertebral OA all had non-significant tests and effect sizes close to zero. SINDEX had the strongest population-level result. Equal-weight SINDEX was higher in Bruckneudorf than Hirschstetten (Welch's $t(60.21) = 2.76$, $p = .008$, $d = 0.67$; Wilcoxon $W = 800$, $p = .006$). The component scores place this difference mainly in PD. PD was higher in Bruckneudorf than Hirschstetten (Welch's $t(65.37) = 3.43$, $p = .001$, $d = 0.83$; Wilcoxon $W = 832$, $p = .002$). PNBF had non-significant tests and a small effect size (Welch's $t(53.45) = 0.80$, $p = .424$, $d = 0.19$; Wilcoxon $W = 612.5$, $p = .644$).

Table 4 Population comparisons for developmental and adult skeletal variables. Positive Cohen's d values indicate higher scores in Bruckneudorf. $p < .05$.

		Bruckneudorf		Hirschstetten						
Domain	**Variable**	**n**	**mean ± SD**	**n**	**mean ± SD**	**Welch's t(df)**	**p**	**Wilcoxon W**	**p**	**Cohen's d**
DED	DED event count	30	1.87 ± 1.01	29	2.10 ± 1.35	−0.76 (51.88)	0.449	397.5	0.561	−0.20
	Maximum DED depth	28	34.52 ± 19.04	26	36.95 ± 18.75	−0.47 (51.81)	0.639	334	0.61	−0.13
	Timing of deepest DED	28	0.42 ± 0.17	26	0.36 ± 0.14	1.50 (51.47)	0.14	432	0.243	0.41
	Timing of earliest DED	28	0.56 ± 0.20	26	0.47 ± 0.20	1.58 (51.70)	0.12	451	0.134	0.43
Appendicular Growth	Estimated stature	30	161.00 ± 7.88	23	160.29 ± 6.97	0.35 (49.89)	0.728	352	0.907	0.1
	Stature z-score	30	−0.28 ± 1.22	23	−0.45 ± 1.12	0.53 (49.35)	0.595	362	0.767	0.15
	CTI	22	0.63 ± 0.07	22	0.62 ± 0.06	0.37 (40.98)	0.713	265	0.597	0.11
	CTI z-score	21	0.06 ± 1.00	21	−0.06 ± 1.00	0.38 (40.00)	0.708	238	0.669	0.12
	BAA	27	0.77 ± 0.40	19	1.54 ± 1.77	−1.85 (19.27)	0.08	219	0.409	−0.60
OA	Total OA score	35	0.43 ± 0.50	33	0.41 ± 0.54	0.15 (64.81)	0.881	592.5	0.857	0.04
	Peripheral OA score	35	0.32 ± 0.41	33	0.34 ± 0.50	−0.21 (61.74)	0.837	612.5	0.667	−0.05
	Vertebral OA score	34	0.55 ± 0.65	33	0.48 ± 0.64	0.49 (65.00)	0.627	595.5	0.64	0.12
SINDEX	**Equal-weight SINDEX**	35	0.18 ± 0.64	33	−0.19 ± 0.44	**2.76 (60.21)**	**.008***	**800**	**.006***	**0.67**
	PD	35	0.26 ± 0.64	33	−0.28 ± 0.67	**3.43 (65.37)**	**.001***	**832**	**.002***	**0.83**
	PNBF	35	0.09 ± 1.21	33	−0.10 ± 0.67	0.80 (53.45)	0.424	612.5	0.644	

5.4 Sex-Specific Patterns

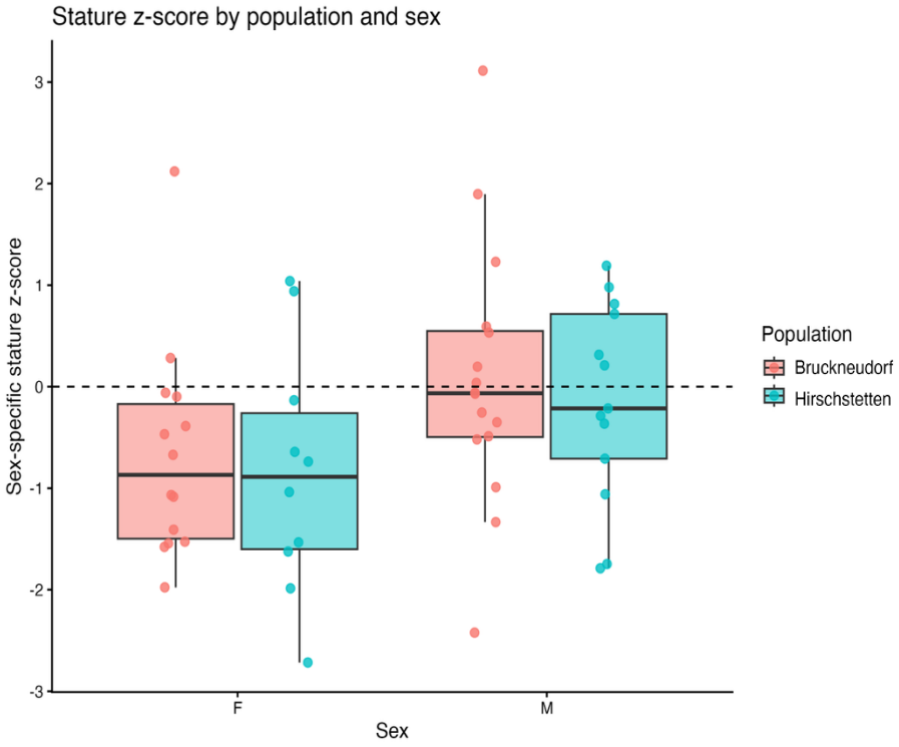

Figure 21 Sex-specific stature z-scores by population. Scores overlapped between populations within each sex; females generally fell below the reference mean, while male scores were centred closer to zero. The dashed line indicates the reference mean.

Stratified analyses examined whether population patterns differed by sex (Table A.2 Table A.3). Estimated stature (Figure 21) showed expected sexual dimorphism, with males taller than females in both populations. Sex-specific stature z-scores reduced this difference, although Bruckneudorf females still had lower stature z-scores than males in the Wilcoxon test. Other appendicular growth measures showed little sex-specific structure. CTI, CTI z-score, and appendicular asymmetry did not differ significantly between females and males within either population.

DED variables also showed limited sex-specific patterning. Within Bruckneudorf and Hirschstetten, females and males had similar DED event counts, maximum defect depths, and DED timing values. Sex-stratified population comparisons followed the same pattern. Among females and males, Bruckneudorf and Hirschstetten did not differ significantly in DED count, maximum depth, deepest timing, or earliest timing. The largest DED effect sizes were for

timing comparisons, especially deepest DED timing among males and earliest DED timing among females, but these did not reach statistical significance.

OA showed more sex-related variation than the developmental stress markers, although the results were inconsistent across tests. In Bruckneudorf, males had higher total, peripheral, and vertebral OA means than females. In Hirschstetten, females had higher peripheral OA means than males. These patterns did not produce consistent significant differences in the Welch tests, although the Hirschstetten peripheral OA comparison approached significance in the Wilcoxon test.

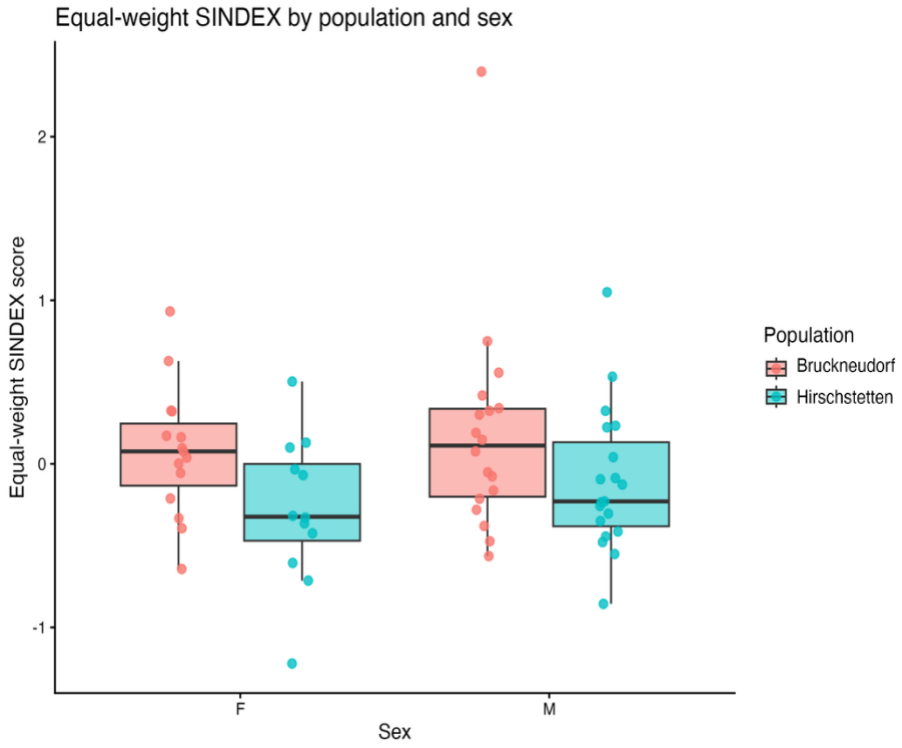

Figure 22 Equal-weight SINDEX scores by population and sex. Bruckneudorf had higher median scores than Hirschstetten in both sex groups, with no clear within-population separation by sex.

SINDEX and PD showed the clearest sex-stratified population pattern (Figure 20 and Figure 22). Bruckneudorf females had higher equal-weight SINDEX and PD scores than Hirschstetten females. The female equal-weight SINDEX comparison was significant by Welch's test, Welch's $t(22.10) = 2.13$, $p = .044$, $d = 0.83$, while the Wilcoxon test followed the same direction but was just above the conventional threshold, $W = 130$, $p = .054$. Female PD scores were higher in Bruckneudorf than Hirschstetten and significant by both Welch and

Wilcoxon tests, Welch's t(23.62) = 2.67, p = .014, d = 1.03; Wilcoxon W = 137, p = .023. Bruckneudorf males also had higher PD scores than Hirschstetten males, with significant Welch and Wilcoxon tests, Welch's t(34.99) = 2.24, p = .032, d = 0.74; Wilcoxon W = 243, p = .030. Equal-weight SINDEX among males followed the same direction but did not reach significance, Welch's t(29.27) = 1.57, p = .128, d = 0.52; Wilcoxon W = 226, p = .098. PNBF did not differ between populations within either sex. The sex-stratified age summaries did not suggest a simple age-structure explanation for the PD pattern. The mean ages were similar between female and male groups in both populations. Bruckneudorf females and males had higher PD values than their Hirschstetten counterparts, while PNBF remained weakly differentiated between populations and sexes.

5.5 Life-Course Correlation Structure

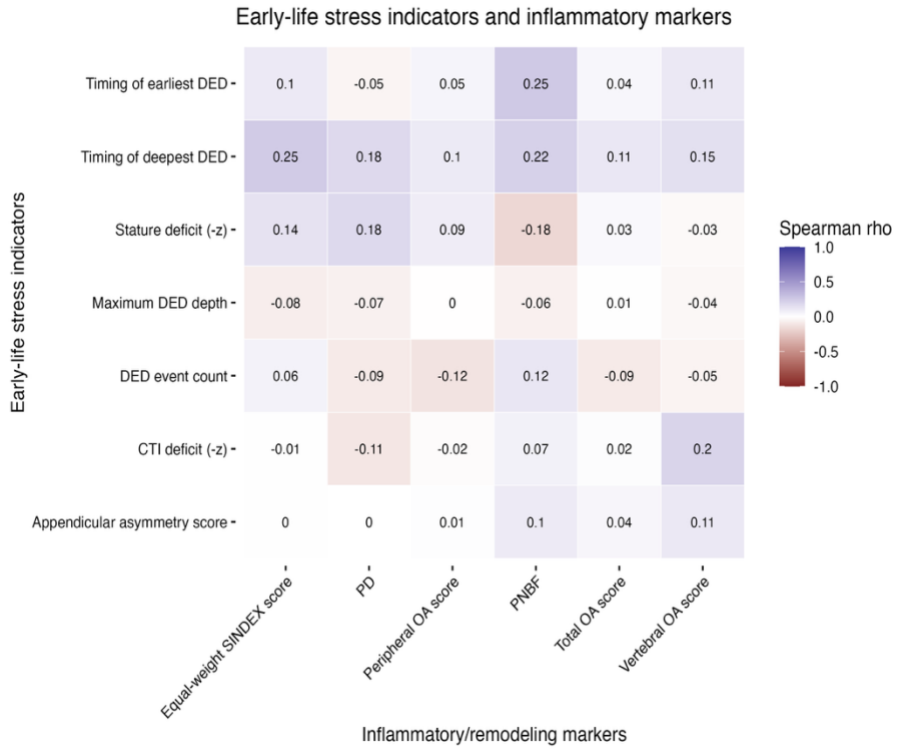

Figure 23 Correlation structure between early-life stress indicators and adult inflammatory/remodelling markers. Associations were sparse and weak (rho ≤ 0.25), with no early-life indicator consistently related to adult marker burden.

Early-life indicators did not cluster strongly with adult inflammatory or OA variables. In the ELS-to-inflammation heatmap, most associations between stature deficit, CTI deficit, appendicular asymmetry, DED variables, PD, PNBF, OA, and equal-weight SINDEX are weak

or negligible (Figure 23). No early-life indicator remained significant after Benjamini-Hochberg (1995) correction (Table A.8). The largest unadjusted coefficients involved DED timing, but these remained weak. Partial correlations controlling for age followed the same pattern (Table A.11). Stature constraint with PD and earliest DED timing with PNBF produced the largest partial coefficients, but both remained weak within the adjusted inferential context. Age was strongly associated to OA in the sample, so age adjustment was necessary before interpreting associations involving OA or inflammatory measures. The clearest early-life correlations were within the DED variables. Deepest and earliest DED timing were strongly correlated, and DED event count was moderately correlated with earliest DED timing (Table A.12).

Component-level analyses separated the population-level and individual-level structure of equal-weight SINDEX (**Error! Reference source not found.**Table A.18). At the population level, the SINDEX contrast was mainly driven by PD. At the individual level, high SINDEX values could result from either high PD or high PNBF. Among individuals in the upper quartile of equal-weight SINDEX, 11 also had high PD, 10 had high PNBF, and four had high PD and PNBF (Table A.23). The highest SINDEX values were driven by PNBF, while the population contrast remained PD-driven. The clearest weak association involving developmental indicators was with the PNBF component. DED event count and DED timing showed weak positive associations with PNBF activity or severity, while PD showed weaker and less consistent associations with developmental indicators. Among component-level PNBF measures, earliest DED timing showed its clearest relationships with PNBF severity, lesion count, and bone count. PNBF severity approached conventional significance before correction (rho = 0.261, p = 0.056), PNBF lesion count showed a similar directional pattern (rho = 0.263, p = 0.054), and PNBF bone count reached nominal significance before correction (rho = 0.292,

p = 0.034). These associations did not remain significant after false-discovery correction and are treated as exploratory directional signals.

The same pattern was visible in the upper tail of the PNBF distribution. Individuals in the upper quartile of PNBF with DED timing data had higher mean earliest DED timing than individuals outside the upper quartile, 0.62 compared with 0.48. Because higher timing values correspond to earlier-forming enamel, high-PNBF individuals tended to have earlier preserved DED timing. The PNBF distribution was influenced by a small number of high-burden individuals in both populations (Table A.20Table A.22; Figure A.11). Several high-PNBF individuals had suspected chronic infectious or complex pathological involvement, including suspected leprosy, tuberculosis signs, osteomyelitis, or cancer differentials. Developmental and inflammatory contrast profiles also showed that high DED count or earlier preserved DED timing did not consistently translate into high equal-weight SINDEX (Table A.24). The strongest developmental pattern involved PNBF response intensity and extent, not equal-weight SINDEX as a whole.

Adult inflammatory and degenerative variables were more strongly correlated with each other than with the early-life indicators (Table 5; **Error! Reference source not found.**). PD was associated with total, peripheral, and vertebral OA. PNBF had negligible correlations with total and peripheral OA and only a weak correlation with vertebral OA. PD and PNBF were also uncorrelated with each other. PD and PNBF do not behave as interchangeable inflammatory components.

Table 5 Spearman correlations among adult inflammatory and osteoarthritis measures. Note. Adjusted p values use the Benjamini–Hochberg correction. ∗p < .05; ∗∗p < .01; ∗∗∗p < .001.

Measure	Correlated variable	n	Spearman's ρ	p	Adjusted p
PD	PNBF	68	−0.10	0.43	0.5
	Total OA score	68	0.5	<.001	**<.001***
	Peripheral OA score	68	0.47	<.001	**<.001***
	Vertebral OA score	67	0.5	<.001	**<.001***
	Equal-weight SINDEX	68	0.74	<.001	**<.001***
PNBF	Total OA score	68	0.03	0.78	0.84
	Peripheral OA score	68	−0.01	0.96	0.96
	Vertebral OA score	67	0.14	0.25	0.31
	Equal-weight SINDEX	68	0.48	<.001	**<.001***
Total OA score	Peripheral OA score	68	0.92	<.001	**<.001***
	Vertebral OA score	67	0.92	<.001	**<.001***
	Equal-weight SINDEX	68	0.37	0.002	**.003****
Peripheral OA score	Vertebral OA score	67	0.76	<.001	**<.001***
	Equal-weight SINDEX	68	0.34	0.01	**.010***
Vertebral OA score	Equal-weight SINDEX	67	0.43	<.001	**<.001***

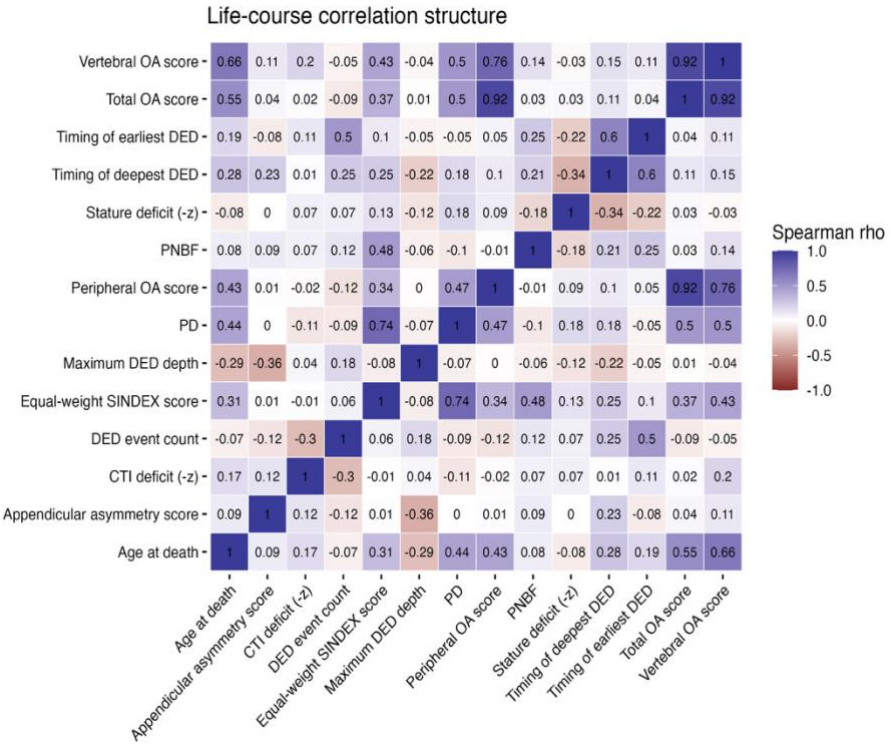

Figure 24 Life-course Spearman correlation matrix. The strongest associations occurred among OA scores (rho = 0.76–0.92), between PD and equal-weight SINDEX (rho = 0.74), and between the two DED timing measures (rho = 0.60).

Age was most closely associated with the OA variables. In the full life-course matrix, age at death was strongly associated with vertebral and total OA and moderately associated with peripheral OA, PD, and equal-weight SINDEX (Table A.13; **Error! Reference source not found.**).

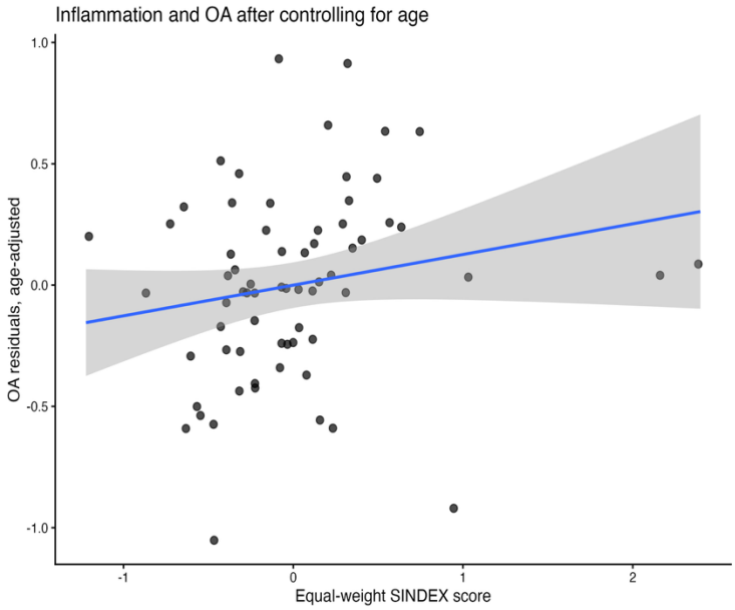

Figure 25 Association between equal-weight SINDEX and age-adjusted OA scores. A weak positive trend remained after controlling for age; the shaded band represents the 95% confidence interval.

The age-adjusted residual plot complicates the SINDEX-OA association (Figure 25). Equal-weight SINDEX and total OA were positively correlated before age adjustment, but the relationship is diffuse once total OA is adjusted for age. Several individuals fall away from the fitted line, and the confidence interval remains broad.

5.6 Covariate-Adjusted Regression Models

Covariate-adjusted regression models provided exploratory checks on the correlation results (Table A.15). The ELS models did not support an adjusted association between developmental indicators and adult inflammatory burden. Stature constraint, CTI constraint, BAA, DED event count, DED depth, and DED timing were not significant in models of equal-weight SINDEX. Age was the only significant term in the combined early-life-to-SINDEX model, b = 0.02, SE = 0.009, p = .042. Component models supported the upper-tail profile structure (Table A.19): PD was more closely related to population and oral variables, while PNBF was less predictable from the measured demographic and oral variables.

The OA models assessed whether OA was associated with inflammatory markers after accounting for age, sex, and population. ELS indicators were not significantly associated with total OA after adjustment, while age remained significant, b = 0.03, SE = 0.009, p = .002. Equal-weight SINDEX was also not significantly associated with total OA once age, sex, and population were included, b = 0.12, SE = 0.11, p = .272. The component-level inflammatory model gave different results for PD and PNBF. PD remained associated with total OA after adjustment, b = 0.23, SE = 0.10, p = .027, while PNBF did not, b = 0.003, SE = 0.04, p = .949. Age also remained significant in this model. PD was not associated with PNBF in the model testing the relationship between the two inflammatory components, b = -0.10, SE = 0.12, p = .368.

5.7 Results Summary

The strongest site-level result was concentrated in periodontal disease. Bruckneudorf had higher equal-weight SINDEX and PD scores than Hirschstetten, and PD had the largest population effect size in the analysis. Age distributions were broadly similar between the cemetery populations, and the PD difference persisted in models that included age, sex, AMTL, and calculus. AMTL was also higher in Bruckneudorf, while calculus presence was widespread in both populations. The strongest population contrast was adult oral inflammatory burden and tooth loss.

PNBF did not produce the site-level pattern seen in PD. It did not differ significantly between populations, was not correlated with PD, and was not predicted by PD, AMTL, calculus, age, sex, or population in exploratory models. Individual-profile inspection showed that high SINDEX values could arise through either PD or PNBF. The population-level SINDEX contrast was PD-driven, while several of the highest individual SINDEX scores were PNBF-driven. The PNBF distribution was shaped partly by individuals with extensive or complex pathological involvement. PNBF contributed to individual inflammatory burden, but it did not reproduce the population-level PD pattern.

ELS indicators showed weaker and more fragmented patterns. Stature, CTI, BAA, DED event count, DED depth, and DED timing had limited associations with adult inflammatory burden in correlation and regression models. DED timing had the clearest developmental pattern, with Bruckneudorf defects more often recorded in earlier-forming enamel. Component-level analyses suggested weak positive relationships between DED timing or DED event count and PNBF activity or severity. Individuals in the upper quartile of PNBF also had earlier preserved DED timing on average than individuals outside the upper quartile. These patterns did not remain significant after correction for multiple testing, but they place the

strongest developmental signal in relation to PNBF rather than PD or equal-weight SINDEX as a whole.

OA did not clearly differ between populations. Age was the strongest OA pattern, and it remained significant in adjusted models. The exploratory inflammatory component model showed that OA aligned more closely with PD than PNBF. This places the strongest adult pattern among age, OA, PD, and AMTL, while PNBF and developmental stress indicators were less consistently connected. These findings indicate that retained developmental markers did not predict adult inflammatory burden in a simple linear pattern within the observable sample.

6. Discussion

Developmental stress can shape later immune regulation, inflammatory response, and repair capacity (Fagundes and Way 2014; Heim et al. 2019; McDade et al. 2017). Clinical, epigenetic, and population studies confirm this biological connection, including the long-term molecular consequences of early adversity and the link between developmental skeletal markers and adult immune function (Anderson et al. 2025; Heijmans et al. 2008). Bioarchaeological work also gives reason to expect adult inflammatory lesions, especially PD and PNBF, to participate in life-course patterns of frailty, survival, and mortality risk. At St Mary Graces, DeWitte and Bekvalac (2010, 2011) found that PD and PNBF co-occurred independently of age, although their developmental stress indicators did not explain that relationship in a simple way. Wigley et al. (2025) likewise places developmental stress, adult inflammatory burden, and mortality risk in the same life-course frame. The Bruckneudorf and Hirschstetten results complicate that expectation. PD showed the strongest cemetery-level contrast, while PNBF did not reproduce the same site pattern. DED timing carried the clearest weak developmental direction, and that direction aligned more closely with PNBF activity and severity than with PD. The results keep the developmental-inflammatory relationship in view, but only at specific tissue scales.

Late Avar social organization gives that separation an archaeological context. Adult cemetery membership is not automatically equivalent to childhood developmental ecology. Patrilocality, female exogamy, remarriage, and household incorporation could bring people with different childhood histories into the same cemetery population, although the sex-stratified results do not make exogamy a demonstrated mechanism in this sample (Gnecchi-Ruscone et al. 2024; Wang et al. 2025). Adult community life added further exposure through food practice, mobility, infection, dental disease, injury, and care (Brooks 2025; Faragó et al. 2022; Klostermann et al. 2025; Vidal-Ronchas et al. 2019).

6.1 Developmental Timing and Tissue-Specific ELS Patterning

Total retained ELS burden appears less informative in these results than the timing of developmental disturbance. Most relationships between ELS indicators and adult inflammatory burden were weak and fragmented. Although DED count, maximum DED depth, stature, CTI, and appendicular asymmetry still describe developmental disturbance, growth investment, or developmental stability, they did not produce a clear directional relationship with adult inflammation. DED timing was also weak and did not survive false-discovery correction, but the direction of the timing pattern was not random within the structure of the results.

DED timing informs when disruption occurred within the forming canine crown. Count records how repetitive retained stress episodes were, and maximum depth records one dimension of defect expression, but neither measure retains the same relation to developmental sequence. This distinction is central because the recorded defects derive from permanent canines. Reid and Dean's anterior tooth formation data place surface-visible permanent canine crown formation broadly from approximately 1.5 to 6 years, with the earlier crown portions falling mainly in the weaning and early post-weaning years (Reid and Dean 2000, 2006). The defects identified in the sample populations record disruption during this childhood interval, when diet, infection, immune development, and care could be changing together. Weaning may also have occurred within this period, although site-specific weaning ages for these cemeteries remain unknown.

The timing signal should not be equated with the timing of immune calibration. Immune and inflammatory regulation begin before, and continue through, the canine formation window, shaped by maternal physiology, infant feeding, microbial exposure, infection, care, and psychosocial stress (Fagundes and Way 2014; Heim et al. 2019; McDade et al. 2017). Earlier-preserved DED may capture a childhood episode within a longer stress trajectory, including recurrence, compounding, or reactivation of vulnerability shaped by earlier conditions.

6.2 Periodontal Burden and Periosteal Response

The component-level results separate periodontal and periosteal inflammation into different life-course patterns. PD and PNBF both fall within the inflammatory life-course frame, but they did not identify the same individuals or reproduce the same population contrast in Bruckneudorf and Hirschstetten. DeWitte and Bekvalac's St Mary Graces analysis showed that PD and periosteal lesions can co-occur independently of age, making shared immune competence, inflammatory response, exposure, or frailty plausible explanations for cross-tissue lesion patterning (DeWitte and Bekvalac 2011). The late Avar data did not reproduce this coupling. High periodontal and periosteal burdens did not consistently identify the same individuals. The expected inflammatory link remains biologically plausible, although in this sample its osteological expression diverged between PD and PNBF.

The periodontal side of this division was concentrated at Bruckneudorf. PD increased with age in both cemeteries, but Bruckneudorf remained higher across much of the age range, despite broadly overlapping age distributions. Calculus presence was widespread in both groups, so the available calculus variable does not explain the PD contrast. The stronger inference is differential disease progression: chronic oral challenge became more destructive at Bruckneudorf, through some combination of duration, severity, tooth retention, wear, host response, repair capacity, or survival with alveolar tissue loss. Retained ELS markers did not explain this pattern directly. If developmental stress shaped periodontal vulnerability, its effect was filtered through later oral conditions and host-mediated tissue response.

PNBF followed a different distribution. It did not reproduce the Bruckneudorf PD pattern, did not increase clearly with age, and did not track PD burden across the combined sample. High-PNBF profiles occurred in both cemeteries and were concentrated in the upper tail of the individual-level PNBF score distribution. Most individuals did not show extensive PNBF; a smaller subset carried more severe, active, or widely distributed periosteal change.

That upper-tail structure is consistent with periosteal response requiring later activation conditions that affected some individuals more strongly than others. Infection, injury, vascular disturbance, chronic irritation, repair stage, duration, and survival can each shape whether periosteal new bone formation occurs (Allen et al. 2023; Klaus 2014; Weston 2008). In Bruckneudorf and Hirschstetten, the conditions producing periodontal destruction and periosteal activation appear to have been distributed differently.

That pattern is compatible with a hyperresponsive inflammatory-repair phenotype, but it does not demonstrate one directly. Macroscopic PNBF cannot identify cytokine activity, immune calibration, pathogen exposure, or osteoimmune signalling. It can show that individuals with earlier-preserved developmental disruption were also more likely to appear in the part of the sample where periosteal response became stronger. If early stress shaped inflammatory thresholds or repair capacity, the effect would only become skeletal when later exposure, infection, injury, or repair demand activated the periosteum. The weak DED timing-PNBF relationship points to differential response intensity, not a simple relationship between developmental stress and lesion presence.

6.3 Case Profiles and Nonlinear Life-Course Patterning

The statistical results showed weak and fragmented ELS-to-inflammation associations. The clearest developmental direction was around DED timing and PNBF, rather than PD or equal-weight SINDEX as a whole. At the individual level, these variables occurred together within the same skeletal histories, along with age, pathology, repair, and survival. Looking at the profiles at this scale helps explain why the developmental-inflammatory pattern is treated as conditional rather than directly predictive.

6.3.1 NHMW-Anthro-Oste-27.291 Grave 836

NHMW-Anthro-Oste-27.291 was estimated 18.5 years old at death and had extensive PNBF across the pelvis and lower limbs, including the ilia, ischia, femora, tibiae, fibulae, tali, and foot elements. The distribution is too widespread for a localized traumatic explanation, but it does not clearly match one named infectious pattern. No specific diagnosis was assigned in the pathology notes. The differential diagnosis remains broad, centred on a chronic inflammatory or infectious process capable of producing extensive periosteal activation across the lower body.

NHMW-Anthro-Oste-27.291 had one of the most severe, active, and anatomically extensive PNBF profiles in the sample, while PD remained low. The high inflammatory score was carried by periosteal response rather than periodontal disease. The developmental profile was mainly dental because stature, sex-standardized CTI, and appendicular asymmetry were not available or not interpretable for this individual. NHMW-Anthro-Oste-27.291 had four recorded DED events, moderate maximum DED depth, and earlier-preserved canine DED timing.

6.3.2 Hirschstetten Individual 109 SE 566 OBJ 154

Hirschstetten 109 was estimated 18.5 years old at death and had a more focal periosteal profile than NHMW-Anthro-Oste-27.291. PNBF was recorded on the left humerus, left femur, and left tibia, with possible fibular involvement. The unilateral distribution keeps the differential diagnosis centred on a local or asymmetrical skeletal process, with a generalized metabolic explanation less likely. Other skeletal observations included abnormal activity near the left radial tuberosity, lumbar vertebral collapse considered extreme for age, and possible porous or blastic activity at the femoral head. A neoplastic process was considered, but no diagnosis was confirmed.

The developmental profile was mixed. 109 had three recorded DED events, a high maximum DED depth, and earlier-preserved DED timing. Stature and CTI did not indicate generalized growth constraint: stature z-score was positive, and CTI was not thinned. PD remained low, while PNBF was elevated through severity, activity, bone count, and lesion count. Severe enamel disruption and earlier-preserved timing occurred alongside a young-age periosteal lesion pattern, while broader growth measures remained unremarkable.

6.3.3 NHMW-Anthro-Oste-27.323 Grave 894_1

NHMW-Anthro-Oste-27.323 was a male adult, approximately 45 years old at death. PNBF was absent and no additional diagnostic pathology was recorded for this individual. PD remained low. CTI was preserved and did not indicate cortical thinning, while stature and appendicular asymmetry were not available.

The developmental record was mainly dental. NHMW-Anthro-Oste-27.323 had three recorded DED events, shallow maximum DED depth, and earlier-preserved canine DED timing. Earlier-preserved developmental disruption was retained in enamel, yet PNBF was absent, PD remained low, and overall inflammatory burden was low. Earlier DED timing could persist without later macroscopic inflammatory expression.

6.3.4 Case Synthesis

Earlier-preserved DED timing recurs across the three profiles, but the later skeletal trajectories diverge. This follows the pattern seen in the wider analysis, where DED timing was the clearest developmental signal but did not translate into a consistent adult inflammatory outcome. In these cases, the same kind of developmental evidence appears with severe periosteal response, focal periosteal response, and little macroscopic inflammatory expression. The shared dental timing therefore does not resolve into one adult lesion pattern.

In the two young individuals, the developmental record was carried into periosteal response through different lesion histories. NHMW-Anthro-Oste-27.291 had severe, active, and anatomically extensive PNBF, suggesting a broad inflammatory or infectious process. Hirschstetten 109 also had elevated PNBF, but the distribution was focal and asymmetrical. These two cases both connect earlier-preserved DED timing with periosteal response, but through different forms of later skeletal activation. In the older adult, NHMW-Anthro-Oste-27.323, earlier-preserved DED timing remained primarily a dental trace. PNBF was absent, PD remained low, and overall inflammatory burden was limited. The contrast is therefore not between developmental stress present or absent, but between different adult conditions under which a similar developmental record became, or did not become, connected to macroscopic inflammatory change.

Age and survival make the contrast less straightforward. The older adult had the longest period in which later exposure could have occurred, but he did not have high PNBF, high PD, or high overall inflammatory burden. Earlier-preserved DED timing remained mainly a dental record. Longer survival meant more time for later exposure, but also more time for healing, remodelling, or for inflammatory episodes to leave little visible periosteal trace. The two young individuals had less adult survival time, but PNBF was already severe or elevated. Their profiles require later activation: some infectious, inflammatory, traumatic, or other pathological demand had to be strong enough for periosteal bone to form and remain visible. This contrast narrows the life-course claim: earlier DED timing may mark developmental disturbance, but adult inflammatory expression depended on later tissue demand, pathology, repair conditions, and survival.

That expression is biocultural as well as physiological. Exposure to infection or injury was shaped by movement, work, household tasks, proximity to people and animals, food access, and care during illness or recovery. Repair required time, energy, and survival long

enough for periosteal response to mineralize. Earlier DED timing may mark developmental disturbance, but it did not determine whether PNBF would appear. That depended on later conditions: the kind of pathology encountered, the intensity of tissue demand, the resources available for repair, and whether new bone formed, remodelled, and remained visible. Developmental disturbance may have altered susceptibility, inflammatory threshold, or repair capacity, but those effects could only become visible when later conditions produced a skeletal response.

6.4 Population, Sex, and Inference Scale

PD was the clearest population-level inflammatory pattern. It crossed estimated sex groups at Bruckneudorf, while DED variables, CTI, appendicular asymmetry, and PNBF did not form the same stable cemetery contrast. The strongest population-level inference is therefore periodontal. Developmental stress and periosteal response remained weaker, more conditional, or more individual. Patrilocality and female exogamy make adult cemetery membership an imperfect proxy for childhood developmental ecology, since some adults buried in a cemetery may have grown elsewhere (Gnecchi-Ruscone et al. 2024; Wang et al. 2025). Female developmental markers did not show a strong site-specific pattern that would support exogamous childhood heterogeneity as the explanation. If local male continuity structured childhood exposure, stronger male site differences might be expected; the male DED timing effects were among the larger directional contrasts but were not stable enough to carry that interpretation. Sex-stratified lifeways remain possible at the level of task, mobility, diet, and care, but the measured variables did not isolate a dominant sex-specific inflammatory pathway.

6.5 Osteoarthritis and Adult Accumulation

OA was included as an exploratory check on whether joint remodelling belonged to the same inflammatory burden pattern as PD, PNBF, or ELS. This was biologically plausible because OA involves inflammatory participation within joint-level degeneration, even though its skeletal expression remains strongly shaped by local mechanics and remodelling (Fernandes et al. 2002; Thielen et al. 2021; Mukherjee and Das 2024). In this sample, OA did not clearly separate Bruckneudorf and Hirschstetten. Age structured OA more consistently than population, placing the OA pattern within age-progressive joint change, mobility, activity, and adult tissue maintenance (Becker 2020; Crubézy et al. 2002; Molnar et al. 2011).

The OA correlations narrowed the exploratory question. OA aligned more clearly with PD than with PNBF, while ELS indicators did not align clearly with OA after adjustment. The OA-PD association stays at the level of co-occurrence between age-associated joint remodelling and periodontal burden. OA also did not behave like the PNBF response-intensity pattern. The macroscopic OA variables recorded here did not capture a developmental-stress pathway, even though developmental calibration of later joint biology remains biologically plausible. In this dataset, OA remains contextual adult accumulation evidence and does not support expansion of equal-weight SINDEX as a comparable inflammatory component.

7. Conclusion

The developmental-inflammatory relationship emerged here as a problem of translation. Clinical and population research makes the biological link plausible, but the Bruckneudorf and Hirschstetten skeletons did not preserve that link as a simple gradient from retained developmental stress to adult inflammatory burden. Equal-weight SINDEX identified visible skeletal-dental inflammatory burden, but the developmental signal became interpretable only after the score was separated into its lesion components. DED timing showed the clearest developmental direction. PD showed the strongest cemetery-level adult contrast and aligned most closely with chronic periodontal burden. PNBF expressed a weak developmental timing signal through severity, activity, and anatomical extent.

Different tissue systems preserved different parts of the life-course pattern. Enamel retained the timing of childhood disruption within the preserved canine crown sequence. Alveolar bone recorded chronic periodontal progression accumulated through later life. Periosteal surfaces recorded response intensity, especially where PNBF became severe, active, or anatomically extensive. Joint surfaces recorded age-structured remodelling and remained contextual to the developmental argument. Population and sex patterns strengthened the Bruckneudorf periodontal finding, but they did not support broader claims about shared childhood ecology, exogamy, or a dominant sex-specific inflammatory pathway.

This thesis treats ELS as conditional vulnerability: a developmental history that may alter inflammatory threshold, repair capacity, or physiological reserve without fixing the lesions that later become visible. Similar retained developmental evidence led into different skeletal outcomes, depending on whether later life produced tissue demand strong enough to activate periosteal response. Exposure to infection or injury, labour, mobility, provisioning, care, recovery, repair demand, and survival shaped whether earlier vulnerability remained latent or became recorded in bone. The DED timing-PNBF pattern is strongest at the level of

response intensity. Earlier-preserved developmental disruption aligned most closely with severe, active, or anatomically extensive PNBF, while lesion presence alone appeared to be less connected. The thesis supports conditional expression of developmental vulnerability, not causal proof of developmental programming.

The skeletal and dental variables used here record retained tissue outcomes: enamel disruption, alveolar destruction, periosteal new bone, and joint remodelling. They cannot directly identify immune calibration, cytokine activity, pathogen exposure, osteoimmune signalling, microbiome, hygiene, diet texture, or childhood residence history. Preservation, dental wear, observable surfaces, and missing data also shaped which relationships could be tested. Cross-domain models required complete cases, reducing sample size where dental, skeletal, inflammatory, demographic, and age data did not overlap. The DED timing-PNBF relationship remains exploratory because it did not survive correction for multiple testing, although its direction is biologically coherent within the tissue structure of the results. The strongest claim stays at the macroscopic scale: these data identify where developmental timing and inflammatory-repair response became retained in mineralized tissue, while the regulatory and molecular processes behind that pattern remain inferred.

The macroscopic pattern developed here provides a contrast-based sampling logic for future work. The strongest contrasts are not limited to the most visually dramatic lesions: high PNBF with earlier-preserved DED timing, earlier-preserved DED timing with low inflammatory burden, high-PD periodontal burden, and lower-burden controls could be used to test a different part of the life-course model. Proteomic analysis could assess whether those contrasts correspond to differences in host inflammatory response, osteoimmune signalling, pathogen-associated signatures, bone matrix remodelling, collagen turnover, or repair phenotype. Kinship and isotopic data could further separate childhood origin, mobility, diet or provisioning, and adult cemetery membership.

Bibliography

Abbas, Abul K., Andrew H. Lichtman, and Shiv Pillai. 2012. *Cellular and Molecular Immunology*. 7th ed. Saunders/Elsevier. http://ebookcentral.proquest.com/lib/umanitoba/detail.action?docID=1430392.

Agarwal, Sabrina C. 2016. 'Bone Morphologies and Histories: Life Course Approaches in Bioarchaeology'. *American Journal of Physical Anthropology* 159 (S61): 131–49. https://doi.org/10.1002/ajpa.22905.

Allen, Hailey, Nicholas C. Barnthouse, and Brian Y. Chan. 2023. 'Periosteal Pathologic Conditions: Imaging Findings and Pathophysiology'. *Radiographics* 43 (2): e220120. https://doi.org/10.1148/rg.220120.

AlQahtani, S. J., M. P. Hector, and H. M. Liversidge. 2010. 'Brief Communication: The London Atlas of Human Tooth Development and Eruption'. *American Journal of Physical Anthropology* 142 (3): 481–90. https://doi.org/10.1002/ajpa.21258.

Anderson, Amy S., Aaron Blackwell, M. Linda Sutherland, et al. 2025. 'Childhood Skeletal Lesions Common in Prehistory Are Present in Living Forager-Farmers and Predict Adult Markers of Immune Function'. *Science Advances*, 1–13. https://doi.org/10.1126/sciadv.adw3697.

Anderson, Amy S., and Sharon N. DeWitte. 2026. 'Known Unknowns and the Osteological Paradox: Why Bioarchaeology Needs Agent-Based Models'. *International Journal of Paleopathology* 52 (March): 32–43. https://doi.org/10.1016/j.ijpp.2025.11.004.

Antoine, Daniel, Charles M. FitzGerald, and Jerome C. Rose. 2018. 'Incremental Structures in Teeth: Keys to Unlocking and Understanding Dental Growth and Development'. In *Biological Anthropology of the Human Skeleton*, 1st edn, edited by M. Anne Katzenberg and Anne L. Grauer. Wiley. https://doi.org/10.1002/9781119151647.ch7.

Antoine, Daniel, Simon Hillson, and M. Christopher Dean. 2009. 'The Developmental Clock of Dental Enamel: A Test for the Periodicity of Prism Cross-Striations in Modern Humans and an Evaluation of the Most Likely Sources of Error in Histological Studies of This Kind'. *Journal of Anatomy* 214 (1): 45–55. https://doi.org/10.1111/j.1469-7580.2008.01010.x.

Armelagos, George J., Alan H. Goodman, Kristin N. Harper, and Michael L. Blakey. 2009. 'Enamel Hypoplasia and Early Mortality: Bioarcheological Support for the Barker Hypothesis'. *Evolutionary Anthropology: Issues, News, and Reviews* 18 (6): 261–71. https://doi.org/10.1002/evan.20239.

Atar, Michael, and Egbert J. Körperich. 2010. 'Systemic Disorders and Their Influence on the Development of Dental Hard Tissues: A Literature Review'. *Journal of Dentistry* 38 (4): 296–306. https://doi.org/10.1016/j.jdent.2009.12.001.

Austin, Christine, Tanya M. Smith, Ramin M. Z. Farahani, et al. 2016. 'Uncovering System-Specific Stress Signatures in Primate Teeth with Multimodal Imaging'. *Scientific Reports* 6 (1): 18802. https://doi.org/10.1038/srep18802.

Baker, Jack, and Osbjorn M. Pearson. 2006. 'Statistical Methods for Bioarchaeology: Applications of Age-Adjustment and Logistic Regression to Comparisons of Skeletal Populations with Differing Age-Structures'. *Journal of Archaeological Science* 33 (2): 218–26. https://doi.org/10.1016/j.jas.2005.07.019.

Barker, DJP. 1986. 'Infant Mortality, Childhood Nutrition, and Ischaemic Heart Disease in England and Wales'. *The Lancet* 327 (8489): 1077–81. https://doi.org/10.1016/S0140-6736(86)91340-1.

Barker, DJP. 1990. 'The Fetal and Infant Origins of Adult Disease'. *BMJ* 301 (6761): 1111–1111. https://doi.org/10.1136/bmj.301.6761.1111.

Barker, DJP. 2012. 'Developmental Origins of Chronic Disease'. *Public Health* 126 (3): 185–89. https://doi.org/10.1016/j.puhe.2011.11.014.

Barker, DJP, A. R. Bull, C. Osmond, and S. J. Simmonds. 1990. 'Fetal and Placental Size and Risk of Hypertension in Adult Life'. *BMJ* 301 (6746): 259–62. https://doi.org/10.1136/bmj.301.6746.259.

Barker, DJP, Johan G. Eriksson, Eero Kajantie, et al. 2010. 'The Maternal and Placental Origins of Chronic Disease'. In *The Placenta and Human Developmental Programming*, 1st edn, edited by Graham J. Burton, DJP Barker, Ashley Moffett, and Kent Thornburg. Cambridge University Press. https://doi.org/10.1017/CBO9780511933806.003.

Barker, DJP, and C. Osmond. 1987. 'Death Rates from Stroke in England and Wales Predicted from Past Maternal Mortality'. *BMJ* 295 (6590): 83–86. https://doi.org/10.1136/bmj.295.6590.83.

Barker, DJP, C. Osmond, and C. M. Law. 1989. 'The Intrauterine and Early Postnatal Origins of Cardiovascular Disease and Chronic Bronchitis'. *Journal of Epidemiology & Community Health* 43 (3): 237–40. https://doi.org/10.1136/jech.43.3.237.

Bateson, Patrick, Peter Gluckman, and Mark Hanson. 2014. 'The Biology of Developmental Plasticity and the Predictive Adaptive Response Hypothesis'. *The Journal of Physiology* 592 (11): 2357–68. https://doi.org/10.1113/jphysiol.2014.271460.

Becker, Sara K. 2020. 'Osteoarthritis, Entheses, and Long Bone Cross-Sectional Geometry in the Andes: Usage, History, and Future Directions'. *International Journal of Paleopathology*, The Paleopathology of Andean South America: 20 Years of Advances and Future Prospects, vol. 29 (June): 45–53. https://doi.org/10.1016/j.ijpp.2019.08.005.

Benjamini, Yoav, and Yosef Hochberg. 1995. 'Controlling the False Discovery Rate: A Practical and Powerful Approach to Multiple Testing'. *Journal of the Royal Statistical Society Series B: Statistical Methodology* 57 (1): 289–300. https://doi.org/10.1111/j.2517-6161.1995.tb02031.x.

Birch, W., and M. C. Dean. 2014. 'A Method of Calculating Human Deciduous Crown Formation Times and of Estimating the Chronological Ages of Stressful Events Occurring During Deciduous Enamel Formation'. *Journal of Forensic and Legal Medicine* 22 (February): 127–44. https://doi.org/10.1016/j.jflm.2013.12.002.

Bocaege, E., and S. Hillson. 2016. ‘Disturbances and Noise: Defining Furrow-Form Enamel Hypoplasia’. *American Journal of Physical Anthropology* 161 (4): 744–51. https://doi.org/10.1002/ajpa.23070.

Brickley, Megan B. 2024. ‘Perspectives on Anemia: Factors Confounding Understanding of Past Occurrence’. *International Journal of Paleopathology* 44 (March): 90–104. https://doi.org/10.1016/j.ijpp.2023.12.001.

Brooks, Alexis. 2025. ‘Observing Tuberculosis and Brucellosis in the Austrian Avar Population’. Master of Arts, University of Manitoba.

Bühler, Birgit, and Sylvia Kirchengast. 2022. ‘Horse-Riding as a Habitual Activity among the Early Medieval Avar Population of the Cemetery of Csokorgasse (Vienna): Sex and Chronological Differences’. *International Journal of Osteoarchaeology* 32 (4): 821–31. https://doi.org/10.1002/oa.3107.

Buikstra, Jane E., Douglas H. Ubelaker, and David Aftandilian, eds. 1994. *Standards for Data Collection from Human Skeletal Remains Proceedings of a Seminar at the Field Museum of Natural History*. With D. Aftandilian, J. E. Buikstra, M. Finnegan, et al. Arkansas Archeological Survey.

Bultink, Irene E. M., and Willem F. Lems. 2013. ‘Osteoarthritis and Osteoporosis: What Is the Overlap?’ *Current Rheumatology Reports* 15 (5): 328. https://doi.org/10.1007/s11926-013-0328-0.

Cares Henriquez, Alejandra, and Marc F. Oxenham. 2020. ‘A New Comprehensive Quantitative Approach for the Objective Identification and Analysis of Linear Enamel Hypoplasia (LEH) in Worn Archaeological Dental Assemblages’. *Journal of Archaeological Science* 113 (January): 105064. https://doi.org/10.1016/j.jas.2019.105064.

Carroll, Joseph, Mathias Clasen, Emelie Jonsson, et al. 2017. ‘Biocultural Theory: The Current State of Knowledge’. *Evolutionary Behavioral Sciences* 11 (1): 1–15. https://doi.org/10.1037/ebs0000058.

Caut, Stéphane, Elena Angulo, and Franck Courchamp. 2009. ‘Variation in Discrimination Factors (Δ^{15} N and Δ^{13} C): The Effect of Diet Isotopic Values and Applications for Diet Reconstruction’. *Journal of Applied Ecology* 46 (2): 443–53. https://doi.org/10.1111/j.1365-2664.2009.01620.x.

Cekici, Ali, Alpdogan Kantarci, Hatice Hasturk, and Thomas E. Van Dyke. 2014. ‘Inflammatory and Immune Pathways in the Pathogenesis of Periodontal Disease’. *Periodontology 2000* 64 (1): 57–80. https://doi.org/10.1111/prd.12002.

Chavda, Vivek P., Jack Feehan, and Vasso Apostolopoulos. 2024. ‘Inflammation: The Cause of All Diseases’. *Cells* 13 (22): 1906. https://doi.org/10.3390/cells13221906.

Chen, Ting, Han-xiao Liu, Hui-yi Yan, Dong-mei Wu, and Jie Ping. 2016. ‘Developmental Origins of Inflammatory and Immune Diseases’. *Molecular Human Reproduction* 22 (8): 858–65. https://doi.org/10.1093/molehr/gaw036.

Cheverko, Colleen M., and Mark Hubbe. 2017. ‘Comparisons of Statistical Techniques to Assess Age-Related Skeletal Markers in Bioarchaeology’. *American Journal of Physical Anthropology* 163 (2): 407–16. https://doi.org/10.1002/ajpa.23206.

Clark, George A., Nicholas R. Hall, George J. Armelagos, Gary A. Borkan, Manohar M. Panjabi, and F. Todd Wetzel. 1986. ‘Poor Growth Prior to Early Childhood: Decreased Health and Life-Span in the Adult’. *American Journal of Physical Anthropology* 70 (2): 145–60. https://doi.org/10.1002/ajpa.1330700202.

Crespo, Fabian. 2020. ‘Reconstructing Immune Competence In Skeletal Samples’. In *Theoretical Approaches in Bioarchaeology*, 1st edn, edited by Colleen M. Cheverko, Julia R. Prince-Buitenhuys, and Mark Hubbe. Routledge. https://doi.org/10.4324/9780429262340-6.

Crubézy, Eric, Jérome Goulet, Bruzek Jaruslav, Jelinek Jan, Rougé Daniel, and Ludes Bertrand. 2002. ‘Epidemiology of Osteoarthritis and Enthesopathies in a European Population Dating Back 7700 Years’. *Joint Bone Spine* 69 (6): 580–88. https://doi.org/10.1016/S1297-319X(02)00455-4.

Csáky, Veronika, Dániel Gerber, István Koncz, et al. 2020. ‘Genetic Insights into the Social Organisation of the Avar Period Elite in the 7th Century AD Carpathian Basin’. *Scientific Reports* 10 (1): 948. https://doi.org/10.1038/s41598-019-57378-8.

Cunningham, Craig, Louise Scheuer, and Sue M. Black. 2016. *Developmental Juvenile Osteology*. Second edition. Elsevier/AP, Academic Press is an imprint of Elsevier.

Curta, Florin. 2021. ‘A Social History of the Avars: Historical and Archaeological Perspectives’. *History Compass* 19 (12): e12697. https://doi.org/10.1111/hic3.12697.

Daim, Falko. 2003. ‘Avars and Avar Archaeology. An Introduction.’ In *Regna and Gentes: The Relationship between Late Antique and Early Medieval Peoples and Kingdoms in the Transformation of the Roman World*, edited by Hans-Werner Goetz, Jörg Jarnut, Walter Pohl, and Sören Kaschke. Transformations of the Roman World, edited by Ian Wood, vol. 13. Brill. https://www.academia.edu/22649118/Avars_and_Avar_Archaeology_An_Introduction_In_Regna_and_gentes_The_relationship_between_late_antique_and_early_medieval_peoples_and_kingdoms_in_the_transformation_of_the_Roman_world_ed_Hans_Werner_Goetz_et_al_Transformation_of_the_Roman_World_13_Leiden_2003_463_570.

Daskalakis, N. P., and R. Yehuda. 2014. ‘Programming The HPA-Axis By Early Life Experience: Mechanisms Of Stress Susceptibility And Adaptation’. *Frontiers*, 8.

De Coster, Greet, Stefan Van Dongen, Phillista Malaki, et al. 2013. ‘Fluctuating Asymmetry and Environmental Stress: Understanding the Role of Trait History’. *PLOS One* 8 (3): e57966. https://doi.org/10.1371/journal.pone.0057966.

De Leon-Oliva, Diego, Silvestra Barrena-Blázquez, Laura Jiménez-Álvarez, et al. 2023. ‘The RANK–RANKL–OPG System: A Multifaceted Regulator of Homeostasis, Immunity, and Cancer’. *Medicina* 59 (10): 1752. https://doi.org/10.3390/medicina59101752.

DeWitte, Sharon N., and Jelena Bekvalac. 2010. ‘Oral Health and Frailty in the Medieval English Cemetery of St Mary Graces’. *American Journal of Physical Anthropology* 142 (3): 341–54. https://doi.org/10.1002/ajpa.21228.

DeWitte, Sharon N., and Jelena Bekvalac. 2011. ‘The Association Between Periodontal Disease and Periosteal Lesions in the St. Mary Graces Cemetery, London, England, A.D. 1350–1538’. *American Journal of Physical Anthropology* 146 (4): 609–18. https://doi.org/10.1002/ajpa.21622.

DeWitte, Sharon N., and Mary Lewis. 2021. ‘Medieval Menarche: Changes in Pubertal Timing before and after the Black Death’. *American Journal of Human Biology* 33 (2): e23439. https://doi.org/10.1002/ajhb.23439.

DeWitte, Sharon N., and James Wood. 2008. ‘Selectivity of Black Death Mortality with Respect to Preexisting Health’. *Proceedings of the National Academy of Sciences* 105 (5): 1436–41. https://doi.org/10.1073/pnas.0705460105.

Dietert, Rodney R., and Amrie C. Grammer. 2016. ‘Immune Disorders, Epigenetics, And The Developmental Origins Of Health And Disease’. In *The Epigenome and Developmental Origins of Health and Disease*. Elsevier. https://doi.org/10.1016/B978-0-12-801383-0.00012-8.

Dutcher, Ethan G., E. A. Claudia Pama, Mary-Ellen Lynall, et al. 2020. ‘Early-Life Stress and Inflammation: A Systematic Review of a Key Experimental Approach in Rodents’. *Brain and Neuroscience Advances* 4 (January): 239821282097804. https://doi.org/10.1177/2398212820978049.

Entringer, Sonja, and Christine Heim. 2024. ‘A Brief Historic Review of Research on Early Life Stress and Inflammation across the Lifespan’. *Neuroimmunomodulation* 32 (1): 24–35. https://doi.org/10.1159/000542676.

Epsley, Scott, Samuel Tadros, Alexander Farid, Daniel Kargilis, Sameer Mehta, and Chamith S. Rajapakse. 2021. ‘The Effect of Inflammation on Bone’. *Frontiers in Physiology* 11 (January): 511799. https://doi.org/10.3389/fphys.2020.511799.

Fagundes, Christopher P., and Baldwin Way. 2014. ‘Early-Life Stress and Adult Inflammation’. *Current Directions in Psychological Science* 23 (4): 277–83. https://doi.org/10.1177/0963721414535603.

Faragó, Norbert, Erwin Gáll, Bence Gulyás, et al. 2022. ‘Dietary and Cultural Differences between Neighbouring Communities: A Case Study on the Early Medieval Carpathian Basin (Avar and Post-Avar Period, 7th–9th/10th Centuries AD)’. *Journal of Archaeological Science: Reports* 42 (April): 103361. https://doi.org/10.1016/j.jasrep.2022.103361.

Farmer, Paul. 2004. ‘An Anthropology of Structural Violence’. *Current Anthropology* 45 (3): 305–25. https://doi.org/10.1086/382250.

Fernandes, Julio C., Johanne Martel-Pelletier, and Jean-Pierre Pelletier. 2002. ‘The Role of Cytokines in Osteoarthritis Pathophysiology’. *Biorheology* 39 (1–2): 237–46.

Fournié, Guillaume, Dirk U. Pfeiffer, and Robin Bendrey. 2017. 'Early Animal Farming and Zoonotic Disease Dynamics: Modelling Brucellosis Transmission in Neolithic Goat Populations'. *Royal Society Open Science* 4 (2): 160943. https://doi.org/10.1098/rsos.160943.

Gaddis, Katherine E. 2018. 'Stress and Frailty in Medieval Prussia: Interpretations From Skeletal Remains at Bezławki'. Master's Thesis. Humboldt State University.

Galson, Deborah L., and G. David Roodman. 2011. 'Origins of Osteoclasts'. In *Osteoimmunology: Interactions of the Immune and Skeletal Systems*, 1st ed, by Joseph Lorenzo. Elsevier/Academic. https://linkinghub.elsevier.com/retrieve/pii/B9780123756701100020.

Gamble, Julia A., and Gillian Bentley. 2022. 'Developmental Origins of Health and Disease (DOHaD): Perspectives From Bioarchaeology'. In *Palaeopathology and Evolutionary Medicine*, by Julia A. Gamble and Gillian Bentley. Oxford University Press. https://doi.org/10.1093/oso/9780198849711.003.0002.

Gamble, Julia A., Michaela Binder, Tobias Bendeguz, Jasmin Özyurt, and Martin Penz. 2024. 'A Possible Case of Leprosy in Avar-Period Austria'.

Gamble, Julia A., and S. B. Milne. 2018. 'Using LEXT Laser-Scanning Confocal Microscopy to Identify Enamel Surface Defects in Archaeological Caribou Dentition: A Pilot Study from Southern Baffin Island, Nunavut, Canada'. *Journal of Archaeological Science: Reports* 18: 847–57.

Gausterer, Christian, Christina Stein, and Maria Teschler-Nicola. 2011. *First Confirmed Evidence of Leprosy in Early Medieval Austria*.

Ghaseminejad-Raeini, Amirhossein, Alireza Azarboo, Negar Zareshahi, et al. 2025. 'Early-Life Famine Exposure and Risk of Osteoporosis and Low Bone Mineral Density: A Systematic Review and Meta-Analysis'. *Osteoporosis International* 36 (1): 21–34. https://doi.org/10.1007/s00198-024-07250-x.

Gluckman, Peter D., and Mark A. Hanson. 2004. 'Developmental Origins of Disease Paradigm: A Mechanistic and Evolutionary Perspective'. *Pediatric Research* 56 (3): 311–17. https://doi.org/10.1203/01.PDR.0000135998.08025.FB.

Gnecchi-Ruscone, Guido Alberto, Zsófia Rácz, Levente Samu, et al. 2024. 'Network of Large Pedigrees Reveals Social Practices of Avar Communities'. *Nature* 629 (8011): 376–83. https://doi.org/10.1038/s41586-024-07312-4.

Godfrey, Keith M., Karen A. Lillycrop, Graham C. Burdge, Peter D. Gluckman, and Mark A. Hanson. 2007. 'Epigenetic Mechanisms and the Mismatch Concept of the Developmental Origins of Health and Disease'. *Pediatric Research* 61 (5 Part 2): 5R-10R. https://doi.org/10.1203/pdr.0b013e318045bedb.

Goldstein, Jeffery A., Kelly Gallagher, Celeste Beck, Rajesh Kumar, and Alison D. Gernand. 2020. 'Maternal-Fetal Inflammation in the Placenta and the Developmental Origins of Health and Disease'. *Frontiers in Immunology* 11 (November): 531543. https://doi.org/10.3389/fimmu.2020.531543.

Goodman, Alan H., and George J. Armelagos. 1989. ‘Infant and Childhood Morbidity and Mortality Risks in Archaeological Populations’. *World Archaeology* 21 (2): 225–43. https://doi.org/10.1080/00438243.1989.9980103.

Goodman, Alan H., and Jerome C. Rose. 1990. ‘Assessment of Systemic Physiological Perturbations From Dental Enamel Hypoplasias and Associated Histological Structures’. *American Journal of Physical Anthropology* 33 (S11): 59–110. https://doi.org/10.1002/ajpa.1330330506.

Gowland, R. L. 2015. ‘Entangled Lives: Implications of the Developmental Origins of Health and Disease Hypothesis for Bioarchaeology and the Life Course’. *American Journal of Physical Anthropology* 158 (4): 530–40. https://doi.org/10.1002/ajpa.22820.

Gowland, R. L., and J. L. Caldwell. 2023. ‘The Developmental Origins of Health and Disease: Implications for Paleopathology’. In *The Routledge Handbook of Paleopathology*, 1st edn, edited by Anne L. Grauer. Routledge. https://doi.org/10.4324/9781003130994.

Gowland, R. L., J. L. Caldwell, and A. Grauer. 2023. ‘The Developmental Origins of Health and Disease: Implications for Paleopathology’. In *The Routledge Handbook of Paleopathology*. University of Veterinary Medicine Vienna. https://www.vetmeduni.ac.at/en/infoservice/presseinformation/press-releases-2015/complete-camel-skeleton-unearthed-in-austria/.

Graham, John, and Bariş Özener. 2016. ‘Fluctuating Asymmetry of Human Populations: A Review’. *Symmetry* 8 (12): 154–89. https://doi.org/10.3390/sym8120154.

Hales, C., and D. Barker. 2013. ‘Type 2 (Non-Insulin-Dependent) Diabetes Mellitus: The Thrifty Phenotype Hypothesis’. *International Journal of Epidemiology* 42 (5): 1215–22. https://doi.org/10.1093/ije/dyt133.

Hanson, M. A., and P. D. Gluckman. 2014. ‘Early Developmental Conditioning of Later Health and Disease: Physiology or Pathophysiology?’ *Physiological Reviews* 94 (4): 1027–76. https://doi.org/10.1152/physrev.00029.2013.

Hassett, Brenna R. 2012. ‘Evaluating Sources of Variation in the Identification of Linear Hypoplastic Defects of Enamel: A New Quantified Method’. *Journal of Archaeological Science* 39 (2): 560–65. https://doi.org/10.1016/j.jas.2011.10.017.

He, Qiang, Zhen Wang, Jie Mei, Chengxin Xie, and Xin Sun. 2024. ‘Relationship Between Systemic Immune-Inflammation Index and Osteoarthritis: A Cross-Sectional Study From the NHANES 2005–2018’. *Frontiers in Medicine* 11 (August). https://doi.org/10.3389/fmed.2024.1433846.

Heijmans, Bastiaan T., Elmar W. Tobi, Aryeh D. Stein, et al. 2008. ‘Persistent Epigenetic Differences Associated With Prenatal Exposure to Famine in Humans’. *Proceedings of the National Academy of Sciences* 105 (44): 17046–49. https://doi.org/10.1073/pnas.0806560105.

Heim, Christine M., Sonja Entringer, and Claudia Buss. 2019. ‘Translating Basic Research Knowledge on the Biological Embedding of Early-Life Stress Into Novel Approaches

for the Developmental Programming of Lifelong Health'. *Psychoneuroendocrinology* 105 (July): 123–37. https://doi.org/10.1016/j.psyneuen.2018.12.011.

Herold, Hajnalka. 2013. *The Avar Period Settlement and the Ceramic Finds from the Cemetery in Zillingtal, Burgenland, Eastern Austria*. Verlag Marie Leidorf. https://ore.exeter.ac.uk/repository/handle/10871/14586.

Herold, Martina. 2008. 'Sex Differences in Mortality in Lower Austria and Vienna in the Early Medieval Period: An Investigation and Evaluation of Possible Contributing Factors'. Dissertation, Universität Wien.

Hillson, S. W., ed. 2014. 'Dental Markers of Disease and Malnutrition'. In *Tooth Development in Human Evolution and Bioarchaeology*. Cambridge University Press. https://doi.org/10.1017/CBO9780511894916.007.

Hillson, S. W., and S. Bond. 1997. 'Relationship of Enamel Hypoplasia to the Pattern of Tooth Crown Growth: A Discussion'. *American Journal of Physical Anthropology* 104 (1): 89–103. https://doi.org/10.1002/(SICI)1096-8644(199709)104:1%3C89::AID-AJPA6%3E3.0.CO;2-8.

Jackson, Alan A., Graham Burdge, and Karen Lillycrop. 2010. 'Pre- and Periconceptual Health and the HPA Axis: Nutrition and Stress'. In *The Placenta and Human Developmental Programming*, 1st edn, edited by Graham J. Burton, D. J. Barker, Ashley Moffett, and Kent Thornburg. Cambridge University Press. https://doi.org/10.1017/CBO9780511933806.004.

Jensby, Matthew. 2022. 'Exploring Enamel Inside and Out: Evidence of Developmental Disruption among Archaeological Barren-Ground Caribou (Rangifer Tarandus Groenlandicus) from Southern Baffin Island, NU'. Master of Arts, University of Manitoba.

Katsimbri, P. 2017. 'The Biology of Normal Bone Remodelling'. *European Journal of Cancer Care* 26 (6): e12740. https://doi.org/10.1111/ecc.12740.

Kerr, N. W. 1988. 'A Method of Assessing Periodontal Status in Archaeologically Derived Skeletal Material'. *Journal of Paleopathology* 2 (2): 67–78.

Kim, Jung-Min, Chujiao Lin, Zheni Stavre, Matthew B. Greenblatt, and Jae-Hyuck Shim. 2020. 'Osteoblast-Osteoclast Communication and Bone Homeostasis'. *Cells* 9 (9): 2073. https://doi.org/10.3390/cells9092073.

Klaus, Haagen D. 2014. 'Frontiers in the Bioarchaeology of Stress and Disease: Cross-Disciplinary Perspectives from Pathophysiology, Human Biology, and Epidemiology'. *American Journal of Physical Anthropology* 155 (2): 294–308. https://doi.org/10.1002/ajpa.22574.

Klostermann, Paul, Sandra Wabnitz, Bendeguz Tobias, et al. 2025. 'Growing up Avar: Osteological and Historical Evidence on the Transition into Adulthood in the Avar Empire and the Plasticity of Development'. *Childhood in the Past*, August 11, 1–15. https://doi.org/10.1080/17585716.2025.2538967.

Kobayashi, Tatiana Yuriko, Luciana Lourenço Ribeiro Vitor, Cleide Felício Carvalho Carrara, et al. 2020. 'Dental Enamel Defect Diagnosis Through Different Technology-Based Devices'. *International Dental Journal* 68 (3): 138–43. https://doi.org/10.1111/idj.12350.

Kondé, Zsófia, Attila Kreiter, Bernadett Bajnóczi, Mária Tóth, and Orsolya Viktorik. 2019. 'The Organization of Ceramic Production: A Comparative Analysis of Typology and Petrography at the Avar Age Settlement of Daruszentmiklós (Hungary)'. *Dissertationes Archaeologicae Ex Instituto Archaeologico Universitatis de Rolando Eötvös Nominatae* (Budapest).

Kramer, Axel, and Ojan Assadian. 2014. 'Survival of Microorganisms on Inanimate Surfaces'. In *Use of Biocidal Surfaces for Reduction of Healthcare Acquired Infections*, edited by Gadi Borkow. Springer International Publishing. https://doi.org/10.1007/978-3-319-08057-4_2.

Krieger, Nancy. 2012. 'Methods for the Scientific Study of Discrimination and Health: An Ecosocial Approach'. *American Journal of Public Health* 102 (5): 936–44. https://doi.org/10.2105/AJPH.2011.300544.

L. Kiss, Anna. 2022. 'Inflammation in Focus: The Beginning and the End'. *Pathology & Oncology Research* 27 (January): 1610136. https://doi.org/10.3389/pore.2021.1610136.

Leatherman, Thomas, and Alan Goodman. 2020. 'Building on the Biocultural Syntheses: 20 Years and Still Expanding'. *American Journal of Human Biology* 32 (4): e23360. https://doi.org/10.1002/ajhb.23360.

Lee, Sooyeon, Benjamin Thilo Krüger, Anita Ignatius, and Jan Tuckermann. 2022. 'Distinct Glucocorticoid Receptor Actions in Bone Homeostasis and Bone Diseases'. *Frontiers in Endocrinology* 12 (January): 815386. https://doi.org/10.3389/fendo.2021.815386.

Lewis, Mary. 2018. *Paleopathology Of Children: Identification Of Pathological Conditions In Human Skeletal Remains Of Non-Adults*. Academic Press.

Lewis, Mary, F. Shapland, and R. Watts. 2016. 'The Influence of Chronic Conditions and the Environment on Pubertal Development: An Example From Medieval England'. *International Journal of Paleopathology* 12 (March): 1–10. https://doi.org/10.1016/j.ijpp.2015.10.004.

Li, Chunyi, and Peter Fennessy. 2021. 'The Periosteum: A Simple Tissue With Many Faces, With Special Reference to the Antler-Lineage Periostea'. *Biology Direct* 16 (1): 17. https://doi.org/10.1186/s13062-021-00310-w.

Lorenzo, Joseph, Mark C. Horowitz, Yongwon Choi, Hiroshi Takayanagi, and Georg Schett. 2016. *Osteoimmunology: Interactions of Hte Immune and Skeletal Systems*. Academic Press.

Maia Ferreira Alencar, Carlos Henrique, Cláudio Régis Sampaio Silveira, Matheus Martins Cavalcante, et al. 2020. '"Periosteum: An Imaging Review"'. *European Journal of Radiology Open* 7: 100249. https://doi.org/10.1016/j.ejro.2020.100249.

Marklein, Kathryn E., Rachael E. Leahy, and Douglas E. Crews. 2016. 'In Sickness and in Death: Assessing Frailty in Human Skeletal Remains'. *American Journal of Physical Anthropology* 161 (2): 208–25. https://doi.org/10.1002/ajpa.23019.

Martín-Márquez, Beatriz Teresita, Flavio Sandoval-García, Fernanda Isadora Corona-Meraz, et al. 2023. 'Osteopontin: A Bone-Derived Protein Involved in Rheumatoid Arthritis and Osteoarthritis Immunopathology'. *Biomolecules* 13 (3): 502. https://doi.org/10.3390/biom13030502.

McDade, Thomas W. 2005. 'The Ecologies of Human Immune Function'. *Annual Review of Anthropology* 34 (1): 495–521. https://doi.org/10.1146/annurev.anthro.34.081804.120348.

McDade, Thomas W., Calen Ryan, Meaghan J. Jones, et al. 2017. 'Social and Physical Environments Early in Development Predict DNA Methylation of Inflammatory Genes in Young Adulthood'. *Proceedings of the National Academy of Sciences* 114 (29): 7611–16. https://doi.org/10.1073/pnas.1620661114.

McEwen, B. 2000. 'Allostasis and Allostatic Load Implications for Neuropsychopharmacology'. *Neuropsychopharmacology* 22 (2): 108–24. https://doi.org/10.1016/S0893-133X(99)00129-3.

McFadden, Clare, and Marc F. Oxenham. 2020. 'A Paleoepidemiological Approach to the Osteological Paradox: Investigating Stress, Frailty, and Resilience Through Cribra Orbitalia'. *American Journal of Physical Anthropology* 173 (2): 205–17. https://doi.org/10.1002/ajpa.24091.

McGrath, Kate, Sireen El-Zaatari, Debbie Guatelli-Steinberg, et al. 2018. 'Quantifying Linear Enamel Hypoplasia in Virunga Mountain Gorillas and Other Great Apes'. *American Journal of Physical Anthropology* 166 (2): 337–52. https://doi.org/10.1002/ajpa.23436.

McGrath, Kate, Laura Sophia Limmer, Annabelle-Louise Lockey, et al. 2021. '3D Enamel Profilometry Reveals Faster Growth but Similar Stress Severity in Neanderthal Versus Homo Sapiens Teeth'. *Scientific Reports* 11 (1): 522. https://doi.org/10.1038/s41598-020-80148-w.

Meinl, A., G. M. Rottensteiner, C. D. Huber, S. Tangl, G. Watzak, and G. Watzek. 2010. 'Caries Frequency and Distribution in an Early Medieval Avar Population from Austria'. *Oral Diseases* 16 (1): 108–16. https://doi.org/10.1111/j.1601-0825.2009.01624.x.

Milner, George R., Sara M. Getz, Svenja Weise, Peter Tarp, Stephen D. Ousley, and Jesper L. Boldsen. 2026. 'Transition Analysis 3: New Skeletal Age Indicators'. *Forensic Science International* 386 (September): 112895. https://doi.org/10.1016/j.forsciint.2026.112895.

Molnar, Petra, Torbjorn P. Ahlstrom, and Ido Leden. 2011. 'Osteoarthritis and Activity—An Analysis of the Relationship Between Eburnation, Musculoskeletal Stress Markers (MSM), and Age in Two Neolithic Hunter–Gatherer Populations From Gotland,

Sweden'. *International Journal of Osteoarchaeology* 21 (3): 283–91. https://doi.org/10.1002/oa.1131.

Morgan, Jennifer A. 2014. 'The Methodological And Diagnostic Applications Of Micro-CT To Paleopathology: A Quantitative Study Of Porotic Hyperostosis'. Doctoral dissertation, University of Western Ontario.

Moro, Claudia, Lucie Biehler-Gomez, Giuseppe Lanza Attisano, et al. 2025. 'Investigating the Etiology and Demographic Distribution of Enamel Hypoplasia'. *Heritage* 8 (10): 421–35. https://doi.org/10.3390/heritage8100420.

Mountain, Rebecca V., Yiwen Zhu, Olivia R. Pickett, et al. 2021. 'Association of Maternal Stress and Social Support During Pregnancy With Growth Marks in Children's Primary Tooth Enamel'. *JAMA Network Open* 4 (11): e2129129. https://doi.org/10.1001/jamanetworkopen.2021.29129.

Mukherjee, Anwesha, and Bodhisatwa Das. 2024. 'The Role of Inflammatory Mediators and Matrix Metalloproteinases (MMPs) in the Progression of Osteoarthritis'. *Biomaterials and Biosystems* 13 (March): 100090. https://doi.org/10.1016/j.bbiosy.2024.100090.

Mündermann, Annegret, Corina Nüesch, Hannah Ewald, and Ilse Jonkers. 2024. 'Osteoarthritis Year in Review 2024: Biomechanics'. *Osteoarthritis and Cartilage* 32 (12): 1530–41. https://doi.org/10.1016/j.joca.2024.09.011.

Nusslock, Robin, and Gregory E. Miller. 2016. 'Early-Life Adversity and Physical and Emotional Health Across the Lifespan: A Neuroimmune Network Hypothesis'. *Biological Psychiatry*, Inflammation and Immune Mechanisms in Neuropsychiatry, vol. 80 (1): 23–32. https://doi.org/10.1016/j.biopsych.2015.05.017.

O'Hara, Mackie C., and Debbie Guatelli-Steinberg. 2020. 'Differences in Enamel Defect Expression and Enamel Growth Variables in Macaca Fascicularis and Trachypithecus Cristatus From Sabah, Borneo'. *Journal of Archaeological Science* 114 (February): 105078. https://doi.org/10.1016/j.jas.2020.105078.

O'Hara, Mackie C., W. Scott McGraw, and Debbie Guatelli-Steinberg. 2023. 'Some Orangutans Acquire Enamel Defects at Regular Intervals, but Not According to Seasonal Cycles'. *American Journal of Biological Anthropology* 180 (3): 519–33. https://doi.org/10.1002/ajpa.24690.

Okamoto, Kazuo, Tomoki Nakashima, Masahiro Shinohara, et al. 2017. 'Osteoimmunology: The Conceptual Framework Unifying the Immune and Skeletal Systems'. *Physiological Reviews* 97 (4): 1295–349. https://doi.org/10.1152/physrev.00036.2016.

Olea-Popelka, Francisco, Adrian Muwonge, Alejandro Perera, et al. 2017. 'Zoonotic Tuberculosis in Human Beings Caused by Mycobacterium Bovis—a Call for Action'. *Lancet Infectious Diseases* 17 (1): e21–25. https://doi.org/10.1016/S1473-3099(16)30139-6.

Pany-Kucera, Doris, and Karin Wiltschke-Schrotta. 2022. 'Die Awarenzeitlichen Skelettreste (7. – 8. Jh. n. Chr.) Aus Der Archäologischen Grabung in Bruckneudorf (Burgenland), Fundstelle 1A: (Mit Ergänzenden Ergebnissen Zu Den Menschlichen Überresten Der Hockerbestattungen Der Frühbronzezeit, Fundstelle 1A, Und Aus Der

Spätantike/Völkerwanderungszeit (300 – 600 n. Chr.), Fundstelle 1B)'. *Annalen Des Naturhistorischen Museums in Wien. Serie A Für Mineralogie Und Petrographie, Geologie Und Paläontologie, Anthropologie Und Prähistorie* 124: 27–72.

Pappalardo, Xena, Gianluca Testa, Rosalia Pellitteri, et al. 2023. 'Early Life Stress (ELS) Effects on Fetal and Adult Bone Development'. *Children* 10 (1): 102. https://doi.org/10.3390/children10010102.

Parsons, P. A. 1992. 'Fluctuating Asymmetry: A Biological Monitor of Environmental and Genomic Stress'. *Heredity* 68 (4): 361–64. https://doi.org/10.1038/hdy.1992.51.

Penz, M., and S. Lehofer. 2023. *Bericht Der Archäologischen Maßnahme (5.–7. Jh. n. Chr.) Aus Hirschstetten (Wien 22), Spange Franz-Fellner-Gasse*. Anschluss 1 Und 2. Museen der Stadt Wien & Novetus.

Pohl, Walter. 2018. *The Avars : A Steppe Empire in Central Europe, 567–822*. Cornell University Press. https://web-p-ebscohost-com.uml.idm.oclc.org/ehost/ebookviewer/ebook/bmxlYmtfXzE3MjgwMDdfX0FO0?sid=b2e68765-b06a-4ce7-9073-35b60c0dccea@redis&vid=0&format=EB&rid=1.

Ponzetti, Marco, and Nadia Rucci. 2021. 'Osteoblast Differentiation and Signaling: Established Concepts and Emerging Topics'. *International Journal of Molecular Sciences* 22 (13): 6651. https://doi.org/10.3390/ijms22136651.

Pópity, Dániel. 2023. 'Avar and Árpádian Age Populations along the Maros River: Settlement History Research in the Hungarian Part of the Maros Valley'. *Dissertationes Archaeologicae Ex Instituto Archaeologico* (Budapest) 3 (10): 401–20.

Preiser-Kapeller, Johannes. 2018. 'The Climate of the Khagan. Observations on Palaeo-Environmental Factors of the History of the Avars (6th-9th Century AD)'. *arXiv:1803.06221 [Nlin, Physics:Physics]*, March 5. http://arxiv.org/abs/1803.06221.

R Core Team. 2020. *R: A Language and Environment for Statistical Computing*. R Foundation for Statistical Computing, released. https://www.R-project.org/.

Reid, D. J., and M. C. Dean. 2000. 'Brief Communication: The Timing of Linear Hypoplasias on Human Anterior Teeth'. *American Journal of Physical Anthropology* 113 (1): 135–39. https://doi.org/10.1002/1096-8644(200009)113:1%3C135::AID-AJPA13%3E3.0.CO;2-A.

Reid, D. J., and M. C. Dean. 2006. 'Variation in Modern Human Enamel Formation Times'. *Journal of Human Evolution* 50 (3): 329–46. https://doi.org/10.1016/j.jhevol.2005.09.003.

Rokade, Rashmi, Abhay Kulkarni, R. S. Birangane, Smita Lahane, Aditee Karkade, and Jyoti Chitgupkar. 2023. 'Enamel Hypoplasia – A Clinical Review'. *Dental Journal of Indira Gandhi Institute of Medical Sciences* 2 (November): 109–15. https://doi.org/10.25259/DJIGIMS_7_2023.

Romero, L. Michael, Molly J. Dickens, and Nicole E. Cyr. 2009. 'The Reactive Scope Model — A New Model Integrating Homeostasis, Allostasis, and Stress'. *Hormones and Behavior* 55 (3): 375–89. https://doi.org/10.1016/j.yhbeh.2008.12.009.

Ruff, Christopher. 2003. ‘Growth in Bone Strength, Body Size, and Muscle Size in a Juvenile Longitudinal Sample’. *Bone* 33 (3): 317–29. https://doi.org/10.1016/S8756-3282(03)00161-3.

Ruff, Christopher, ed. 2018. *Skeletal Variation and Adaptation in Europeans: Upper Paleolithic to the Twentieth Century*. Wiley Blackwell. https://doi.org/10.1002/9781118628430.

Schaefer, Maureen, Louise Scheuer, and Sue M. Black. 2009. *Juvenile Osteology: A Laboratory and Field Manual*. Elsevier/Academic Press.

Schrader, Sarah A., and Christina Torres-Rouff. 2020. ‘Embodying Bioarchaeology’. In *Theoretical Approaches in Bioarchaeology*, 1st edn, edited by Colleen M. Cheverko, Julia R. Prince-Buitenhuys, and Mark Hubbe. Routledge. https://doi.org/10.4324/9780429262340-2.

Skinner, Mark F. 2021. ‘Cold Discomfort: A Model to Explain Repetitive Linear Enamel Hypoplasia Among Pan Troglodytes and Pan Paniscus’. *International Journal of Primatology* 42 (3): 370–403. https://doi.org/10.1007/s10764-021-00206-6.

Skinner, Mark F., Mao Asami, Matthew M. Skinner, and Akiko Kato. 2025. ‘Potential of Japanese Macaques for Understanding Etiology and Seasonality of Repetitive Linear Enamel Hypoplasia in Nonhuman Primates’. *American Journal of Primatology* 87 (1): e23713. https://doi.org/10.1002/ajp.23713.

Spekker, Olga, Balázs Tihanyi, Luca Kis, et al. 2022. ‘Life and Death of a Leprosy Sufferer from the 8th-Century-CE Cemetery of Kiskundorozsma–Kettőshatár I (Duna-Tisza Interfluve, Hungary)—Biological and Social Consequences of Having Hansen’s Disease in a Late Avar Age Population from Hungary’. *PLOS One* 17 (2): e0264286. https://doi.org/10.1371/journal.pone.0264286.

Spekker, Olga, Balázs Tihanyi, Luca Kis, et al. 2023. ‘Leprosy: The Age-Old Companion of Humans – Re-Evaluation and Comparative Analysis of Avar-Period Cases with Hansen’s Disease from the Danube-Tisza Interfluve, Hungary’. *Tuberculosis* 142 (September): 102393. https://doi.org/10.1016/j.tube.2023.102393.

Stadler, Peter. 2008. ‘Avar Chronology Revisited, And The Question Of Ethnicity In The Avar Qaganate’. In *The Other Europe in the Middle Ages, 450-1450*, edited by Florin Curta and Roman Kivalev, vol. 2. Brill. http://brill.com/view/book/edcoll/9789047423560/Bej.9789004163898.i-492_004.xml.

Stephens, Ryan B., Andrew P. Ouimette, Erik A. Hobbie, and Rebecca J. Rowe. 2022. ‘Reevaluating Trophic Discrimination Factors ($\Delta\Delta^{13}$C and $\Delta\Delta^{15}$N) for Diet Reconstruction’. *Ecological Monographs* 92 (3): e1525. https://doi.org/10.1002/ecm.1525.

Temple, Daniel H. 2019. ‘Bioarchaeological Evidence for Adaptive Plasticity and Constraint: Exploring Life-History Trade-Offs in the Human Past’. *Evolutionary Anthropology: Issues, News, and Reviews* 28 (1): 34–46. https://doi.org/10.1002/evan.21754.

Temple, Daniel H., and Ashley N. Edes. 2022. ‘Stress in Bioarchaeology, Epidemiology, and Evolutionary Medicine: An Integrated Conceptual Model of Shared History From the Descriptive to the Developmental’. In *Palaeopathology and Evolutionary Medicine*, by Daniel H. Temple and Ashley N. Edes. Oxford University Press. https://doi.org/10.1093/oso/9780198849711.003.0014.

Temple, Daniel H., and Haagen D. Klaus. 2022. ‘Synthesizing Stress in Paleopathological Perspective’. In *The Routledge Handbook of Paleopathology*, 1st edn, by Anne L. Grauer. Routledge. https://doi.org/10.4324/9781003130994.

Thielen, Nathalie, Margot Neefjes, Renske Wiegertjes, et al. 2021. ‘Osteoarthritis-Related Inflammation Blocks TGF-a’s Protective Effect on Chondrocyte Hypertrophy via (de)Phosphorylation of the SMAD2/3 Linker Region’. *International Journal of Molecular Sciences* 22 (15): 15. https://doi.org/10.3390/ijms22158124.

Tihanyi, Balázs, Levente Samu, István Koncz, et al. 2024. ‘A Glimpse into the Past of Hansen’s Disease – Re-Evaluation and Comparative Analysis of Cases with Leprosy from the Avar Period of the Trans-Tisza Region, Hungary’. *Tuberculosis* 148 (September): 102552. https://doi.org/10.1016/j.tube.2024.102552.

Torres, Haydee M., Katherine M. Arnold, Manuela Oviedo, Jennifer J. Westendorf, and Samantha R. Weaver. 2023. ‘Inflammatory Processes Affecting Bone Health and Repair’. *Current Osteoporosis Reports* 21 (6): 842–53. https://doi.org/10.1007/s11914-023-00824-4.

Vaughan, Owen R., Alison J. Forhead, and Abigail L. Fowden. 2010. ‘Glucocorticoids and Placental Programming’. In *The Placenta and Human Developmental Programming*, 1st edn, edited by Graham J. Burton, DJP Barker, Ashley Moffett, and Kent Thornburg. Cambridge University Press. https://doi.org/10.1017/CBO9780511933806.015.

Ventades, Nerea G., Imanol M. Laza, Montserrat Hervella, and Concepción de-la-Rúa. 2018. ‘A Recording Form for Differential Diagnosis of Arthropathies’. *International Journal of Paleopathology* 20 (March): 45–49. https://doi.org/10.1016/j.ijpp.2018.01.004.

Vidal-Ronchas, Rocio, Petra Rajić Šikanjić, Zrinka Premužić, Anita Rapan Papeša, and Emma Lightfoot. 2019. ‘Diet, Sex, and Social Status in the Late Avar Period: Stable Isotope Investigations at Nuštar Cemetery, Croatia’. *Archaeological and Anthropological Sciences* 11 (5): 1727–37. https://doi.org/10.1007/s12520-018-0628-4.

Wang, Ke, Bendeguz Tobias, Doris Pany-Kucera, et al. 2025. ‘Ancient DNA Reveals Reproductive Barrier despite Shared Avar-Period Culture’. *Nature*, 1–8. https://doi.org/10.1038/s41586-024-08418-5.

Waterland, Robert A., and Karin B. Michels. 2007. ‘Epigenetic Epidemiology of the Developmental Origins Hypothesis’. *Annual Review of Nutrition* 27 (1): 363–88. https://doi.org/10.1146/annurev.nutr.27.061406.093705.

Watts, Rebecca. 2013. ‘Childhood Development and Adult Longevity in an Archaeological Population From Barton-upon-Humber, Lincolnshire, England’. *International Journal of Paleopathology* 3 (2): 95–104. https://doi.org/10.1016/j.ijpp.2013.05.001.

Weitzmann, M. Neale, and Ighovwerha Ofotokun. 2016. ‘Physiological and Pathophysiological Bone Turnover — Role of the Immune System’. *Nature Reviews Endocrinology* 12 (9): 518–32. https://doi.org/10.1038/nrendo.2016.91.

Weston, Darlene A. 2008. ‘Investigating the Specificity of Periosteal Reactions in Pathology Museum Specimens’. *American Journal of Physical Anthropology* 137 (1): 48–59. https://doi.org/10.1002/ajpa.20839.

Wigley, B. R., E. C. Stillman, and E. Craig-Atkins. 2025. ‘What Doesn’t Kill You Makes You Stronger? Examining Relationships Between Early-Life Stress, Later-Life Inflammation and Mortality Risk in Skeletal Remains’. *American Journal of Biological Anthropology* 186 (2): e70005. https://doi.org/10.1002/ajpa.70005.

Wippert, Pia-Maria, Michael Rector, Gisela Kuhn, and Karin Wuertz-Kozak. 2017. ‘Stress and Alterations in Bones: An Interdisciplinary Perspective’. *Frontiers in Endocrinology* 8 (May): 96. https://doi.org/10.3389/fendo.2017.00096.

Wissler, Amanda, Kelly E. Blevins, and Jane E. Buikstra. 2022. ‘Missing Data in Bioarchaeology I: A Review of the Literature’. *American Journal of Biological Anthropology* 179 (3): 339–48. https://doi.org/10.1002/ajpa.24609.

Witzel, C., U. Kierdorf, M. Schultz, and H. Kierdorf. 2008. ‘Insights From the Inside: Histological Analysis of Abnormal Enamel Microstructure Associated With Hypoplastic Enamel Defects in Human Teeth’. *American Journal of Physical Anthropology* 136 (4): 400–414. https://doi.org/10.1002/ajpa.20822.

Wood, James, George R. Milner, Henry C. Harpending, et al. 1992. ‘The Osteological Paradox: Problems of Inferring Prehistoric Health from Skeletal Samples [and Comments and Reply]’. *Current Anthropology* 33 (4): 343–70. https://doi.org/10.1086/204084.

Wuertz-Kozak, Karin, Martin Roszkowski, Elena Cambria, et al. 2020. ‘Effects of Early Life Stress on Bone Homeostasis in Mice and Humans’. *International Journal of Molecular Sciences* 21 (18): 6634. https://doi.org/10.3390/ijms21186634.

Xu, Jie, Linxin Yu, Feng Liu, Longbiao Wan, and Zhenhua Deng. 2023. ‘The Effect of Cytokines on Osteoblasts and Osteoclasts in Bone Remodeling in Osteoporosis: A Review’. *Frontiers in Immunology* 14 (July): 122–29. https://doi.org/10.3389/fimmu.2023.1222129.

Zhou, Mi, and Dana T. Graves. 2022. ‘Impact of the Host Response and Osteoblast Lineage Cells on Periodontal Disease’. *Frontiers in Immunology* 13 (October): 998244. https://doi.org/10.3389/fimmu.2022.998244.

Appendix A

Figures

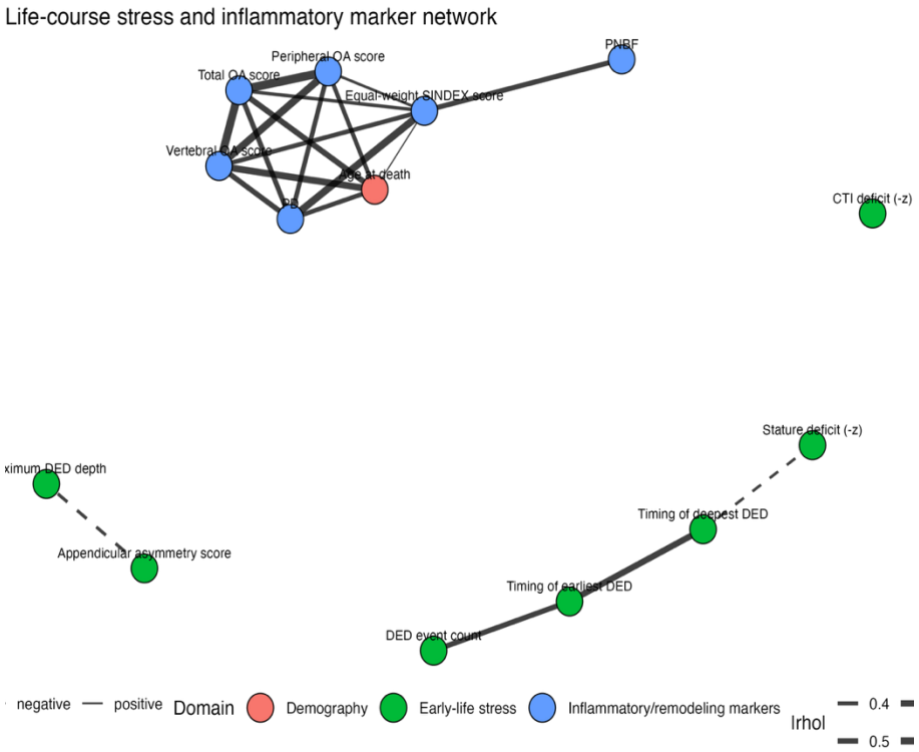

Figure A.1 Life-course correlation network. Adult inflammatory and remodelling markers formed a densely connected cluster with age, whereas early-life stress indicators were more weakly connected and largely separate. Node colours identify analytical domains; solid and dashed edges indicate positive and negative correlations, and line thickness represents correlation strength.

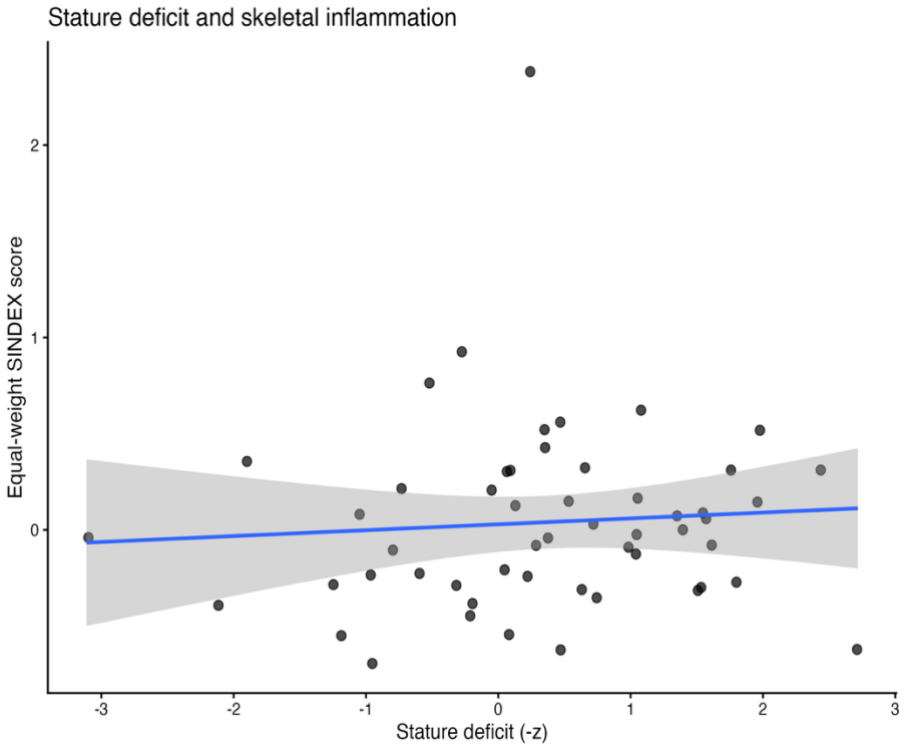

Figure A.2 Association between stature deficit and equal-weight SINDEX. The fitted trend was nearly flat, indicating little relationship between shorter standardized stature and skeletal inflammation. The shaded band represents the 95% confidence interval.

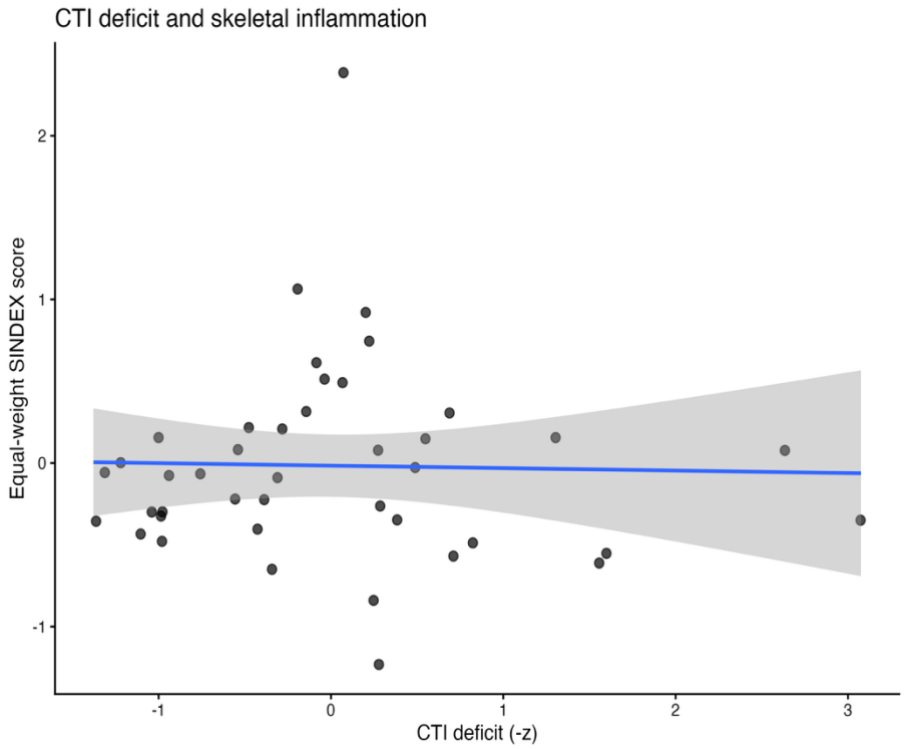

Figure A.3 Association between CTI deficit and equal-weight SINDEX. The fitted trend was nearly flat, indicating no clear relationship between reduced cortical thickness and skeletal inflammation. The shaded band represents the 95% confidence interval.

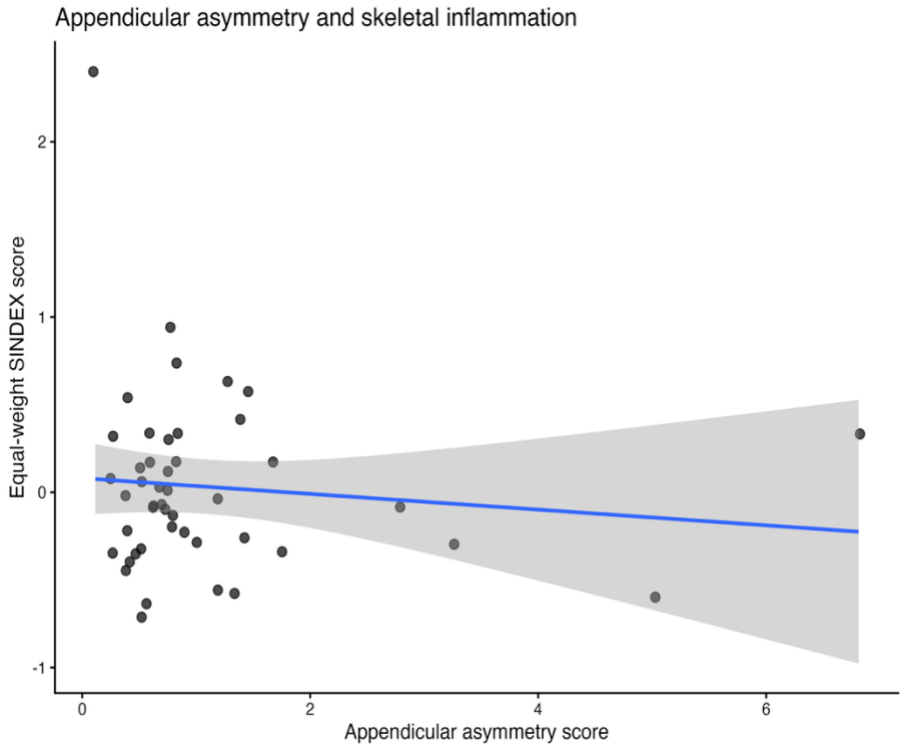

Figure A.4 Association between appendicular asymmetry and equal-weight SINDEX. The fitted trend was weakly negative, with substantial uncertainty at higher asymmetry scores.

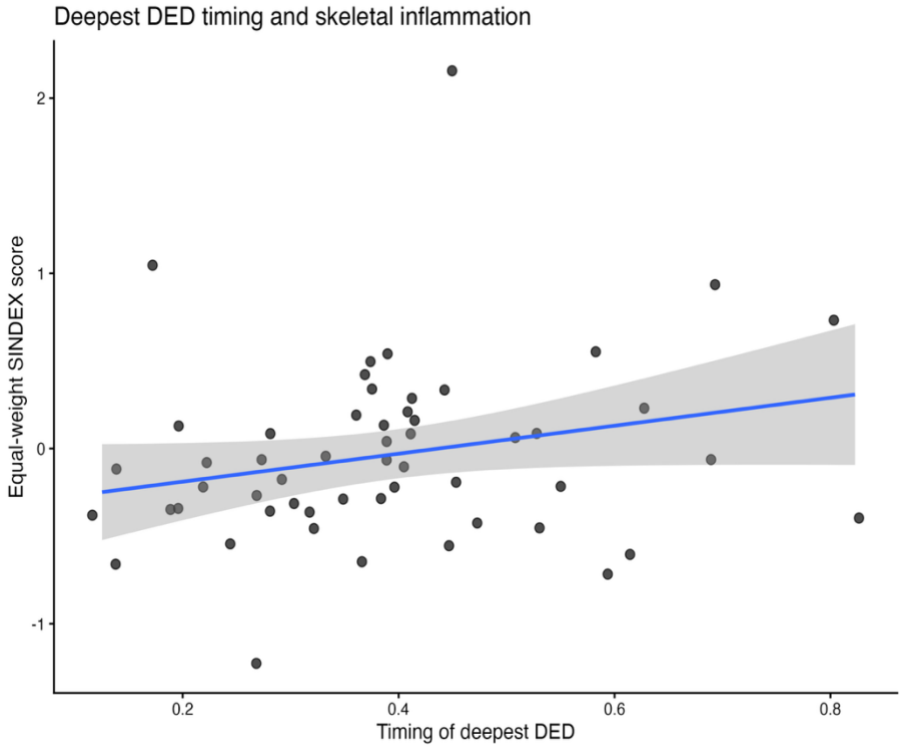

Figure A.5 Association between deepest DED timing and equal-weight SINDEX. Higher timing values, representing defects in earlier-forming enamel, showed a weak positive association with skeletal inflammation.

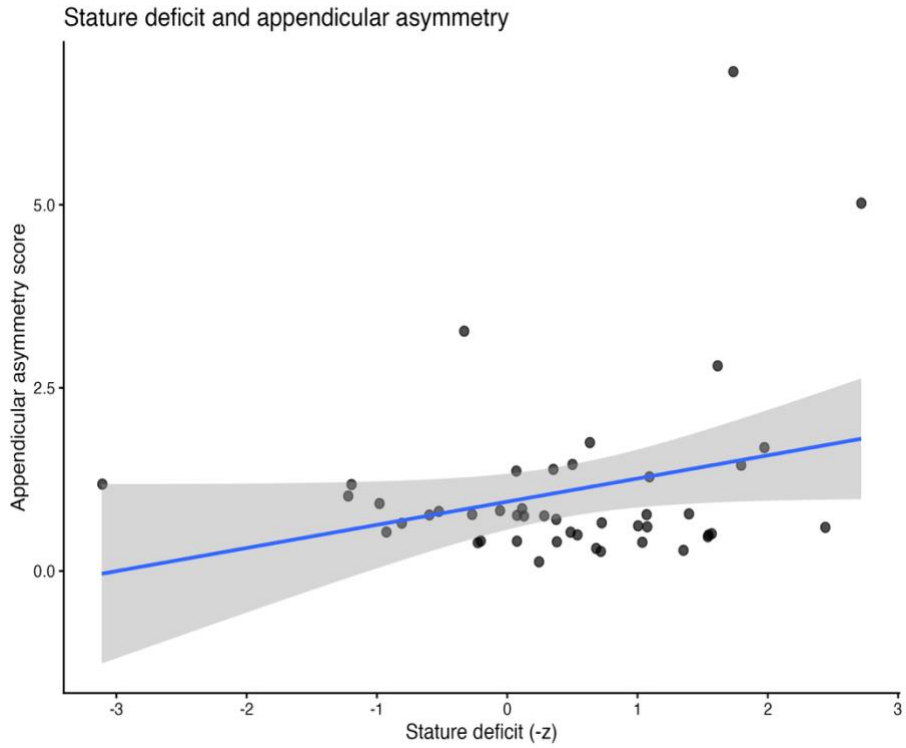

Figure A.6 Association between stature deficit and appendicular asymmetry. The fitted trend was positive but influenced by a small number of high-asymmetry observations.

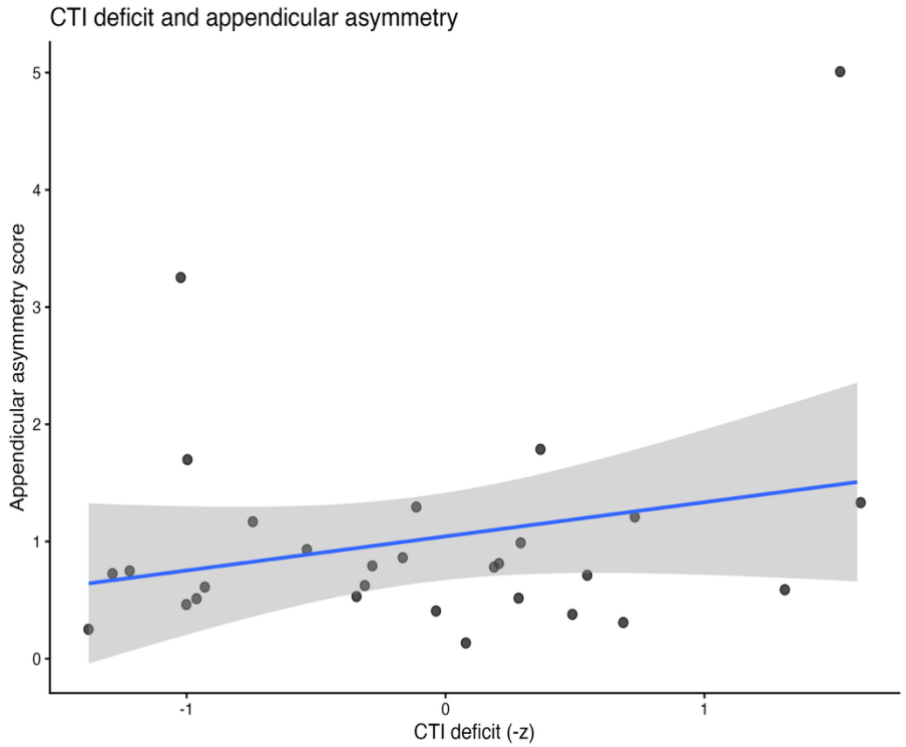

Figure A.7 Association between CTI deficit and appendicular asymmetry. The fitted trend was weakly positive, with substantial variation and several high-asymmetry observations.

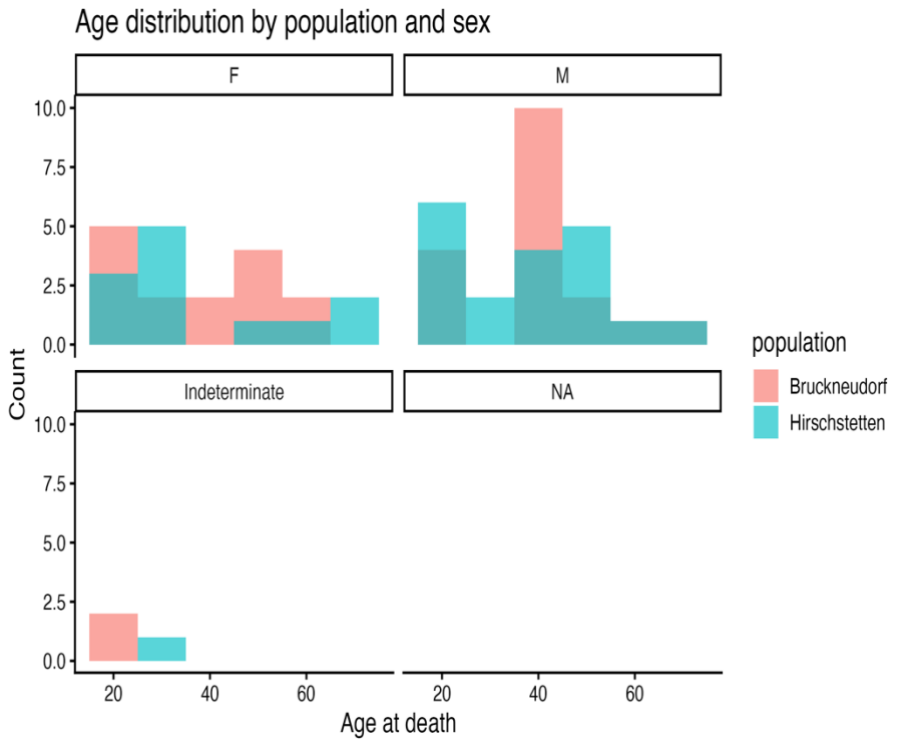

Figure A.8 Age-at-death distributions by population and sex. Female and male age profiles overlapped between Bruckneudorf and Hirschstetten, with no clear population-level age imbalance.

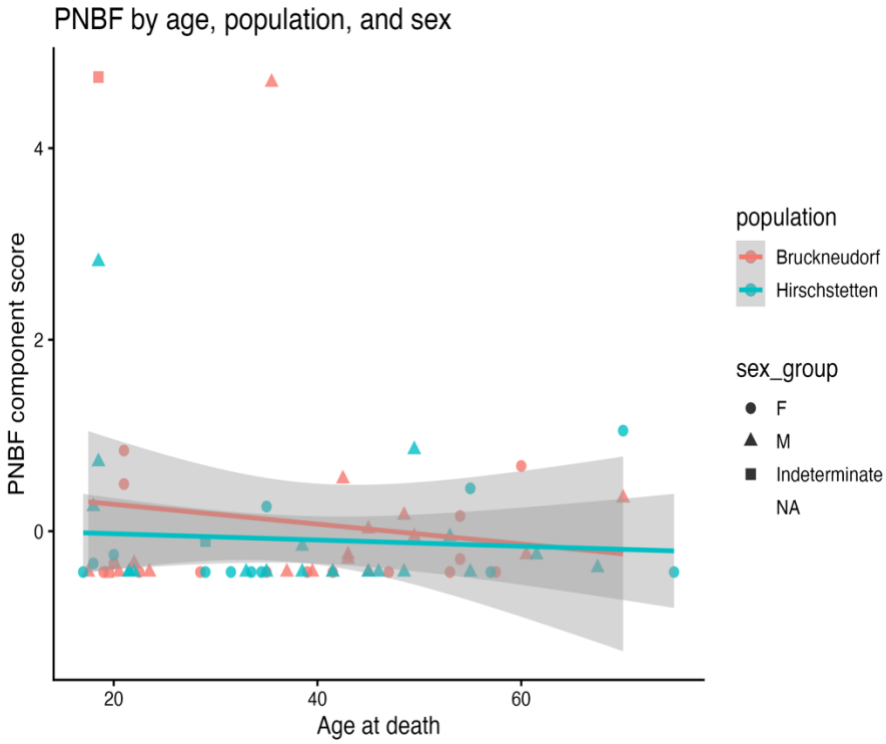

Figure A.9 PNBF scores by age, population, and sex. Scores showed no clear increase with age or separation by population or sex; high values were limited to a small number of individuals. Shaded bands represent 95% confidence intervals.

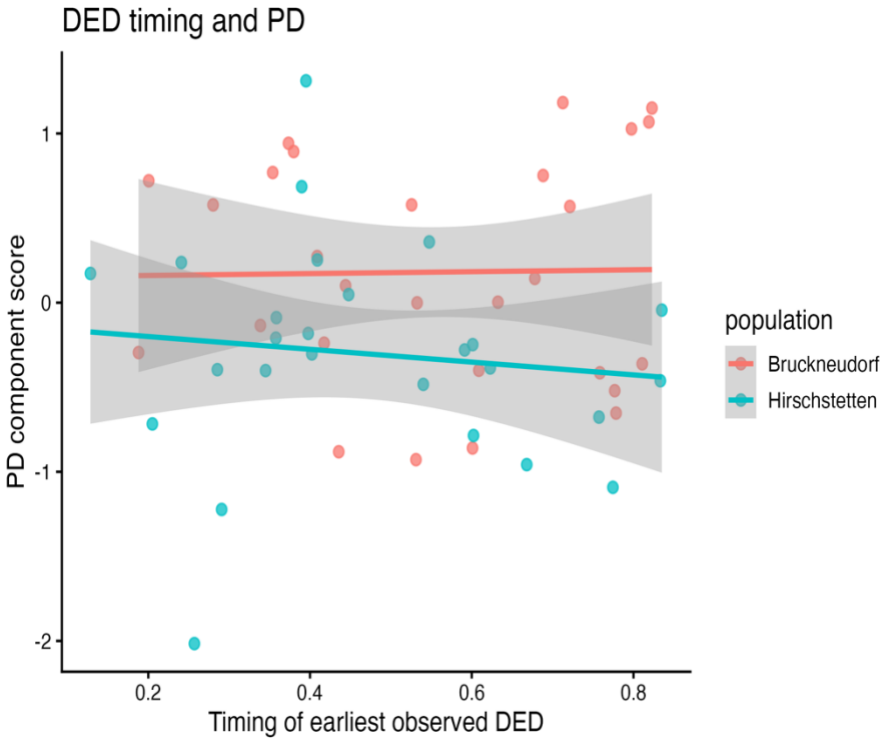

Figure A.10 Earliest DED timing and PD scores by population. Bruckneudorf showed a nearly flat trend, while Hirschstetten showed a weak negative trend; neither population displayed a clear association. Shaded bands represent 95% confidence intervals.

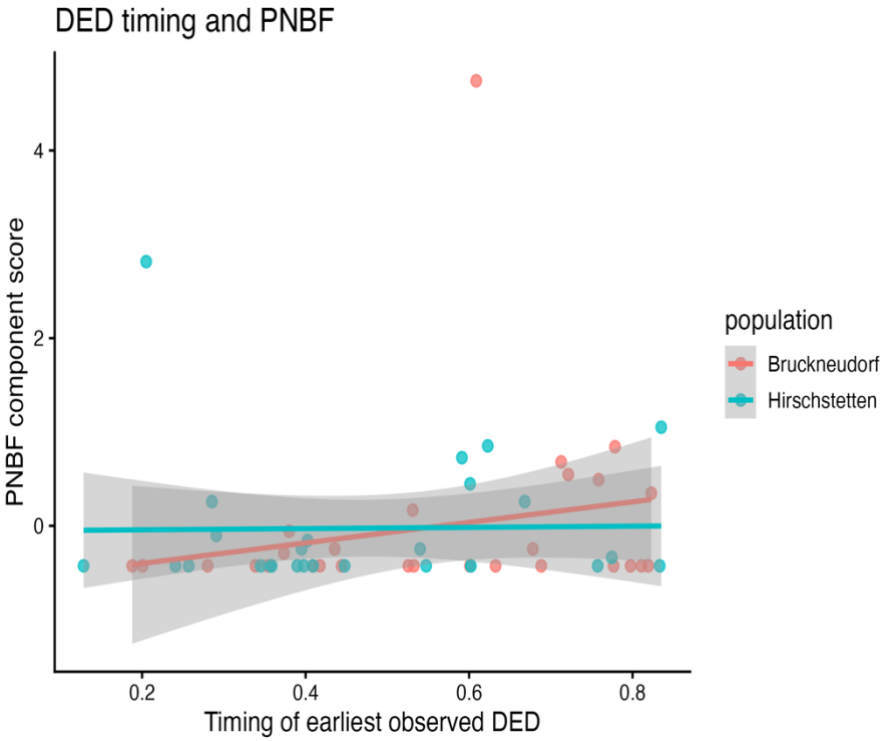

Figure A.11 Earliest DED timing and PNBF scores by population. Bruckneudorf showed a weak positive trend, while Hirschstetten showed little overall change; high PNBF scores were limited to a small number of individuals.

Tables

Table A.1 Population-specific distributions of developmental and adult skeletal variables. Values are presented as n, mean ± SD, and median (minimum–maximum). Note. B = Bruckneudorf; H = Hirschstetten. Sample sizes vary with preservation and observability.

		Bruckneudorf			Hirschstetten		
Domain	**Variable**	**n**	**mean ± SD**	**median (range)**	**n**	**mean ± SD**	**median (range)**
Appendicular Growth	BAA	27	0.77 ± 0.40	0.76 (0.12–1.69)	19	1.54 ± 1.77	0.74 (0.27–6.81)
	CTI	22	0.63 ± 0.07	0.64 (0.42–0.73)	22	0.62 ± 0.06	0.63 (0.47–0.74)
	CTI z-score	21	0.06 ± 1.00	0.16 (−2.62–1.30)	21	−0.06 ± 1.00	0.02 (−3.08–1.38)
	Estimated stature (cm)	30	161.00 ± 7.88	159.36 (150.54–183.77)	23	160.29 ± 6.97	160.83 (147.96–172.23)
	Stature z-score	30	−0.28 ± 1.22	−0.37 (−2.42–3.11)	23	−0.45 ± 1.12	−0.36 (−2.72–1.19)
DED	DED event count	30	1.87 ± 1.01	2.00 (0–4)	29	2.10 ± 1.35	2.00 (0–5)
	Maximum DED depth (µm)	28	34.52 ± 19.04	30.26 (11.56–86.79)	26	36.95 ± 18.75	33.79 (10.35–81.40)
	Timing of deepest DED	28	0.42 ± 0.17	0.40 (0.17–0.82)	26	0.36 ± 0.14	0.39 (0.13–0.62)
	Timing of earliest DED	28	0.56 ± 0.20	0.57 (0.19–0.82)	26	0.47 ± 0.20	0.41 (0.13–0.84)
OA	Peripheral OA score	35	0.32 ± 0.41	0.18 (0–1.82)	33	0.34 ± 0.50	0.10 (0–1.73)
	Total OA score	35	0.43 ± 0.50	0.18 (0–1.77)	33	0.41 ± 0.54	0.11 (0–1.70)
	Vertebral OA score	34	0.55 ± 0.65	0.00 (0–1.71)	33	0.48 ± 0.64	0.00 (0–2.00)
SINDEX	Equal-weight SINDEX	35	0.18 ± 0.64	0.08 (−0.64–2.40)	33	−0.19 ± 0.44	−0.23 (−1.22–1.05)
	PD	35	0.26 ± 0.64	0.27 (−0.93–1.18)	33	−0.28 ± 0.67	−0.30 (−2.02–1.31)
	PNBF	35	0.09 ± 1.21	−0.43 (−0.43–4.74)	33	−0.10 ± 0.67	−0.43 (−0.43–2.82)

Table A.2 Sex-stratified descriptive statistics for developmental and adult skeletal variables by population. Sample sizes vary according to preservation and observability. Values are reported separately for estimated females and males.

		n				Mean ± SD				Mean ± 95% CI margin				Median Range				Skew			
		Bruckneudorf		Hirschstetten		Bruckneudorf		Hirschstetten		Bruckneudorf		Hirschstetten		Bruckneudorf		Hirschstetten		Bruckneudorf		Hirschstette	
		F	M	F	M	F	M	F	M	F	M	F	M	F	M	F	M	F	M	F	M
Appendicular Growth	BAA	12	15	8	11	0.74 ± 0.4	0.8 ± 0.41	1.5 ± 1.67	1.57 ± 1.92	0.74 ± 0.25	0.8 ± 0.22	1.5 ± 1.39	1.57 ± 1.29	0.65 (0.29-1.69)	0.78 (0.12-1.46)	0.63 (0.27-5.02)	0.79 (0.39-6.81)	1.149	0.097	1.084	1.8
	CTI	13	8	9	12	0.63 ± 0.09	0.63 ± 0.04	0.62 ± 0.07	0.63 ± 0.06	0.63 ± 0.05	0.63 ± 0.04	0.62 ± 0.05	0.63 ± 0.04	0.64 (0.42-0.73)	0.63 (0.55-0.68)	0.6 (0.5-0.74)	0.64 (0.47-0.69)	-0.912	-0.681	0.089	-1.4
	CTI z-score	13	8	9	12	0.03 ± 1.11	0.1 ± 0.85	-0.05 ± 0.88	-0.06 ± 1.12	0.03 ± 0.67	0.1 ± 0.71	-0.05 ± 0.68	-0.06 ± 0.71	0.16 (-2.62-1.3)	0.1 (-1.59-0.97)	-0.27 (-1.54-1.38)	0.24 (-3.08-1.12)	-0.912	-0.681	0.089	-1.4
	Estimated stature	14	16	10	13	155.86 ± 4.08	165.5 ± 7.71	155.22 ± 4.7	164.18 ± 5.89	155.86 ± 2.36	165.5 ± 4.11	155.22 ± 3.36	164.18 ± 3.56	155.12 (150.83-166.7)	164.69 (150.54-183.77)	155.04 (147.96-162.51)	163.8 (154.34-172.23)	1.131	0.478	0.215	-0.3
	Stature z-score	14	16	10	13	-0.68 ± 1.05	0.07 ± 1.28	-0.84 ± 1.21	-0.15 ± 0.98	-0.68 ± 0.61	0.07 ± 0.68	-0.84 ± 0.87	-0.15 ± 0.59	-0.87 (-1.98-2.12)	-0.06 (-2.42-3.11)	-0.89 (-2.72-1.04)	-0.21 (-1.79-1.19)	1.131	0.478	0.215	-0.3
DED	DED event count	13	15	11	16	1.77 ± 0.93	1.87 ± 0.99	2.18 ± 1.4	2.12 ± 1.41	1.77 ± 0.56	1.87 ± 0.55	2.18 ± 0.94	2.12 ± 0.75	2 (0-3)	2 (0-3)	2 (0-5)	2 (0-5)	-0.165	-0.17	0.305	0.1
	Maximum DED depth	12	14	10	14	37.61 ± 21.04	32.19 ± 19.06	38.66 ± 19.24	37.74 ± 19.64	37.61 ± 13.37	32.19 ± 11	38.66 ± 13.77	37.74 ± 11.34	33.34 (11.68-83.48)	25 (11.56-86.79)	38.6 (17.28-74.94)	34.33 (10.35-81.4)	0.847	1.548	0.39	0.7
	Timing of deepest DED	12	14	10	14	0.42 ± 0.18	0.45 ± 0.17	0.38 ± 0.16	0.35 ± 0.14	0.42 ± 0.12	0.45 ± 0.1	0.38 ± 0.11	0.35 ± 0.08	0.39 (0.17-0.81)	0.42 (0.2-0.82)	0.35 (0.13-0.6)	0.4 (0.13-0.62)	0.867	0.667	0.125	0.1
	Timing of earliest DED	12	14	10	14	0.6 ± 0.2	0.54 ± 0.19	0.52 ± 0.2	0.45 ± 0.21	0.6 ± 0.12	0.54 ± 0.11	0.52 ± 0.14	0.45 ± 0.12	0.66 (0.28-0.82)	0.53 (0.2-0.82)	0.54 (0.26-0.84)	0.4 (0.13-0.83)	-0.409	0.026	0.163	0.2
OA	Peripheral OA score	15	18	12	19	0.22 ± 0.29	0.43 ± 0.48	0.49 ± 0.6	0.27 ± 0.45	0.22 ± 0.16	0.43 ± 0.24	0.49 ± 0.38	0.27 ± 0.22	0.05 (0-0.82)	0.32 (0-1.82)	0.25 (0-1.73)	0 (0-1.45)	0.912	1.447	1.075	1.4
	Total OA score	15	18	12	19	0.3 ± 0.44	0.58 ± 0.54	0.46 ± 0.62	0.37 ± 0.53	0.3 ± 0.24	0.58 ± 0.27	0.46 ± 0.39	0.37 ± 0.26	0.05 (0-1.19)	0.63 (0-1.77)	0.12 (0-1.7)	0.05 (0-1.58)	1.1	0.473	1.037	1.2
	Vertebral OA score	14	18	12	19	0.4 ± 0.64	0.73 ± 0.66	0.42 ± 0.66	0.46 ± 0.65	0.4 ± 0.37	0.73 ± 0.33	0.42 ± 0.42	0.46 ± 0.31	0 (0-1.57)	0.85 (0-1.71)	0 (0-1.67)	0 (0-2)	1.016	0.009	0.897	1.0

SINDEX	Equal-weight SINDEX score	15	18	12	19	0.07 ± 0.4	0.18 ± 0.66	-0.28 ± 0.45	-0.11 ± 0.44	0.07 ± 0.22	0.18 ± 0.33	-0.28 ± 0.29	-0.11 ± 0.21	0.08 (-0.64-0.93)	0.11 (-0.56-2.4)	-0.32 (-1.22-0.5)	-0.23 (-0.86-1.05)	0.289	1.93	-0.301	0.8
	PD	15	18	12	19	0.3 ± 0.68	0.3 ± 0.62	-0.41 ± 0.69	-0.17 ± 0.65	0.3 ± 0.38	0.3 ± 0.31	-0.41 ± 0.44	-0.17 ± 0.31	0.43 (-0.86-1.18)	0.42 (-0.93-1.15)	-0.32 (-2.02-0.69)	-0.3 (-1.29-1.31)	-0.242	-0.56	-0.694	0.6
	PNBF	15	18	12	19	-0.15 ± 0.46	0.07 ± 1.19	-0.15 ± 0.48	-0.05 ± 0.8	-0.15 ± 0.25	0.07 ± 0.59	-0.15 ± 0.31	-0.05 ± 0.38	-0.43 (-0.43-0.84)	-0.31 (-0.43-4.69)	-0.43 (-0.43-1.05)	-0.43 (-0.43-2.82)	1.166	3.213	1.397	2.4

Table A.3 Sex-stratified within- and between-population comparisons of developmental and adult skeletal variables. Group values are reported as n and mean ± SD. Welch's t-tests and Wilcoxon rank-sum tests assess group differences; Cohen's d indicates effect size. Note. G1 and G2 follow the order shown in the Comparison column. F = estimated female; M = estimated male. Positive Cohen's d values indicate higher values in Group 1. ∗p < .05; ∗∗p < .01; ∗∗∗p < .001.

			Group 1		Group 2						
Comparison	**Domain**	**Variable**	**n**	**mean ± SD**	**n**	**mean ± SD**	**Welch's t(df)**	**p**	**W**	**p**	**Cohen's d**
Bruckneudorf F vs M	**DED**	DED event count	13	1.77 ± 0.93	15	1.87 ± 0.99	−0.27 (25.83)	0.79	92	0.809	−0.10
		Maximum DED depth	12	37.61 ± 21.04	14	32.19 ± 19.06	0.68 (22.50)	0.501	100	0.425	0.27
		Timing of deepest DED	12	0.42 ± 0.18	14	0.45 ± 0.17	−0.42 (22.71)	0.68	72	0.554	−0.16
		Timing of earliest DED	12	0.60 ± 0.20	14	0.54 ± 0.19	0.79 (23.23)	0.439	96	0.554	0.31
	Appendicular Growth	Estimated stature	14	155.86 ± 4.08	16	165.50 ± 7.71	−4.35 (23.38)	**<.001***	28	**<.001***	−1.56
		Stature z-score	14	−0.68 ± 1.05	16	0.07 ± 1.28	−1.75 (27.90)	0.092	63	**.044***	−0.64
		CTI	13	0.63 ± 0.09	8	0.63 ± 0.04	−0.16 (18.36)	0.877	53	0.971	−0.07
		CTI z-score	13	0.03 ± 1.11	8	0.10 ± 0.85	−0.15 (17.88)	0.886	56	0.8	−0.06
		Appendicular asymmetry	12	0.74 ± 0.40	15	0.80 ± 0.41	−0.42 (23.93)	0.679	73	0.421	−0.16
	OA	Total OA score	15	0.30 ± 0.44	18	0.58 ± 0.54	−1.70 (30.99)	0.1	91	0.112	−0.59
		Peripheral OA score	15	0.22 ± 0.29	18	0.43 ± 0.48	−1.61 (28.34)	0.118	90.5	0.108	−0.55
		Vertebral OA score	14	0.40 ± 0.64	18	0.73 ± 0.66	−1.43 (28.48)	0.163	92	0.173	−0.51
	SINDEX	Equal-weight SINDEX	15	0.07 ± 0.40	18	0.18 ± 0.66	−0.59 (28.39)	0.563	128	0.814	−0.20
		PD	15	0.30 ± 0.68	18	0.30 ± 0.62	0.00 (28.80)	0.997	140	0.871	0
		PNBF	15	−0.15 ± 0.46	18	0.07 ± 1.19	−0.72 (22.68)	0.48	118	0.521	−0.24

Hirschstetten F vs M	**DED**	DED event count	11	2.18 ± 1.40	16	2.13 ± 1.41	0.10 (21.73)	0.919	89.5	0.959	0.04
		Maximum DED depth	10	38.66 ± 19.24	14	37.74 ± 19.64	0.11 (19.79)	0.91	72	0.93	0.05
		Timing of deepest DED	10	0.38 ± 0.16	14	0.35 ± 0.14	0.41 (17.80)	0.683	73	0.884	0.17
		Timing of earliest DED	10	0.52 ± 0.20	14	0.45 ± 0.21	0.78 (20.35)	0.445	80	0.578	0.32
	Appendicular Growth	Estimated stature	10	155.22 ± 4.70	13	164.18 ± 5.89	−4.06 (20.95)	**<.001***	15	**.002****	−1.68
		Stature z-score	10	−0.84 ± 1.21	13	−0.15 ± 0.98	−1.48 (17.09)	0.158	44	0.204	−0.63
		CTI	9	0.62 ± 0.07	12	0.63 ± 0.06	−0.11 (15.09)	0.917	47	0.644	−0.05
		CTI z-score	9	−0.05 ± 0.88	12	−0.06 ± 1.12	0.03 (18.92)	0.973	48	0.696	0.01
		Appendicular asymmetry	8	1.50 ± 1.67	11	1.57 ± 1.92	−0.08 (16.34)	0.937	36	0.536	−0.04
	OA	Total OA score	12	0.46 ± 0.62	19	0.37 ± 0.53	0.41 (20.89)	0.685	135	0.398	0.15
		Peripheral OA score	12	0.49 ± 0.60	19	0.27 ± 0.45	1.09 (18.68)	0.291	157	0.076	0.41
		Vertebral OA score	12	0.42 ± 0.66	19	0.46 ± 0.65	−0.17 (23.35)	0.867	107	0.764	−0.06
	SINDEX	Equal-weight SINDEX	12	−0.28 ± 0.45	19	−0.11 ± 0.44	−1.05 (22.95)	0.305	94	0.429	−0.39
		PD	12	−0.41 ± 0.69	19	−0.17 ± 0.65	−0.97 (22.43)	0.343	101	0.612	−0.36
		PNBF	12	−0.15 ± 0.48	19	−0.05 ± 0.80	−0.46 (28.98)	0.652	112.5	0.964	−0.16
Bruckneudorf F vs Hirschstetten F	**DED**	DED event count	13	1.77 ± 0.93	11	2.18 ± 1.40	−0.83 (16.85)	0.416	59.5	0.489	−0.35
		Maximum DED depth	12	37.61 ± 21.04	10	38.66 ± 19.24	−0.12 (19.79)	0.904	57	0.869	−0.05
		Timing of deepest DED	12	0.42 ± 0.18	10	0.38 ± 0.16	0.50 (19.98)	0.622	67	0.668	0.21
		Timing of earliest DED	12	0.60 ± 0.20	10	0.52 ± 0.20	0.99 (19.25)	0.333	75	0.339	0.43
	Appendicular Growth	Estimated stature	14	155.86 ± 4.08	10	155.22 ± 4.70	0.35 (17.75)	0.73	78	0.661	0.15
		Stature z-score	14	−0.68 ± 1.05	10	−0.84 ± 1.21	0.35 (17.75)	0.73	78	0.661	0.15
		CTI	13	0.63 ± 0.09	9	0.62 ± 0.07	0.20 (19.50)	0.846	67	0.593	0.08
		CTI z-score	13	0.03 ± 1.11	9	−0.05 ± 0.88	0.20 (19.50)	0.846	67	0.593	0.08
		Appendicular asymmetry	12	0.74 ± 0.40	8	1.50 ± 1.67	−1.27 (7.53)	0.243	45	0.847	−0.63
	OA	Total OA score	15	0.30 ± 0.44	12	0.46 ± 0.62	−0.75 (19.11)	0.461	69.5	0.323	−0.30
		Peripheral OA score	15	0.22 ± 0.29	12	0.49 ± 0.60	−1.44 (14.99)	0.17	61	0.158	−0.58
		Vertebral OA score	14	0.40 ± 0.64	12	0.42 ± 0.66	−0.08 (23.11)	0.94	83	0.976	−0.03
	SINDEX	Equal-weight SINDEX	15	0.07 ± 0.40	12	−0.28 ± 0.45	2.13 (22.10)	**.044***	130	0.054	0.83
		PD	15	0.30 ± 0.68	12	−0.41 ± 0.69	2.67 (23.62)	**.014***	137	**.023***	1.03

		PNBF	15	−0.15 ± 0.46	12	−0.15 ± 0.48	−0.01 (23.15)	0.993	89	0.978	0
Bruckneudorf M vs Hirschstetten M	**DED**	DED event count	15	1.87 ± 0.99	16	2.13 ± 1.41	−0.59 (26.96)	0.558	108.5	0.652	−0.21
		Maximum DED depth	14	32.19 ± 19.06	14	37.74 ± 19.64	−0.76 (25.98)	0.455	77	0.346	−0.29
		Timing of deepest DED	14	0.45 ± 0.17	14	0.35 ± 0.14	1.56 (24.87)	0.131	129	0.161	0.59
		Timing of earliest DED	14	0.54 ± 0.19	14	0.45 ± 0.21	1.17 (25.76)	0.254	125	0.223	0.44
	Appendicular Growth	Estimated stature	16	165.50 ± 7.71	13	164.18 ± 5.89	0.52 (26.92)	0.607	109	0.844	0.19
		Stature z-score	16	0.07 ± 1.28	13	−0.15 ± 0.98	0.52 (26.92)	0.607	109	0.844	0.19
		CTI	8	0.63 ± 0.04	12	0.63 ± 0.06	0.37 (17.59)	0.719	48	1	0.16
		CTI z-score	8	0.10 ± 0.85	12	−0.06 ± 1.12	0.37 (17.59)	0.719	48	1	0.16
		Appendicular asymmetry	15	0.80 ± 0.41	11	1.57 ± 1.92	−1.30 (10.66)	0.222	69	0.5	−0.55
	OA	Total OA score	18	0.58 ± 0.54	19	0.37 ± 0.53	1.24 (34.86)	0.225	222	0.12	0.41
		Peripheral OA score	18	0.43 ± 0.48	19	0.27 ± 0.45	1.08 (34.45)	0.287	228.5	0.076	0.36
		Vertebral OA score	18	0.73 ± 0.66	19	0.46 ± 0.65	1.25 (34.87)	0.22	212	0.191	0.41
	SINDEX	Equal-weight SINDEX	18	0.18 ± 0.66	19	−0.11 ± 0.44	1.57 (29.27)	0.128	226	0.098	0.52
		PD	18	0.30 ± 0.62	19	−0.17 ± 0.65	2.24 (34.99)	**.032***	243	**.030***	0.74
		PNBF	18	0.07 ± 1.19	19	−0.05 ± 0.80	0.33 (29.47)	.			

Table A.4 Population comparisons of categorical developmental and osteoarthritis variables using Fisher's exact tests. Note. Odds ratios were not estimated for the multicategory DED timing comparisons. No population comparison was statistically significant at $p < .05$.

Domain	Variable	p	Odds ratio	95% CI
DED	Timing bin of deepest DED	0.091	—	—
	Timing bin of earliest DED	0.198	—	—
OA	Any OA	1	0.92	0.28–2.98
	Peripheral OA	0.606	0.7	0.22–2.19
	Vertebral OA	0.812	0.88	0.30–2.54
Appendicular Growth	CTI-thinned classification	1	1	0.01–82.32
	Growth-constraint classification	1	1.31	0.02–106.90

Table A.5 Sex-stratified and population-stratified comparisons of categorical appendicular-growth and osteoarthritis variables using Fisher's exact tests. Note. F = estimated female; M = estimated male. Dashes indicate that odds ratios could not be estimated. Zero and infinite estimates, together with wide confidence intervals, reflect sparse contingency-table cells. Odds-ratio direction follows the original group coding. $*p < .05$.

Comparison	Domain	Variable	p	Odds ratio	95% CI
Bruckneudorf: F vs M	**Appendicular Growth**	CTI-thinned classification	1	0	0.00–63.31
		Growth-constraint classification	1	∞	0.02–∞
	OA	Any OA	0.24	—	—
		Peripheral OA	0.24	—	—
		Vertebral OA	0.121	—	—
Hirschstetten: F vs M	**Appendicular Growth**	CTI-thinned classification	1	∞	0.02–∞
		Growth-constraint classification	0.435	0	0.00–30.00
	OA	Any OA	0.296	—	—
		Peripheral OA	0.089	—	—
		Vertebral OA	0.447	—	—
Females: Bruckneudorf vs Hirschstetten	**Appendicular Growth**	CTI-thinned classification	1	0	0.00–56.28
		Growth-constraint classification	0.417	∞	0.04–∞
	OA	Any OA	0.236	3.19	0.42–40.28
		Peripheral OA	0.236	3.19	0.42–40.28
		Vertebral OA	1	1	0.14–6.55
Males: Bruckneudorf vs Hirschstetten	**Appendicular Growth**	CTI-thinned classification	1	∞	0.02–∞
		Growth-constraint classification	1	0	0.00–47.96
	OA	Any OA	0.151	0.29	0.04–1.54
		Peripheral OA	**.038***	**0.19**	**0.03–1.00**
		Vertebral OA	0.33	0.47	0.10–2.06

Table A.6 DED: Distribution of deepest DED timing categories by population. Values are counts of individuals. No Hirschstetten individuals were classified in the early timing category.

Population	Early	Mid	Late	Total
Bruckneudorf	4	16	8	**28**
Hirschstetten	0	14	12	**26**
Total	**4**	**30**	**20**	**54**

Table A.7 Distribution of earliest DED timing categories by population. Note: Values are counts of individuals.

Population	Early	Mid	Late	Total
Bruckneudorf	11	14	3	**28**
Hirschstetten	5	15	6	**26**
Total	**16**	**29**	**9**	**54**

Table A.8 Overall Spearman correlations between early-life stress indicators and adult inflammatory/remodelling markers. Note. Adjusted p values use the Benjamini–Hochberg correction. Correlations were weak or negligible, and none remained statistically significant after adjustment.

Early-Life Indicator	Adult Marker	n	Spearman's rho	p	Adjusted p
Stature Constraint (−z)	PD	53	0.178	0.203	0.993
	PNBF	53	−0.177	0.204	0.993
	Total OA score	53	0.03	0.832	0.993
	Peripheral OA score	53	0.086	0.542	0.993
	Vertebral OA score	52	−0.027	0.85	0.993
	Equal-weight SINDEX	53	0.135	0.336	0.993
CTI Constraint (−z)	PD	42	−0.111	0.486	0.993
	PNBF	42	0.067	0.673	0.993
	Total OA score	42	0.016	0.921	0.993
	Peripheral OA score	42	−0.016	0.92	0.993
	Vertebral OA score	41	0.203	0.204	0.993
	Equal-weight SINDEX	42	−0.006	0.972	0.993
BAA	PD	46	0.001	0.993	0.993
	PNBF	46	0.095	0.531	0.993
	Total OA score	46	0.044	0.773	0.993
	Peripheral OA score	46	0.008	0.957	0.993
	Vertebral OA score	46	0.106	0.483	0.993
	Equal-weight SINDEX	46	0.005	0.973	0.993
DED Event Count	PD	59	−0.094	0.478	0.993
	PNBF	59	0.117	0.379	0.993
	Total OA score	59	−0.092	0.489	0.993
	Peripheral OA score	59	−0.124	0.349	0.993
	Vertebral OA score	58	−0.053	0.694	0.993
	Equal-weight SINDEX	59	0.062	0.643	0.993
Maximum DED Depth	PD	54	−0.067	0.628	0.993
	PNBF	54	−0.064	0.646	0.993
	Total OA score	54	0.006	0.965	0.993
	Peripheral OA score	54	−0.004	0.976	0.993

	Vertebral OA score	53	−0.037	0.795	0.993
	Equal-weight SINDEX	54	−0.079	0.569	0.993
Timing of Deepest DED	PD	54	0.176	0.204	0.993
	PNBF	54	0.215	0.119	0.993
	Total OA score	54	0.11	0.43	0.993
	Peripheral OA score	54	0.098	0.482	0.993
	Vertebral OA score	53	0.146	0.298	0.993
	Equal-weight SINDEX	54	0.246	0.073	0.993
Timing of Earliest DED	PD	54	−0.047	0.734	0.993
	PNBF	54	0.253	0.065	0.993
	Total OA score	54	0.043	0.758	0.993
	Peripheral OA score	54	0.052	0.708	0.993
	Vertebral OA score	53	0.107	0.447	0.993
	Equal-weight SINDEX	54	0.102	0.465	0.993

Table A.9 Sex-Stratified Spearman Correlations Between Early-Life Stress Indicators and Adult Inflammatory/Remodelling Markers. Note. F = estimated female; M = estimated male. Adjusted p values use the Benjamini–Hochberg correction. No sex-stratified correlation remained statistically significant after adjustment.

Sex	Early-Life Indicator	Adult Marker	n	Spearman's rho	p	Adjusted p
F	**Stature Constraint (−z)**	PD	24	−0.038	0.859	0.942
		PNBF	24	−0.034	0.875	0.942
		Total OA Score	24	−0.044	0.838	0.942
		Peripheral OA Score	24	−0.054	0.801	0.942
		Vertebral OA Score	23	−0.024	0.915	0.961
		Equal-Weight SINDEX	24	0.088	0.683	0.942
	CTI Constraint (−z)	PD	22	0.075	0.74	0.942
		PNBF	22	−0.096	0.672	0.942
		Total OA Score	22	0.125	0.581	0.942
		Peripheral OA Score	22	0.037	0.871	0.942
		Vertebral OA Score	21	0.4	0.072	0.942
		Equal-Weight SINDEX	22	0.181	0.42	0.942
	BAA	PD	20	0.09	0.705	0.942
		PNBF	20	0.222	0.348	0.942
		Total OA Score	20	0.159	0.502	0.942
		Peripheral OA Score	20	0.166	0.485	0.942
		Vertebral OA Score	20	0.193	0.414	0.942
		Equal-Weight SINDEX	20	0.174	0.462	0.942
	DED Event Count	PD	24	−0.107	0.62	0.942
		PNBF	24	0.348	0.096	0.942
		Total OA Score	24	−0.281	0.184	0.942
		Peripheral OA Score	24	−0.256	0.227	0.942
		Vertebral OA Score	23	−0.191	0.383	0.942
		Equal-Weight SINDEX	24	0.108	0.617	0.942

	Maximum DED Depth	PD	22	0.091	0.687	0.942
		PNBF	22	0.153	0.498	0.942
		Total OA Score	22	0.271	0.223	0.942
		Peripheral OA Score	22	0.232	0.299	0.942
		Vertebral OA Score	21	0.237	0.301	0.942
		Equal-Weight SINDEX	22	0.151	0.503	0.942
	Timing of Deepest DED	PD	22	0.063	0.782	0.942
		PNBF	22	0.216	0.334	0.942
		Total OA Score	22	−0.061	0.786	0.942
		Peripheral OA Score	22	−0.069	0.76	0.942
		Vertebral OA Score	21	0.108	0.643	0.942
		Equal-Weight SINDEX	22	0.222	0.321	0.942
	Timing of Earliest DED	PD	22	−0.006	0.978	0.978
		PNBF	22	0.363	0.097	0.942
		Total OA Score	22	−0.124	0.582	0.942
		Peripheral OA Score	22	−0.080	0.724	0.942
		Vertebral OA Score	21	0.011	0.963	0.978
		Equal-Weight SINDEX	22	0.199	0.374	0.942
M	Stature Constraint (−z)	PD	29	0.416	0.025	0.674
		PNBF	29	−0.239	0.212	0.674
		Total OA Score	29	0.23	0.229	0.674
		Peripheral OA Score	29	0.297	0.117	0.674
		Vertebral OA Score	29	0.124	0.522	0.783
		Equal-Weight SINDEX	29	0.267	0.161	0.674
	CTI Constraint (−z)	PD	20	−0.352	0.128	0.674
		PNBF	20	0.226	0.337	0.674
		Total OA Score	20	−0.122	0.609	0.81
		Peripheral OA Score	20	−0.060	0.801	0.897
		Vertebral OA Score	20	−0.023	0.924	0.924
		Equal-Weight SINDEX	20	−0.215	0.363	0.692
	Appendicular Asymmetry	PD	26	−0.103	0.617	0.81
		PNBF	26	0.021	0.918	0.924
		Total OA Score	26	−0.097	0.637	0.811
		Peripheral OA Score	26	−0.145	0.48	0.747
		Vertebral OA Score	26	−0.033	0.873	0.924
		Equal-Weight SINDEX	26	−0.160	0.436	0.709
	DED Event Count	PD	31	−0.045	0.811	0.897
		PNBF	31	−0.179	0.335	0.674
		Total OA Score	31	0.105	0.575	0.806
		Peripheral OA Score	31	0.028	0.883	0.924
		Vertebral OA Score	31	0.059	0.752	0.878
		Equal-Weight SINDEX	31	−0.064	0.732	0.878

Maximum DED Depth	PD	28	−0.220	0.261	0.674
	PNBF	28	−0.213	0.276	0.674
	Total OA Score	28	−0.160	0.417	0.709
	Peripheral OA Score	28	−0.152	0.439	0.709
	Vertebral OA Score	28	−0.190	0.333	0.674
	Equal-Weight SINDEX	28	−0.258	0.185	0.674
Timing of Deepest DED	PD	28	0.195	0.319	0.674
	PNBF	28	0.23	0.239	0.674
	Total OA Score	28	0.31	0.109	0.674
	Peripheral OA Score	28	0.222	0.255	0.674
	Vertebral OA Score	28	0.235	0.229	0.674
	Equal-Weight SINDEX	28	0.196	0.318	0.674
Timing of Earliest DED	PD	28	−0.117	0.555	0.803
	PNBF	28	0.189	0.336	0.674
	Total OA Score	28	0.236	0.227	0.674
	Peripheral OA Score	28	0.165	0.401	0.709
	Vertebral OA Score	28	0.237	0.224	0.674
	Equal-Weight SINDEX	28	−0.077	0.696	0.86

Table A.10 Population-Stratified Spearman Correlations Between Early-Life Stress Indicators and Adult Inflammatory/Remodelling Markers. Note. Adjusted p values use the Benjamini–Hochberg correction. No population-stratified correlation remained statistically significant after adjustment.

Population	Early-Life Indicator	Adult Marker	n	Spearman's rho	p	Adjusted p
Bruckneudorf	Stature Constraint (−z)	PD	30	0.152	0.423	0.807
		PNBF	30	−0.228	0.226	0.799
		Total OA Score	30	−0.140	0.462	0.809
		Peripheral OA Score	30	−0.123	0.518	0.837
		Vertebral OA Score	29	−0.177	0.357	0.799
		Equal-Weight SINDEX	30	0.082	0.668	0.884
	CTI Constraint (−z)	PD	21	0.086	0.712	0.884
		PNBF	21	0.348	0.122	0.799
		Total OA Score	21	0.059	0.798	0.884
		Peripheral OA Score	21	−0.040	0.863	0.884
		Vertebral OA Score	20	0.284	0.225	0.799
		Equal-Weight SINDEX	21	0.295	0.195	0.799
	BAA	PD	27	0.189	0.344	0.799
		PNBF	27	0.304	0.123	0.799
		Total OA Score	27	0.194	0.333	0.799
		Peripheral OA Score	27	0.221	0.269	0.799
		Vertebral OA Score	27	0.224	0.262	0.799
		Equal-Weight SINDEX	27	0.172	0.392	0.807
	DED Event Count	PD	30	−0.141	0.457	0.809
		PNBF	30	0.132	0.488	0.82
		Total OA Score	30	−0.209	0.268	0.799
		Peripheral OA Score	30	−0.193	0.306	0.799

		Vertebral OA Score	29	−0.189	0.326	0.799
		Equal-Weight SINDEX	30	0.114	0.549	0.845
	Maximum DED Depth	PD	28	−0.037	0.851	0.884
		PNBF	28	−0.159	0.419	0.807
		Total OA Score	28	0.051	0.796	0.884
		Peripheral OA Score	28	0.046	0.815	0.884
		Vertebral OA Score	27	−0.015	0.939	0.939
		Equal-Weight SINDEX	28	−0.061	0.757	0.884
	Timing of Deepest DED	PD	28	0.253	0.193	0.799
		PNBF	28	0.408	0.031	0.799
		Total OA Score	28	0.114	0.563	0.845
		Peripheral OA Score	28	0.089	0.651	0.884
		Vertebral OA Score	27	0.183	0.361	0.799
		Equal-Weight SINDEX	28	0.373	0.051	0.799
	Timing of Earliest DED	PD	28	0.041	0.838	0.884
		PNBF	28	0.312	0.106	0.799
		Total OA Score	28	−0.039	0.845	0.884
		Peripheral OA Score	28	−0.062	0.755	0.884
		Vertebral OA Score	27	0.054	0.789	0.884
		Equal-Weight SINDEX	28	0.192	0.329	0.799
Hirschstetten	**Stature Constraint (−z)**	PD	23	0.261	0.229	0.944
		PNBF	23	−0.154	0.484	0.944
		Total OA Score	23	0.175	0.423	0.944
		Peripheral OA Score	23	0.285	0.187	0.944
		Vertebral OA Score	23	0.115	0.602	0.944
		Equal-Weight SINDEX	23	0.144	0.511	0.944
	CTI Constraint (−z)	PD	21	−0.240	0.294	0.944
		PNBF	21	−0.164	0.477	0.944
		Total OA Score	21	−0.030	0.899	0.944
		Peripheral OA Score	21	0.014	0.952	0.96
		Vertebral OA Score	21	0.156	0.499	0.944
		Equal-Weight SINDEX	21	−0.234	0.308	0.944
	BAA	PD	19	−0.061	0.803	0.944
		PNBF	19	−0.170	0.487	0.944
		Total OA Score	19	−0.071	0.773	0.944
		Peripheral OA Score	19	−0.103	0.676	0.944
		Vertebral OA Score	19	0.052	0.832	0.944
		Equal-Weight SINDEX	19	−0.012	0.96	0.96
	DED Event Count	PD	29	0.065	0.739	0.944
		PNBF	29	0.107	0.58	0.944
		Total OA Score	29	0.038	0.845	0.944
		Peripheral OA Score	29	−0.040	0.836	0.944

		Vertebral OA Score	29	0.111	0.567	0.944
		Equal-Weight SINDEX	29	0.086	0.656	0.944
	Maximum DED Depth	PD	26	−0.064	0.756	0.944
		PNBF	26	0.034	0.868	0.944
		Total OA Score	26	−0.042	0.837	0.944
		Peripheral OA Score	26	−0.053	0.797	0.944
		Vertebral OA Score	26	−0.064	0.757	0.944
		Equal-Weight SINDEX	26	−0.098	0.633	0.944
	Timing of Deepest DED	PD	26	0.052	0.8	0.944
		PNBF	26	0.027	0.895	0.944
		Total OA Score	26	0.082	0.69	0.944
		Peripheral OA Score	26	0.085	0.681	0.944
		Vertebral OA Score	26	0.064	0.756	0.944
		Equal-Weight SINDEX	26	0.063	0.761	0.944
	Timing of Earliest DED	PD	26	−0.145	0.479	0.944
		PNBF	26	0.198	0.331	0.944
		Total OA Score	26	0.136	0.509	0.944
		Peripheral OA Score	26	0.144	0.483	0.944
		Vertebral OA Score	26	0.163	0.427	0.944
		Equal-Weight SINDEX	26	−0.079	0.701	0.944

Table A.11 Age-Adjusted Partial Spearman Correlations Between Early-Life Stress Indicators and Adult Inflammatory/Remodelling Markers. Partial correlations control for age at death. Adjusted p values use the Benjamini–Hochberg correction. No association remained statistically significant after adjustment.

Early-Life Indicator	Adult Marker	n	Partial Spearman's rho	p	Adjusted p
Stature Constraint (−z)	PD	53	0.232	0.094	0.921
	PNBF	53	−0.165	0.239	0.921
	Total OA Score	53	0.115	0.412	0.921
	Peripheral OA Score	53	0.157	0.263	0.921
	Vertebral OA Score	52	0.027	0.852	0.921
	Equal-Weight SINDEX	53	0.185	0.186	0.921
CTI Constraint (−z)	PD	42	−0.216	0.169	0.921
	PNBF	42	0.048	0.763	0.921
	Total OA Score	42	−0.084	0.598	0.921
	Peripheral OA Score	42	−0.103	0.515	0.921
	Vertebral OA Score	41	0.079	0.623	0.921
	Equal-Weight SINDEX	42	−0.061	0.703	0.921
BAA	PD	46	−0.041	0.788	0.921
	PNBF	46	0.074	0.623	0.921
	Total OA Score	46	−0.019	0.899	0.921
	Peripheral OA Score	46	−0.042	0.78	0.921
	Vertebral OA Score	46	0.056	0.712	0.921
	Equal-Weight SINDEX	46	−0.035	0.819	0.921

DED Event Count	PD	58	−0.062	0.646	0.921
	PNBF	58	0.116	0.387	0.921
	Total OA Score	58	−0.056	0.677	0.921
	Peripheral OA Score	58	−0.098	0.465	0.921
	Vertebral OA Score	57	−0.008	0.952	0.952
	Equal-Weight SINDEX	58	0.09	0.503	0.921
Maximum DED Depth	PD	53	0.1	0.477	0.921
	PNBF	53	−0.057	0.686	0.921
	Total OA Score	53	0.201	0.15	0.921
	Peripheral OA Score	53	0.136	0.33	0.921
	Vertebral OA Score	52	0.224	0.111	0.921
	Equal-Weight SINDEX	53	0.029	0.839	0.921
Timing of Deepest DED	PD	53	0.043	0.762	0.921
	PNBF	53	0.214	0.123	0.921
	Total OA Score	53	−0.054	0.703	0.921
	Peripheral OA Score	53	−0.025	0.859	0.921
	Vertebral OA Score	52	−0.080	0.573	0.921
	Equal-Weight SINDEX	53	0.165	0.237	0.921
Timing of Earliest DED	PD	53	−0.157	0.261	0.921
	PNBF	53	0.24	0.083	0.921
	Total OA Score	53	−0.055	0.694	0.921
	Peripheral OA Score	53	−0.019	0.893	0.921
	Vertebral OA Score	52	−0.040	0.778	0.921
	Equal-Weight SINDEX	53	0.037	0.793	0.921

Table A.12 Spearman Correlations Among Early-Life Stress Indicators. Note. Adjusted p values use the Benjamini–Hochberg correction. ∗∗p < .01; ∗∗∗p < .001.

Indicator 1	Indicator 2	n	Spearman's rho	p	Adjusted p
Stature Constraint (−z)	CTI Constraint (−z)	35	0.073	0.676	0.832
	BAA	46	0	1	1
	DED Event Count	44	0.072	0.642	0.832
	Maximum DED Depth	42	−0.123	0.439	0.821
	Timing of Deepest DED	42	−0.340	0.028	0.165
	Timing of Earliest DED	42	−0.221	0.159	0.4
CTI Constraint (−z)	BAA	29	0.125	0.519	0.821
	DED Event Count	36	−0.298	0.077	0.27
	Maximum DED Depth	33	0.041	0.819	0.905
	Timing of Deepest DED	33	0.01	0.956	1
	Timing of Earliest DED	33	0.109	0.547	0.821
BAA	DED Event Count	38	−0.116	0.487	0.821
	Maximum DED Depth	36	−0.359	0.031	0.165
	Timing of Deepest DED	36	0.226	0.185	0.4
	Timing of Earliest DED	36	−0.082	0.634	0.832

DED Event Count	Maximum DED Depth	54	0.181	0.191	0.4
	Timing of Deepest DED	54	0.247	0.072	0.27
	Timing of Earliest DED	54	**0.496**	**<.001**	**.001**∗∗
Maximum DED Depth	Timing of Deepest DED	54	−0.216	0.116	0.348
	Timing of Earliest DED	54	−0.051	0.713	0.832
Timing of Deepest DED	**Timing of Earliest DED**	54	**0.596**	**<.001**	**<.001***

Table A.13 Strongest Life-Course Spearman Correlations, Ranked by Absolute Correlation Strength. Note. Correlations are ordered by absolute Spearman's ρ. Adjusted p values use the Benjamini–Hochberg correction. ∗p < .05; ∗∗p < .01; ∗∗∗p < .001.

Variable 1	Variable 2	n	Spearman's ρ	p	Adjusted p
Total OA Score	**Peripheral OA Score**	68	**0.924**	**<.001**	**<.001***
Total OA Score	**Vertebral OA Score**	67	**0.917**	**<.001**	**<.001***
Peripheral OA Score	**Vertebral OA Score**	67	**0.759**	**<.001**	**<.001***
PD	**Equal-Weight SINDEX**	68	**0.743**	**<.001**	**<.001***
Age at Death	**Vertebral OA Score**	66	**0.658**	**<.001**	**<.001***
Timing of Deepest DED	**Timing of Earliest DED**	54	**0.596**	**<.001**	**<.001***
Age at Death	**Total OA Score**	67	**0.547**	**<.001**	**<.001***
PD	**Vertebral OA Score**	67	**0.504**	**<.001**	**<.001***
PD	**Total OA Score**	68	**0.496**	**<.001**	**<.001***
DED Event Count	**Timing of Earliest DED**	54	**0.496**	**<.001**	**.001**∗∗
PNBF	**Equal-Weight SINDEX**	68	**0.479**	**<.001**	**<.001***
PD	**Peripheral OA Score**	68	**0.467**	**<.001**	**<.001***
Age at Death	**PD**	67	**0.438**	**<.001**	**.002**∗∗
Vertebral OA Score	**Equal-Weight SINDEX**	67	**0.432**	**<.001**	**.002**∗∗
Age at Death	**Peripheral OA Score**	67	**0.432**	**<.001**	**.002**∗∗
Total OA Score	**Equal-Weight SINDEX**	68	**0.366**	**0.002**	**.012**∗
BAA	Maximum DED Depth	36	−0.359	0.032	0.143
Stature Constraint (−z)	Timing of Deepest DED	42	−0.340	0.028	0.133
Peripheral OA Score	**Equal-Weight SINDEX**	68	**0.337**	**0.005**	**.026**∗
Age at Death	**Equal-Weight SINDEX**	67	**0.315**	**0.01**	**.048**∗

Table A.14 Spearman Correlations Among Adult Inflammatory and Osteoarthritis Measures. Note. Adjusted p values use the Benjamini–Hochberg correction. ∗∗p < .01; ∗∗∗p < .001.

Variable 1	Variable 2	n	Spearman's rho	p	Adjusted p
PD	PNBF	68	−0.097	0.43	0.496
	Total OA Score	68	**0.496**	**<.001**	**<.001***
	Peripheral OA Score	68	**0.467**	**<.001**	**<.001***
	Vertebral OA Score	67	**0.504**	**<.001**	**<.001***
	Equal-Weight SINDEX	68	**0.743**	**<.001**	**<.001***
PNBF	Total OA Score	68	0.034	0.783	0.839
	Peripheral OA Score	68	−0.006	0.964	0.964
	Vertebral OA Score	67	0.143	0.25	0.312
	Equal-Weight SINDEX	68	**0.479**	**<.001**	**<.001***

Total OA Score	**Peripheral OA Score**	68	**0.924**	**<.001**	**<.001***
	Vertebral OA Score	67	**0.916**	**<.001**	**<.001***
	Equal-Weight SINDEX	68	**0.366**	**0.002**	**.003****
Peripheral OA Score	**Vertebral OA Score**	67	**0.759**	**<.001**	**<.001***
	Equal-Weight SINDEX	68	**0.337**	**0.005**	**.007****
Vertebral OA Score	**Equal-Weight SINDEX**	67	**0.432**	**<.001**	**<.001***

*Table A.15 Multivariable Regression Coefficients for Life-Course Models. Note. Reference categories are Bruckneudorf and estimated female. SE = standard error. Statistical significance is marked for predictor terms only. *p < .05; **p < .01; ***p < .001.*

Model	Predictor	Estimate	SE	Statistic	p
Early Life → SINDEX	Intercept	−0.793	0.57	−1.391	0.185
	Stature Constraint (−z)	0.047	0.143	0.326	0.749
	CTI Constraint (−z)	−0.105	0.14	−0.750	0.465
	BAA	−0.031	0.151	−0.202	0.842
	DED Event Count	−0.011	0.137	−0.082	0.936
	Hirschstetten	−0.079	0.2	−0.393	0.7
	Estimated Male	−0.039	0.281	−0.138	0.892
	Age at Death	**0.02**	**0.009**	**2.228**	**.042***
Early Life → PD	Intercept	−0.696	0.89	−0.782	0.446
	Stature Constraint (−z)	0.134	0.19	0.707	0.49
	CTI Constraint (−z)	−0.163	0.259	−0.631	0.538
	BAA	−0.102	0.243	−0.418	0.682
	DED Event Count	−0.100	0.168	−0.596	0.56
	Hirschstetten	−0.048	0.361	−0.132	0.897
	Estimated Male	−0.022	0.434	−0.051	0.96
	Age at Death	0.029	0.014	2.033	0.06
Early Life → PNBF	Intercept	−0.890	0.373	−2.389	0.031
	Stature Constraint (−z)	−0.041	0.122	−0.337	0.741
	CTI Constraint (−z)	−0.047	0.085	−0.555	0.587
	BAA	0.041	0.078	0.523	0.609
	DED Event Count	0.077	0.132	0.587	0.566
	Hirschstetten	−0.110	0.12	−0.913	0.376
	Estimated Male	−0.055	0.244	−0.226	0.825
	Age at Death	0.012	0.006	1.882	0.079
Early Life → OA	Intercept	−1.113	0.608	−1.831	0.087
	Stature Constraint (−z)	0.202	0.133	1.514	0.151
	CTI Constraint (−z)	−0.240	0.146	−1.645	0.121
	BAA	−0.016	0.11	−0.144	0.887
	DED Event Count	−0.084	0.138	−0.608	0.552
	Hirschstetten	−0.008	0.232	−0.036	0.972
	Estimated Male	0.542	0.369	1.47	0.162
	Age at Death	**0.034**	**0.009**	**3.789**	**.002****
Appendicular Growth → SINDEX	Intercept	−0.216	0.394	−0.550	0.588
	Stature Constraint (−z)	0.135	0.15	0.897	0.38

	CTI Constraint (−z)	0.016	0.176	0.091	0.929
	BAA	−0.179	0.144	−1.240	0.228
	Hirschstetten	−0.322	0.193	−1.669	0.109
	Estimated Male	0.364	0.462	0.786	0.44
	Age at Death	0.009	0.007	1.305	0.205
DED → SINDEX	Intercept	−0.687	0.386	−1.779	0.082
	DED Event Count	0.124	0.133	0.935	0.355
	Maximum DED Depth	0.001	0.003	0.308	0.759
	Timing of Deepest DED	0.767	0.706	1.086	0.283
	Timing of Earliest DED	−0.453	0.633	−0.716	0.478
	Hirschstetten	−0.242	0.172	−1.408	0.166
	Estimated Male	0.035	0.125	0.281	0.78
	Indeterminate Sex	0.586	1.037	0.565	0.575
	Age at Death	0.009	0.005	1.788	0.081
Stature Constraint → Appendicular Stress	Intercept	1.456	1.551	0.938	0.362
	CTI Constraint (−z)	0.16	0.374	0.428	0.675
	BAA	0.163	0.376	0.433	0.671
	DED Event Count	0.128	0.336	0.383	0.707
	Hirschstetten	−0.023	0.636	−0.036	0.972
	Estimated Male	**−1.634**	**0.635**	**−2.573**	**.020***
	Age at Death	−0.020	0.028	−0.710	0.488
SINDEX → OA	Intercept	−0.475	0.159	−2.979	0.004
	Equal-Weight SINDEX	0.122	0.109	1.11	0.272
	Hirschstetten	0.01	0.103	0.095	0.925
	Estimated Male	0.076	0.105	0.722	0.473
	Indeterminate Sex	0.128	0.276	0.463	0.645
	Age at Death	**0.022**	**0.004**	**5.313**	**<.001***
PD and PNBF → OA	Intercept	−0.393	0.168	−2.346	0.022
	PD	**0.232**	**0.102**	**2.271**	**.027***
	PNBF	0.003	0.04	0.064	0.949
	Age at Death	**0.019**	**0.005**	**4**	**<.001***
	Estimated Male	0.068	0.105	0.648	0.52
	Indeterminate Sex	0.281	0.233	1.206	0.233
	Hirschstetten	0.1	0.1	0.999	0.322
PD → PNBF	Intercept	−0.043	0.293	−0.145	0.885
	PD	−0.104	0.115	−0.907	0.368
	Age at Death	<−0.001	0.007	−0.058	0.954
	Estimated Male	0.183	0.207	0.885	0.38
	Indeterminate Sex	1.461	2.048	0.713	0.478
	Hirschstetten	−0.213	0.254	−0.841	0.404

Table A.16 Age-at-Death Distributions by Population and Estimated Sex. Note. F = estimated female; M = estimated male; I = indeterminate sex. SD was not calculated for the single Hirschstetten individual of indeterminate sex.

Population	Sex	n	Mean ± SD	Median	Range
Bruckneudorf	F	15	38.20 ± 15.35	39	19.00–60.00
	M	18	40.50 ± 13.49	42.75	17.50–70.00
	I	2	19.00 ± 0.71	19	18.50–19.50
Hirschstetten	F	12	39.63 ± 19.87	34	17.00–75.00
	M	19	38.55 ± 15.45	38.5	18.00–67.50
	I	1	29.00 ± —	29	29.00–29.00

Table A.17 Population-Level Age and Oral-Health Summaries. Note. PD = periodontal disease component score; AMTL = antemortem tooth-loss count. Calculus is summarized as the individual-level proportion with calculus present.

Population	n	Mean Age	PD Mean (Median)	AMTL Mean (Median)	Calculus Mean (Median)
Bruckneudorf	35	38.29	0.26 (0.27)	4.71 (2.00)	1.00 (1.00)
Hirschstetten	33	38.66	−0.28 (−0.30)	3.70 (1.00)	0.98 (1.00)

Spearman Correlations Between Early-Life Stress Indicators and Component-Level Adult Inflammatory Measures. Note. Adjusted p values use the Benjamini–Hochberg correction. No component-level association remained statistically significant after adjustment.

Early-Life Indicator	Inflammatory Measure	n	Spearman's rho	p	Adjusted p
CTI Constraint (−z)	PD Component	42	−0.11	0.49	0.82
	Kerr Score Sum	42	−0.17	0.27	0.82
	SLB/SLI Score Sum	42	−0.15	0.36	0.82
	PNBF Activity Count	42	0.11	0.48	0.82
	PNBF Severity Sum	42	0.08	0.63	0.82
	PNBF Component	42	0.07	0.67	0.82
DED Event Count	PD Component	59	−0.09	0.48	0.82
	Kerr Score Sum	59	−0.04	0.75	0.82
	SLB/SLI Score Sum	59	0.02	0.89	0.92
	PNBF Activity Count	59	**0.27**	**0.04**	**0.79**
	PNBF Severity Sum	59	0.09	0.51	0.82
	PNBF Component	59	0.12	0.38	0.82
BAA	PD Component	46	0	0.99	0.99
	Kerr Score Sum	46	−0.03	0.85	0.92
	SLB/SLI Score Sum	46	−0.06	0.68	0.82
	PNBF Activity Count	46	0.11	0.48	0.82
	PNBF Severity Sum	46	0.09	0.56	0.82
	PNBF Component	46	0.09	0.53	0.82
Maximum DED Depth	PD Component	54	−0.07	0.63	0.82
	Kerr Score Sum	54	−0.11	0.43	0.82
	SLB/SLI Score Sum	54	−0.10	0.47	0.82
	PNBF Activity Count	54	−0.05	0.73	0.82
	PNBF Severity Sum	54	−0.06	0.68	0.82
	PNBF Component	54	−0.06	0.65	0.82

Stature Constraint (−z)	PD Component	53	0.18	0.2	0.79
	Kerr Score Sum	53	0.17	0.21	0.79
	SLB/SLI Score Sum	53	−0.07	0.64	0.82
	PNBF Activity Count	53	−0.10	0.47	0.82
	PNBF Severity Sum	53	−0.17	0.23	0.79
	PNBF Component	53	−0.18	0.2	0.79
Timing of Deepest DED	PD Component	54	0.18	0.2	0.79
	Kerr Score Sum	54	0.16	0.25	0.81
	SLB/SLI Score Sum	54	0.13	0.36	0.82
	PNBF Activity Count	54	0.17	0.22	0.79
	PNBF Severity Sum	54	0.22	0.11	0.79
	PNBF Component	54	0.21	0.12	0.79
Timing of Earliest DED	PD Component	54	−0.05	0.73	0.82
	Kerr Score Sum	54	0.02	0.9	0.92
	SLB/SLI Score Sum	54	−0.14	0.33	0.82
	PNBF Activity Count	54	***0.24***	***0.08***	***0.79***
	PNBF Severity Sum	54	***0.26***	***0.06***	***0.79***
	PNBF Component	54	***0.25***	***0.07***	***0.79***

*Table A.18 Age-Adjusted Partial Spearman Correlations Between Early-Life Stress Indicators and Component-Level Adult Inflammatory Measures. Note. Partial correlations control for age at death. Adjusted p values use the Benjamini–Hochberg correction. * indicates a nominal unadjusted association at p < .05; † indicates a trend-level unadjusted association at .05 ≤ p < .10. No association remained statistically significant after correction.*

Early-Life Indicator	Inflammatory Measure	n	Partial Spearman's rho	p	Adjusted p
CTI Constraint (−z)	PD Component	42	−0.22	0.17	0.7
	Kerr Score Sum	42	−0.24	0.12	0.65
	SLB/SLI Score Sum	42	−0.16	0.3	0.78
	PNBF Activity Count	42	0.11	0.47	0.84
	PNBF Severity Sum	42	0.06	0.71	0.84
	PNBF Component	42	0.05	0.76	0.84
DED Event Count	PD Component	58	−0.06	0.65	0.84
	Kerr Score Sum	58	−0.03	0.8	0.84
	SLB/SLI Score Sum	58	0.07	0.63	0.84
	PNBF Activity Count	58	**0.27**	**.04***	0.65
	PNBF Severity Sum	58	0.09	0.52	0.84
	PNBF Component	58	0.12	0.39	0.84
BAA	PD Component	46	−0.04	0.79	0.84
	Kerr Score Sum	46	−0.06	0.69	0.84
	SLB/SLI Score Sum	46	−0.06	0.7	0.84
	PNBF Activity Count	46	0.09	0.56	0.84
	PNBF Severity Sum	46	0.07	0.65	0.84
	PNBF Component	46	0.07	0.62	0.84

Maximum DED Depth	PD Component	53	0.1	0.48	0.84
	Kerr Score Sum	53	−0.02	0.87	0.89
	SLB/SLI Score Sum	53	−0.01	0.95	0.95
	PNBF Activity Count	53	−0.05	0.7	0.84
	PNBF Severity Sum	53	−0.05	0.72	0.84
	PNBF Component	53	−0.06	0.69	0.84
Stature Constraint (−z)	***PD Component***	53	***0.23***	***.09†***	0.65
	Kerr Score Sum	53	0.2	0.14	0.66
	SLB/SLI Score Sum	53	−0.07	0.64	0.84
	PNBF Activity Count	53	−0.09	0.54	0.84
	PNBF Severity Sum	53	−0.16	0.26	0.74
	PNBF Component	53	−0.16	0.24	0.74
Timing of Deepest DED	PD Component	53	0.04	0.76	0.84
	Kerr Score Sum	53	0.09	0.53	0.84
	SLB/SLI Score Sum	53	0.05	0.71	0.84
	PNBF Activity Count	53	0.18	0.21	0.72
	PNBF Severity Sum	53	0.22	0.11	0.65
	PNBF Component	53	0.21	0.12	0.65
Timing of Earliest DED	PD Component	53	−0.16	0.26	0.74
	Kerr Score Sum	53	−0.04	0.75	0.84
	SLB/SLI Score Sum	53	−0.19	0.18	0.7
	PNBF Activity Count	53	***0.23***	***.09†***	0.65
	PNBF Severity Sum	53	***0.25***	***.07†***	0.65
	PNBF Component	53	***0.24***	***.08†***	0.65

Table A.19 Regression Coefficients for Developmental, Demographic, and Oral-Health Models of Adult Inflammatory Outcomes. Note. Reference categories are Bruckneudorf and estimated female. SE = standard error; AMTL = antemortem tooth loss. ∗ indicates p < .05; † indicates a trend-level result at .05 ≤ p < .10. Intercept significance is reported for completeness but is not interpreted as a substantive predictor effect.

Model	Predictor	Estimate	SE	Statistic	p
Developmental Indicators → PD	Intercept	−0.75	0.92	−0.82	0.43
	Timing of Earliest DED	0.3	2.07	0.15	0.89
	DED Event Count	−0.11	0.46	−0.24	0.81
	Stature Constraint (−z)	0.14	0.3	0.48	0.64
	CTI Constraint (−z)	−0.15	0.29	−0.52	0.61
	BAA	−0.12	0.25	−0.49	0.63
	Age at Death	0.03	0.02	1.35	0.2
	Hirschstetten	−0.02	0.39	−0.04	0.97
	Estimated Male	0.02	0.52	0.03	0.97
Developmental Indicators → PNBF	Intercept	***−0.96***	***0.47***	***−2.04***	***.06†***
	Timing of Earliest DED	−0.35	1.55	−0.22	0.83
	DED Event Count	0.21	0.41	0.51	0.62
	Stature Constraint (−z)	−0.08	0.17	−0.49	0.63
	CTI Constraint (−z)	0	0.1	−0.03	0.97

	BAA	0.02	0.07	0.3	0.77
	Age at Death	0.01	0.01	1.03	0.32
	Hirschstetten	−0.12	0.26	−0.47	0.65
	Estimated Male	−0.04	0.38	−0.11	0.92
Oral Ecology → PD	Intercept	−0.61	1.63	−0.37	0.71
	Age at Death	0.01	0.01	1.04	0.3
	Hirschstetten	**−0.46**	**0.13**	**−3.53**	**<.001***
	Estimated Male	0.15	0.13	1.16	0.25
	AMTL Count	**0.06**	**0.01**	**5.82**	**<.001***
	Calculus Presence Proportion	0.35	1.62	0.22	0.83
Oral Ecology and PD → PNBF	Intercept	−0.06	2.84	−0.02	0.98
	Age at Death	0	0.01	0.01	0.99
	Hirschstetten	−0.15	0.21	−0.70	0.49
	Estimated Male	0.16	0.22	0.74	0.46
	PD Component	−0.24	0.19	−1.27	0.21
	AMTL Count	0.01	0.02	0.55	0.58
	Calculus Presence Proportion	−0.05	2.81	−0.02	0.99
PNBF → PD	Intercept	**−0.50**	**0.24**	**−2.06**	**.04***
	PNBF Component	−0.07	0.06	−1.16	0.25
	Age at Death	**0.02**	**0.01**	**3.64**	**<.001***
	Hirschstetten	**−0.56**	**0.15**	**−3.68**	**<.001***
	Estimated Male	0.11	0.15	0.72	0.48
PD → PNBF	Intercept	−0.14	0.25	−0.56	0.58
	PD Component	−0.13	0.1	−1.23	0.22
	Age at Death	0	0.01	0.19	0.85
	Hirschstetten	−0.14	0.23	−0.59	0.56
	Estimated Male	0.18	0.21	0.87	0.39

Table A.20 High-Burden PNBF Outlier Profiles and Associated Life-Course Indicators. Note. Individuals are ranked by descending PNBF component score. These profiles represent the upper end of the observed PNBF distribution and are described as outliers in a distributional, rather than diagnostic, sense. F = estimated female; M = estimated male; I = indeterminate sex; AMTL = antemortem tooth-loss count; DED = dental enamel defects. Dashes indicate unavailable data, and diagnostic descriptions reflect differential considerations rather than confirmed diagnoses.

Rank	Population	Individual	Sex	Age	PNBF Score	Severity Sum	Activity Count	PD	AMTL	DED Events	Earliest / Deepest DED	Contextual Summary
1	Bruckneudorf	NHMW-Anthro-Oste-27.291	I	18.5	4.74	56	14	−0.40	1	4	0.61 / 0.47	Highest PNBF burden; diffuse multi-element involvement, including the pelvis, limbs, feet, hands, and ribs. Rib lesions require caution because fracture and taphonomic alteration were recorded.
2	Bruckneudorf	NHMW-Anthro-Oste-27.335	M	35.5	4.69	59	13	0.11	0	—	—	Severe upper- and lower-limb involvement with possible rib lesions. Subperiosteal deposits were recorded; possible gout-like and taphonomic changes complicate interpretation.

3	Hirschstetten	57	M	18.5	2.82	30	10	−0.72	2	2	0.21 / 0.18	Extensive bilateral lower-extremity and foot involvement. Leprosy was considered during assessment but remains a differential diagnosis.
4	Hirschstetten	125	F	70	1.05	16	4	−0.04	16	5	0.84 / 0.39	PNBF affects the tibia, ulna, and ribs. Possible tuberculosis and multi-system pathology require cautious interpretation.
5	Hirschstetten	5	M	49.5	0.85	20	2	−0.39	6	1	0.62 / 0.62	Femoral, tibial, and rib involvement; poor preservation may mimic extensive PNBF. Retained as a low-confidence surface assessment.

6	Bruckneudorf	NHMW-Anthro-Oste-27.354	F	21	0.84	24	1	−0.65	2	3	0.78 / 0.40	Extensive pelvic and lower-limb PNBF with destructive vertebral change. Tuberculosis was considered, but preservation limits diagnostic attribution.
7	Hirschstetten	109	M	18.5	0.73	13	3	−0.28	0	3	0.59 / 0.43	Strongly unilateral PNBF with associated lytic and vertebral changes. Localized infection, trauma, or another focal destructive process remain possible.
8	Bruckneudorf	NHMW-Anthro-Oste-27.404	F	60	0.68	12	3	1.18	7	3	0.71 / 0.71	Severe right-femoral osteomyelitic change after probable fracture, with additional pelvic and vertebral lesions. Burden is likely dominated by trauma-related infection.

9	Bruckneudorf	NHMW-Anthro-Oste-27.556	M	42.5	0.55	9	3	0.57	0	3	0.72 / 0.59	Rib PNBF with possible pleuritic deposits and respiratory involvement. Degenerative and other skeletal changes complicate interpretation.
10	Bruckneudorf	NHMW-Anthro-Oste-27.225	F	21	0.49	12	2	−0.41	0	2	0.76 / 0.40	Bilateral femoral and tibial PNBF with cranial porosity and focal lytic activity. Associated lesions should be interpreted cautiously.
11	Hirschstetten	108	F	55	0.45	11	2	−0.25	1	3	0.60 / 0.54	PNBF affects the clavicle, tibia, and femur. Moderate burden with limited additional pathological context.
12	Bruckneudorf	NHMW-Anthro-Oste-27.246	M	70	0.35	13	1	1.15	25	2	0.82 / 0.82	Lower-limb PNBF accompanied by dental infection, widespread OA, and possible traumatic or compressive changes.

13	Hirschstetten	12	M	18	0.26	11	1	−0.96	0	2	0.67 / 0.28	Lower-limb PNBF with OA despite young age. Available observations do not support a specific diagnosis.
14	Hirschstetten	180	F	35	0.26	11	1	−0.40	1	1	0.29 / 0.29	Bilateral femoral and tibial PNBF with limited additional diagnostic context.

Table A.21 High-Burden Appendicular Asymmetry Outlier Profiles and Associated Life-Course Indicators. Note. Individuals are ranked by descending appendicular asymmetry score. These profiles represent the upper end of the observed distribution and are described as outliers in a distributional, rather than diagnostic, sense. F = estimated female; M = estimated male; DED = dental enamel defects; PD = periodontal disease component; PNBF = periosteal new bone formation component. Dashes indicate unavailable data, and diagnostic descriptions reflect differential considerations, not confirmed diagnoses.

						(-z)					
Rank	**Population**	**Individual**	**Sex**	**Age**	**BAA**	**Asymmetry**	**Stature**	**CTI**	**DED Events**	**Earliest / Deepest DED**	**PD**
1	Hirschstetten	65	M	48.5	6.81	4.7	−1.75	—	—	—	1.07
2	Hirschstetten	202	F	33.5	5.02	3.23	−2.72	−1.54	3	0.60 / 0.60	−0.79
3	Hirschstetten	199	M	21.5	3.26	1.78	0.31	1.04	2	0.40 / 0.40	−0.18
4	Hirschstetten	180	F	35	2.8	1.4	−1.62	—	1	0.29 / 0.29	−0.40
5	Hirschstetten	54	F	75	1.77	0.56	−0.64	−0.38	—	—	−0.23
6	Bruckneudorf	NHMW-Anthro-Oste-27.326	F	22.5	1.69	0.49	−1.98	1.01	3	0.69 / 0.42	0.75
7	Bruckneudorf	NHMW-Anthro-Oste-27.556	M	42.5	1.46	0.3	−0.49	—	3	0.72 / 0.59	0.57
8	Hirschstetten	111	M	21.5	1.43	0.28	−1.79	—	3	0.36 / 0.26	−0.09
9	Bruckneudorf	NHMW-Anthro-Oste-27.358	M	49.5	1.37	0.23	−0.35	—	1	0.38 / 0.38	0.89
10	Bruckneudorf	NHMW-Anthro-Oste-27.366	M	43	1.35	0.21	−0.07	−1.59	1	0.44 / 0.44	−0.88
11	Bruckneudorf	NHMW-Anthro-Oste-27.591	F	54	1.29	0.17	−1.08	0.09	0	—	1.1
12	Hirschstetten	117	M	41.5	1.2	0.09	1.19	−0.72	3	0.76 / 0.25	−0.68
13	Bruckneudorf	NHMW-Anthro-Oste-27.424	M	60.5	1.17	0.07	3.11	0.75	1	0.68 / 0.68	0.14
14	Bruckneudorf	NHMW-Anthro-Oste-27.204	M	20.5	1.01	−0.07	1.23	−0.28	1	0.34 / 0.34	−0.14

Table A.22 Selected Life-Course Contrast and Outlier Profiles. Note. Profiles were selected to illustrate high-burden, discordant, or otherwise distinctive combinations of developmental and adult skeletal indicators. F = estimated female; M = estimated male; I = indeterminate sex; AMTL = antemortem tooth loss; OA = total osteoarthritis score; DED = dental enamel defects; BAA = bilateral appendicular asymmetry. Dashes indicate unavailable data. Diagnostic descriptions represent differential considerations rather than confirmed diagnoses.

Population	**Individual**	**Sex**	**Age**	**Profile Type**	**SINDEX / PD / PNBF**	**AMTL / OA**	**DED Count / Earliest Timing**	**BAA**	**Pathological Co**

Bruckneudorf	NHMW-Anthro-Oste-27.335	M	35.5	High SINDEX; PNBF-driven	2.40 / 0.11 / 4.69	0 / 0.46	—	0.12	Diffuse subperioste deposits and PNBF possible gout-like c
Bruckneudorf	NHMW-Anthro-Oste-27.291	I	18.5	High PNBF at young age	2.17 / −0.40 / 4.74	1 / 0.00	4 / 0.61	—	Extensive severe Pl involving the pelvis lower limbs, and fe
Hirschstetten	57	M	18.5	High PNBF; suspected leprosy	1.05 / −0.72 / 2.82	2 / 0.00	2 / 0.21	—	Lower-limb PNBF porous palate and s inflammation; lepro remains a differenti diagnosis.
Hirschstetten	125	F	70	High PNBF, DED, and AMTL	0.50 / −0.04 / 1.05	16 / 1.56	5 / 0.84	—	Skeletal changes interpreted during assessment as possi tuberculosis.
Bruckneudorf	NHMW-Anthro-Oste-27.404	F	60	High PD and PNBF; complex infection	0.93 / 1.18 / 0.68	7 / 0.00	3 / 0.71	0.76	Right-femoral osteomyelitis and vertebral destructio tuberculosis and brucellosis were considered as differentials.
Hirschstetten	27	M	61.5	High PD, AMTL, and OA	0.53 / 1.31 / −0.25	30 / 1.58	1 / 0.40	0.39	Severe oral disease possible tuberculos noted during assess
Bruckneudorf	NHMW-Anthro-Oste-27.246	M	70	High PD, AMTL, and OA	0.75 / 1.15 / 0.35	25 / 1.77	2 / 0.82	0.82	Multiple dental abs severe OA, and per lesions.

Bruckneudorf	NHMW-Anthro-Oste-27.354	F	21	PNBF at young age; TB signs	0.09 / −0.65 / 0.84	2 / 0.00	3 / 0.78	—	Vertebral destructio remodelling; tuberc was considered dur assessment.
Hirschstetten	65	M	48.5	Asymmetry outlier; high PD/OA	0.32 / 1.07 / −0.43	15 / 1.57	—	6.81	Severe asymmetry possible early-life fracture or dislocati
Hirschstetten	202	F	33.5	Asymmetry outlier; low inflammation	−0.61 / −0.79 / −0.43	0 / 0.00	3 / 0.60	5.02	Skeletal dysplasia v recor

Table A.23 Selected Developmental–Inflammatory Contrast Profiles. Note. Profiles were selected to illustrate contrasting combinations of retained developmental disruption and adult inflammatory burden. F = estimated female; M = estimated male; I = indeterminate sex; DED = dental enamel defects; LEH = linear enamel hypoplasia; AMTL = antemortem tooth loss; OA = total osteoarthritis score. Higher DED timing values represent defects in earlier-forming enamel. Diagnostic descriptions reflect differential considerations rather than confirmed diagnoses.

Population	Individual	Sex	Age	Contrast Shown	DED Count / Earliest Timing	SINDEX / PD / PNBF	AMTL / OA	Pathological Context
Bruckneudorf	NHMW-Anthro-Oste-27.291	I	18.5	High DED count with extreme PNBF	4 / 0.61	2.17 / −0.40 / 4.74	1 / 0.00	Extensive severe PNBF.
Hirschstetten	125	F	70	Highest DED count with high PNBF and OA	5 / 0.84	0.50 / −0.04 / 1.05	16 / 1.56	Possible tuberculosis.
Hirschstetten	129	M	33	High DED count with low SINDEX	5 / 0.35	−0.41 / −0.40 / −0.43	0 / 0.05	Severe foot injury or infection noted.
Hirschstetten	78	M	46	High DED count and early timing with low SINDEX	4 / 0.83	−0.44 / −0.46 / −0.43	1 / 1.10	Some OA was recorded.
Bruckneudorf	NHMW-Anthro-Oste-27.387	F	47	Severe LEH with low SINDEX	2 / 0.60	−0.64 / −0.86 / −0.43	0 / 0.00	Severe LEH was recorded.

Bruckneudorf	NHMW-Anthro-Oste-27.354	F	21	Early DED timing with PNBF at young age	3 / 0.78	0.09 / −0.65 / 0.84	2 / 0.00	Vertebral destruction and remodelling; tuberculosis was considered.
Bruckneudorf	NHMW-Anthro-Oste-27.246	M	70	Early DED timing with high PD, AMTL, and OA	2 / 0.82	0.75 / 1.15 / 0.35	25 / 1.77	Multiple dental abscesses and severe OA.
Hirschstetten	57	M	18.5	High PNBF with later DED timing	2 / 0.21	1.05 / −0.72 / 2.82	2 / 0.00	Leprosy was considered as a differential diagnosis.
Bruckneudorf	NHMW-Anthro-Oste-27.323	M	45	Early DED timing with low SINDEX	3 / 0.78	−0.47 / −0.52 / −0.43	2 / 0.00	No major associated pathological observation.
Hirschstetten	202	F	33.5	Asymmetry and dysplasia with low inflammation	3 / 0.60	−0.61 / −0.79 / −0.43	0 / 0.00	Skeletal dysplasia was recorded.

Recording Forms

Form 1 Crespo SINDEX periosteal new bone formation recording form. The form was used to record periosteal new bone formation by skeletal element and anatomical region, including observability, lesion presence, distribution, severity, and activity state. PNBF variables recorded from this form were used to construct the PNBF severity and PNBF activity components of SINDEX (Crespo 2020)

PERIOSTEAL LESION SEVERITY - PLS

V: Nov 2024

LOCALITY: **CHRONOLOGY:** **DATE:**
SITE: **SEX:** **OBSERVER:**
FUNERARY UNIT: **AGE:**
INDIVIDUAL:

TIBIA[1]

	LEFT				RIGHT			
Completeness of anteromedial surface	<25%	25-50%	>50%	WB	<25%	25-50%	>50%	WB

WB: whole bone

COVERAGE SCORE[2]

Lesion Coverage[2]

Score 1: Coverage < 25%
Score 2: Coverage 25%-50%
Score 3: Coverage >50%

SEVERITY SCORE

Lesion Severity

Score 0: unobservable (no bone or too damage)
Score 1: no periosteal lesion
Score 2: mild striae, **no thickening**
Score 3: **moderate** striae, **mild** thickening
Score 4: moderate to extreme thickening

		LEFT	RIGHT
Lesion Activity	Active		
	Healing		
	Healed		

PHOTOS REFERENCE (FT samples)

FT 43.012
Lesion Form Score: 2

FT 37.006
Lesion Form Score: 2-3

FT 3.1.043
Lesion Form Score: 4

(1) Only **anteromedial diaphysis** of the bone will be evaluated

(2) Coverage of the periosteal lesion on the complete or partial bone (this will be corrected by the completeness of the bone)

Scoring criteria modified from Cook Collins D. 1976

Form 2 Crespo PDS/SINDEX periodontal disease recording form. The form records labial and lingual CEJ–alveolar crest distances as DLB and DLI, and the corresponding CEJ–alveolar crest scores as SLB and SLI. Kerr-based alveolar remodelling was recorded separately (Crespo 2020; Kerr 1988).

PERIODONTAL DISEASE SEVERITY - PDS

V: Nov 2024

LOCALITY: **CHRONOLOGY:** **DATE:**
SITE: **SEX:** **OBSERVER:**
FUNERARY UNIT: **AGE:**
INDIVIDUAL:

	RIGHT MAXILLA								LEFT MAXILLA							
TOOTH =	18	17	16	15	14	13	12	11	21	22	23	24	25	26	27	28
TS																
AP																
DLB																
SLB																
DLI																
SLI																
KERR																
LEH																
CARIES																
CALC																
OTHER																

	RIGHT MANDIBLE								LEFT MANDIBLE							
TOOTH =	48	47	46	45	44	43	42	41	31	32	33	34	35	36	37	38
TS																
AP																
DLB																
SLB																
DLI																
SLI																
KERR																
LEH																
CARIES																
CALC																
OTHER																

Form 3 Arthropathy identification and diagnosis recording form from Ventades et al. (2018). The form was used to structure macroscopic recording of osteoarthritis and other arthropathic changes, including osteophyte formation, porosity, eburnation, articular surface alteration, and joint distribution. Variables recorded from this form were used to construct peripheral, vertebral, and total OA scores for this study.

Data 1

RECORDING FORM FOR THE IDENTIFICATION AND DIAGNOSIS OF ARTHROPATHIES IN SKELETAL REMAINS

- **Reference:**

- **Sex estimation:**

☐ Male ☐ Probable male ☐ Indeterminate

☐ Female ☐ Probable female

- **Age-at-Death estimation:**

☐ Young Adult (19-40) ☐ Middle Adult (41-60) ☐ Old Adult (>61)

Estimated age:

- **Relevant aspects:**

- **Skull:**
- **Vertebrae:**
- **Pelvis:**
- **Hands and feet:**
- **Limbs:**
- **Others**

1

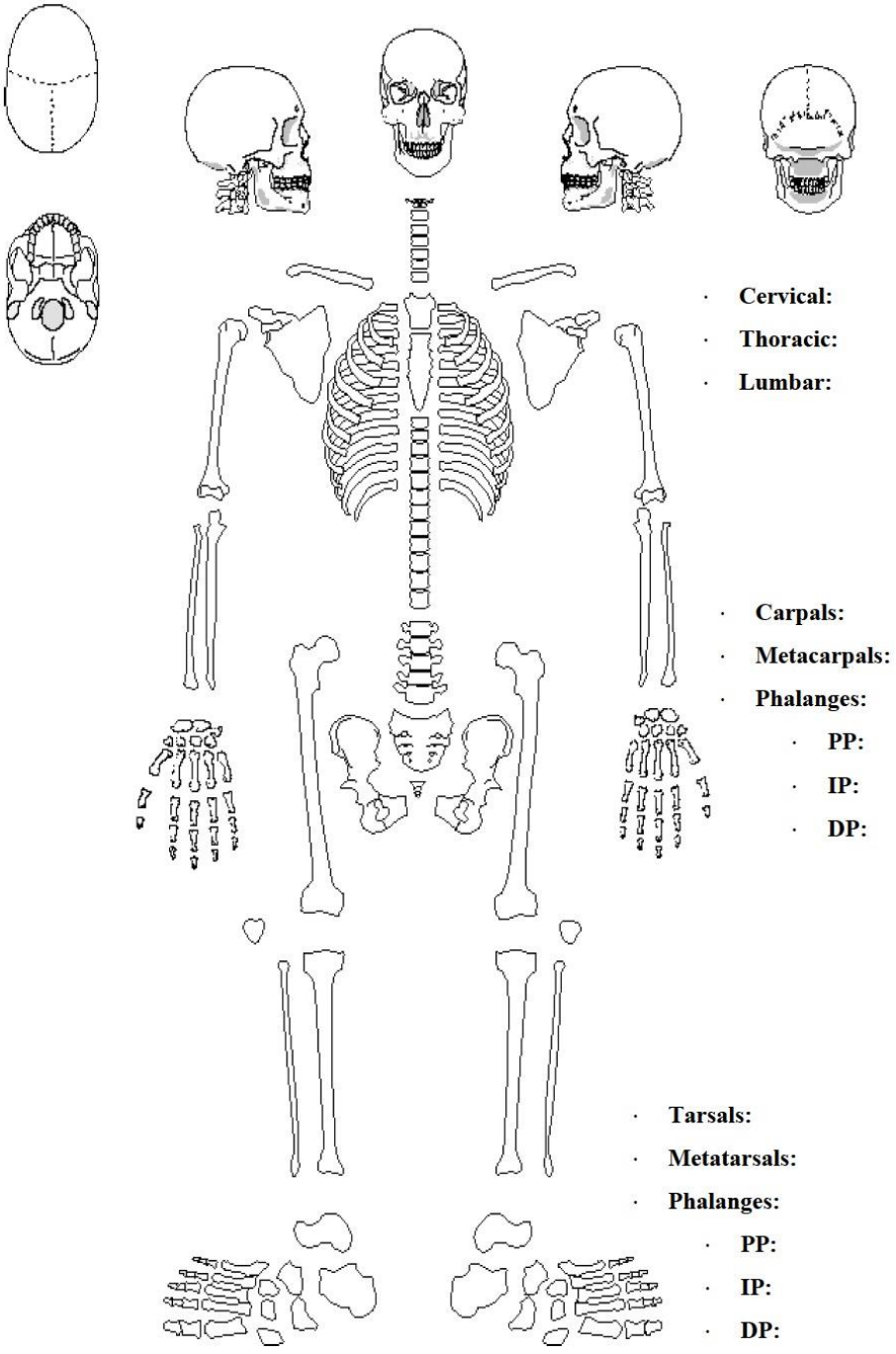

PP: Proximal Phalanges; IP: Intermediate Phalanges; DP: Distal Phalanges

2

- **Vertebral column:**
  - Vertebrae involvement (YES / NO)
  - Type of involvement (BONY OUTGROWTH / FUSION / OSTEOLYSIS)
  - Spine segment (CERVICAL / THORACIC / LUMBAR)
  - Degree affected (1 / 2 / 3) / (1 / 2 / 3) / (1 / 2 / 3)
  - Apophyseal involvement (YES / NO)
  - Degree affected (1 / 2 / 3)
  - Osteophytes (YES / NO)
    - Orientation (VERTICAL / HORIZONTAL / INDETERMINATE)
    - Symmetry (YES / NO / INDETERMINATE)
    - Degree affected (1 / 2 / 3)
  - Preservation of intervertebral space (YES / NO)
- **Pelvis:**
  - Sacroiliac joint involvement (YES / NO)
    - Symmetry (YES / NO / INDETERMINATE)
    - Degree affected (1 / 2 / 3)
- **Hands and feet:**
  - Hand joints involved (YES / NO)
    - Joint (MCP / PIP / DIP)
  - Feet joints involved (YES / NO)
    - Joint (MTP / PIP / DIP)
- **Other joints:**
  - Shoulder (RIGHT / LEFT)
  - Elbow (RIGHT / LEFT)
  - Hip (RIGHT / LEFT)
  - Knee (RIGHT / LEFT)
- **Probable diagnosis:**
- **Observer´s name and date:**

Severity of the joint lesion:

- **Grade 1**: joint slightly affected, with well-defined edges.
- **Grade 2**: joint moderately to severely affected, without well-defined edges but not fused.
- **Grade 3**: joint severely affected and fused.

Severity of the osteophytes:

- **Grade 1**: slight alteration (not measurable)
- **Grade 2**: ≤ 5 mm in length
- **Grade 3**: > 5 mm in length

MCP: metacarpophalangeal joint; MTP: metatarsophalangeal joint; PIP: proximal interphalangeal joint; DIP: distal interphalangeal joint